Reports of the Department of Geodetic Science

Report No. 201

APPLICATION OF KINEMATICAL GEODESY FOR DETERMINING THE SHORT WAVE LENGTH COMPONENTS OF THE GRAVITY FIELD BY SATELLITE GRADIOMETRY

by

George B. Reed

The Ohio State University
Department of Geodetic Science
1958 Neil Avenue
Columbus, Ohio 43210

March, 1973

Foreword

This report was prepared by George B. Reed, a graduate student in the Department of Geodetic Science of The Ohio State University. The typing and preparation of this report was supported by Air Force Contract No. F19628-720C-0120, The Ohio State University Research Foundation Project No. 3368B1. The contract covering this research is administed by the Air Force Cambridge Research Laboratories, L.G. Hanscom Field, Bedford, Massachusetts, with Mr. Belz Szabo, Project Scientist.

This report was also presented to the Graduate School of The Ohio State University in partial fulfillment of the requirements for the Ph.D degree. The original reproduction and distribution of this report was carried out through funds supplied by the Department of Geodetic Science. This report was also distributed by the Air Force Cambridge Research Laboratories as Scientific Report No. 9 under contract F19628-72-C-0120.

Several corrections, supplied by the author, have been made to the original version, for this October 1982 printing.

ACKNOWLEDGMENTS

The author expresses his sincere gratitude to the Faculty and Staff of the Department of Geodetic Science, The Ohio State University, and particularly to his adviser, Professor Richard H. Rapp, who provided not only encouragement and guidance, but also arranged for resources which enabled this work to be completed in a timely manner, and to Professors Urho A. Uotila and Ivan I. Mueller, who, as members of the author's reading committee gave many helpful suggestions.

Special thanks are due to the Department of the Army for giving the author the opportunity to participate in the U.S. Army Civil Schools Program, and to the Instruction and Research Computer Center of The Ohio State University for providing free computer facilities without which this work could not have been accomplished.

The author is deeply indebted to his wife, Bettye, for her patience and understanding during his years of study, and for typing the draft of this paper.

Finally, the author extends his sincere thanks to Miss Janet I. Wancho and Miss Kimberly R. Focht who did an exceptional job of typing this dissertation.

Abstract

This report describes an investigation into the use of satellite borne gravity gradient devices for the recovery of terrestrial gravity information in terms of discrete mean gravity anomalies, point masses or potential coefficients. Simulation studies were conducted considering two possible instrument configurations: 1) a hand-mounted system capable of sensing five independent components of the gravity gradient tensor and 2) a rotating gravity gradient system.

The spatial partial derivatives of a gravitational potential are developed using the methods of tensor calculus with specialization to the potential in spherical harmonics. A method is presented for estimating the root mean square magnitudes of all components of the gravity gradient tensor. The resulting estimates and the simulated solutions for the hard-mounted system strongly indicate that the measuring sensitivities required for the cross-gradient terms are beyond practical limits for satellite gradiometers. In addition, the effect of altitude attenuation on the gradients was evaluated.

The simulation experiments demonstrated that a rotating gradiometer with a sensitivity and accuracy of 0.01 E can satisfactorily resolve 2° x 2° mean gravity anomalies (equivalent to degree 90) with an accuracy of 0.5 to 1 milligals at 250 to 300 kilometers altitude.

TABLE OF CONTENTS

TABLE OF CONTENTS (continued)

TABLE OF CONTENTS (continued)

LIST OF TABLES

LIST OF FIGURES

LIST OF FIGURES (continued)

LIST OF FIGURES (continued)

INTRODUCTION

A long standing goal of geodesy is the determination of the gravity field of the earth. The qualitative and quantitative achievement of this goal has been essentially an evolutionary process associated with the needs and state-of-the-art of technology and science. Today socio-economic pressures coupled with unprecendented technological achievement is placing ever increasing demands on the geosciences. Among these are increasing scientific and functional requirements for detailed knowledge of the fine structure of the earth's gravity field. The applications are to be found in numerous civil and military endeavors. Among those applications of greatest significance are satellite navigation, inertial navigation, earth and ocean physics, earth resources, surveying and mapping, and trajectory computations for strategic weaponry and artificial satellites.

In the past, the acquisition of detailed gravity data through classical gravimetric methods was limited by inaccessability or denial of large regions of the earth. With the advent of the space age and the development of the satellite gravimetry, geodesy experienced a quantum jump in capability to refine and survey the gravity field on a global basis. As a consequence, progressively over the last decade, more detailed and accurate models of the earth's gravity field have been produced. Such models have normally been in the form of coefficients of the spherical harmonic expansion of the

geopotential:

$$V = \frac{kM}{r}\left[1 + \sum_{n=2}^{\infty}\sum_{m=0}^{n}\left(\frac{a}{r}\right)^{n}\left(C_{nm}\cos m\lambda + S_{nm}\sin m\lambda\right)P_{nm}(\sin\varphi)\right] \qquad (0.1)$$

The detail expressed by such a model depends on the number of coefficients (C_{nm}, S_{nm}) which it contains. Such models have been developed by satellite orbit perturbation analysis and by combinations of satellite determined harmonic coefficients and surface gravimetry (Kaula, 1966a; Rapp, 1969; Gasposchkin and Lambeck, 1970).

While dynamic satellite methods have been eminently successful in advancing our knowledge of the earth's gravity field, there are apparent limitations in detecting the short wavelength components which make up the so called fine structure of the gravity field. As a consequence, impetus has been given to various proposals for satellite-borne hybrid measuring systems which, in general, provide a capability to sense or measure some spectrum of the earth's gravitational field directly. The requirements for such systems are discussed in the report of the Williamstown Conference (Kaula, 1969a) and the JPL Earth and Ocean Physics Applications Planning Study (Loomis et al., 1972).

Proposed systems currently in an advanced stage of development are satellite altimeters, satellite-to-satellite Doppler and satellite gradiometers. The concepts of altimetry and satellite-to-satellite tracking have been studied in substantial detail with respect to exploitation in geodesy (Hudson, 1970; Lundquist, et al., 1969; Wolff, 1969; Schwarz, 1970). On the other hand, satellite gradiometry has received minimal attention for geodetic implications

(Forward, 1971a; Glaser and Sherry, 1971; Kaula, 1971; Bell et al., 1970; Moritz, 1971; Glaser, 1972). With the exception of Moritz and Glaser, the investigations published to date have been limited in scope and rather non-specific as to how the gradient measurements are to be used in forming more detailed geopotential models. Although Moritz specifically addresses the use of airborne gravimetry and gradiometry, he presents some extrapolation of the airborne system to satellite gradiometry. However, in all published studies, the implied proposed uses of satellite gradiometer measurements are based on global solutions in terms of harmonic coefficients and/or direct geophysical interpretation in combination with data such as geomagnetic field measurements, surface gravimetry and tectonic plate movements, etc.

The JPL Study (Loomis, et al., 1972) suggests the following probable order of decreasing resolving power for satellite gravimetric techniques:

(1) radar altimetry (Ocean areas only)

(2) gravity gradiometry

(3) high-low satellite-to-satellite tracking

(4) low-low satellite-to-satellite tracking

(5) Upgraded orbit analysis from improved tracking and lower satellites.

Comparative analyses (Forward, 1971a; Sherry and Glaser, 1972; Gardner, et al., 1972; Loomis,et al., 1972) of the above systems indicate that each has an optimum range of sensitivity in terms of harmonic degree and the

associated wavelength. In fact, the analyses point out that theoretically the various systems are complimentary rather than competitive. In the case of satellite gradiometry, the resulting measurements are expected to yield significant information to harmonic degree 90. Of interest is the evaluation in the JPL Gravity Gradiometer Study (Gardner, et al, 1972) that while present state-of-the-art orbit determination is adequate for a satellite gradiometer mission, it is not adequate for an altimeter mission. Their analyses show that about a two order of magnitude improvement in the gravitational uncertainies is necessary to the success of an altimeter mission. Satellite gradiometry can provide such improvement according to that evaluation.

Satellite gradiometry thus presents an exciting possibility of developing global gravity maps in heretofore unprecedented detail. As a consequence, the principal purpose of this investigation was pointed to development of a possible procedure for use of satellite gradient measurements in obtaining gravity boundary values and to determine if gradiometry can provide, with sufficient accuracy, discrete geopotential information equivalent to harmonic degree 90.

Since real data was not available, the study relied heavily on computer simulation experiments. Further, because of various proposals for gradiometer instrumentation which are under development (Anthony, 1971), simulations were limited to two possible instrument configurations: (1) A hard-mounted system capable of sensing five independent components of the gravity

gradient tensor; (2) A rotating system which produces a signal which can be analyzed in terms of signal amplitude as a function of three components of the gradient tensor.

Chapter 1 discusses the general concept of satellite gradiometry and the mission parameter considerations which governed the simulation experiments. Chapter 2 presents some current thinking with respect to gravity field representations and discusses the choice of representations used in this study. In Chapter 3 the first and second derivatives of a potential function are developed by the methods of tensor calculus. These derivatives are then specialized for the spherical harmonic expansion of the geopotential. Chapter 4 presents a discussion of various investigators attempts to evaluate the magnitude of the anomalous gravity gradients at orbital altitudes and the gradiometry sensitivity required to resolve the anomalous spectrum of the gravity field. Formulae for gravity gradient estimation are developed along the lines of classical estimation theory in physical geodesy. The results of estimates obtained are evaluated in terms of gradiometer resolution and sensitivity. Additionally, the effect of altitude attenuation on the gradients are considered. An algorithm for generating simulated satellite gradiometer data is presented in Chapter 5. In Chapter 6, least squares solutions with gradiometer data are mathematically formulated and the physical nature of the solutions are discussed. Development of the simulation models, the simulation experiments, and numerical results are presented in Chapter 7. Chapter 8 briefly summarizes the study and presents relevant conclusions.

1. THE CONCEPT OF SATELLITE GRAVITY GRADIOMETRY

1.1 General Principles

In the usual convention of physical geodesy, the total gravity potential is separated into a normal or reference potential, U, and a disturbing or anomalous potential, T:

$$W = U + T \tag{1.1}$$

Normally, the function U represents the potential of an equipotential ellipsoid (Heiskanen and Moritz, 1967). It also may represent the potential of a high order equipotential spherop (Needham, 1970). On the surface, W and U include the potential of the centrifugal force due to the earth's angular rotation. For points in external space, the centrifugal potential does not act. In this case it is appropriate to express the total gravitational potential by:

$$V = U + T \tag{1.2}$$

where it is understood that U does not contain a centrifugal term.

In principle, gradiometers in orbiting artificial satellites measure the second spatial derivatives of the total gravitational potential. Defining a local earth space Cartesian coordinate system (ξ, η, ζ) where the ξ-axis is directed Northward, the η-axis Eastward, and the ζ-axis is perpendicular to the $\xi\eta$ plane and is directed outward from the earth, these second

derivatives can be expressed in matrix form by:

$$\begin{bmatrix} V_{\xi\xi} & V_{\xi\eta} & V_{\xi\zeta} \\ V_{\eta\xi} & V_{\eta\eta} & V_{\eta\zeta} \\ V_{\zeta\xi} & V_{\zeta\eta} & V_{\zeta\zeta} \end{bmatrix} \tag{1.3}$$

where $V_{\xi\xi} = \frac{\partial^2 V}{\partial \xi^2}$, $V_{\xi\eta} = \frac{\partial^2 V}{\partial \xi \partial \eta}$, etc. are called the "gravity gradients". The term "gravity gradient" is a misnomer since the first derivatives of the potential form a vector or gradient of the potential. A vector has no gradient; therefore it would be more accurate to call the second derivatives the components of the gravity tensor. However, since the usage is well established, no confusion should result from retaining the designation "gravity gradients". The matrix, equation (1.3) will be referred to as the "gravity gradient tensor".

Of fundamental importance to the application of gradiometry is the nature of the earth's external gravitational field. From classical potential theory (MacMillan, 1958), any gravitational field in empty space belongs to the class of force fields in which no dissipative losses of energy occur when a mass particle is moved from point to point. Such a field is said to be conservative. In addition, the potential energy differences between points in the field are a function of position only i.e., independent of the path along which the particle moves. The basic properties of the gravitational vector force field $\bar{g}$ in empty space (external to the masses producing the field) is associated with a scalar potential $V(x, y, z)$ such that:

$$\begin{aligned} \bar{\nabla} V &= -\bar{g} \\ \bar{\nabla} \cdot \bar{g} = \bar{\nabla}^2 V &= 0 \\ \bar{\nabla} \times \bar{g} &= 0 \end{aligned} \tag{1.4}$$

These equations indicate that $V(x, y, z)$ and its gradient $\bar{\nabla} V$ are harmonic functions. Further, since the divergence of the field, $\bar{\nabla} \bar{g}$, is zero, the field is said to be solenoidal, i.e., the flux of the field in empty space along a "tube of force" is constant. The curl, $\bar{\nabla} \times \bar{g}$, is also zero; hence, the field is both conservative and irrotational. The significance of these properties to gradiometry are:

(1) The harmonic nature of the gravitational field requires that the first and second derivatives of the potential function exist.

(2) The solenoidal nature requires that in a stationary system of reference: $V_{xx} + V_{yy} + V_{zz} = 0$.

(3) The irrotational nature imposes the conditions:

$$V_{xy} = V_{yx}$$

$$V_{xz} = V_{zx}$$

$$V_{yz} = V_{zy}$$

(4) From (2) and (3) we see that of the nine gradient components in equation (1.3) only five are independent.

(5) The field is independent of the coordinate system.

(6) The first and second derivatives are non-zero, unless the potential is everywhere constant in space. This means that any possible field except the zero field is non-uniform in space.

The non-uniformity of the external gravitational field has two features. One pertains to variation of field strength along a line of force (the plumb line), while the other appears as a variation of its direction when passing from one line of force to another. The latter feature is called "curvature effect".

These properties and features make gradiometry a viable method of surveying the gravitational field provided the inertial effects can be separated from the gravitational effects. The earliest method devised for such separation is attributed to Roland von Eötvös. Early in this century, Eötvös designed a "torsion balance" or pendulum which he made insensitive to the influence of gravity at the origin of the instrument's coordinate axes by confining its motion to a horizontal plane (Flugge, 1956, Mueller, 1960). In the case of a moving platform such as an aircraft, Moritz (1967) has shown that the inertial part of the gravity field can be separated by inertially stabilizing the gradiometer instrument axes. For field separation, an artificial satellite provides the ideal environment for a gradiometer. In an orbiting vehicle, the gravitational force at the center of mass is in equilibrium with the centrifugal force thus the inertial part of the field is zero. In fact, the only direct measurements of the gravitational field possible in a satellite are the gradients of gravity.

As pointed out previously, this study considers two possible types of satellite gradiometer systems. Both systems are conceptually feasible and have been the subject of analytical studies and/or active research and development. Numerous references found in the bibliography to this report provide detailed information on specific instrumentation. Discussion here will be limited to describing in general terms a hard-mounted system and a

rotating system.

The hard-mounted or strap-down type gradiometer hypothesized could, for example, be assembled from a set of vibrating string transducers described by American Bosch Arma (1966) or from seismic devices proposed by Savet, et al., (1967). Five independent components of the gravity gradient tensor are assumed to be measured. In addition, the orientation of the gradiometer with respect to inertial space is maintained by active attitude control and gradient torque stabilization of the satellite carrier. The satellite is assumed to have on-board attitude sensors which provide a read-out of the spatial orientation of the local Cartesian coordinate axes along which the gradients are measured. Details of the hard-mounted gradiometer orientation are given in section 5.6.1. The gravity gradient tensor components which may be measured by the hard-mounted system include the off-diagonal terms:

$$V_{12},\ V_{13},\ V_{23}$$

and any two of the diagonal terms:

$$V_{11},\ V_{22},\ V_{33},$$

where the subscripts denote the gradiometer and satellite fixed coordinate axes along which the gravity gradients are measured. In general, the 1-axis lies in the satellite's orbital plane, and 3-axis is directed outward from the earth in the direction of the local vertical; and the 2-axis is perpendicular to the 1-3 plane forming a right-handed (1,2,3) coordinate system. Only two of the diagonal terms or components are independent by virtue of the condition imposed by the Laplace equation $\nabla^2 V = 0$.

For satellite-borne systems, rotating type gradiometers, such as described by Forward (1971c) and Glaser (1972), are the most likely to be operational in the near future. The signal output for a typical rotating gradiometer may be expressed by:

$$\text{Signal} = (V_{33} - V_{11}) \sin wt - 2V_{13} \cos wt \tag{1.5}$$

where w is the spin rate and t is the time interval from some initial epoch. This is simply a harmonic oscillator which may be evaluated in terms of signal amplitude given by:

$$\text{Amplitude} = [(V_{33} - V_{11})^2 + 4V_{13}^2]^{\frac{1}{2}} \tag{1.6}$$

Attitude control for this system is provided by spin stabilization of the satellite. The orientation of rotating gradiometer fixed coordinate axes is described in section 5.6.2. As in the case of the hard-mounted system we have assumed that on-board attitude sensors will be provided. Further, the rotating system requires sensors to provide in-flight spin rate correction or telemetry of data for post-mission corrections. For more detailed discussion of gradiometer attitude control concepts, the reader is referred to Chapter VI and VII of the JPL gradiometer study (Gardner, et al., 1972).

In simulating the gradiometer systems, the output signals in terms of gradients or functions of gradients have been assumed to be exact. Actually these signals differ from the output of a real gradiometer by some proportionality factor. This factor depends on the characteristics of the particular instrumentation employed. The constancy of the proportionality

is subject to various dynamic and thermal noise effects. Mallove (1972) analyzed the equations of motion for a dynamic model of a rotating gradiometer in a spin stabilized satellite. Dynamic errors were evaluated using parameters for an Earth orbiting experiment. The reported results show that the dynamic errors produce inaccuracies less than 0.01E[1] at a system integration time of about 30 seconds (Forward, 1971a, 1971c). Since similar accuracy data was not available for the hard-mounted gradiometer system, 0.01E at 30 seconds was assumed to be applicable.

Satellite gradiometry offers several advantages when compared to surface gravimetry and other satellite gravimetric techniques. First of all, a gradiometer instrument package mounted in a single satellite in low polar orbit can obtain complete global coverage in a period of days. Gravimetric methods based on orbit pertubation analysis and satellite-to-satellite tracking require two or more satellites at various altitudes and inclinations to obtain complete sampling of the gravity field. Pertubation methods are highly dependent on orbit determination and indirect; whereas direct measurements are made by a gradiometer which permits on-board data storage and less stringent orbit determination. Satellite altimetry as currently conceived is limited to measurements over ocean areas and in order to achieve its full potential will probably require orbit determination one or two orders of magnitude above current technology. Further, the more conventional satellite techniques and satellite-to-satellite tracking measure responses due to the gravitational acceleration. It is well known that the acceleration signals

[1] 1E(Eotvos) = 10^{-9} Gal/cm where 1 Gal = 1 cm/sec^2

are most responsive to the longer wavelength components of the field and tend to filter out the short wavelengths at orbital altitudes. With gradiometry, the high frequency short wavelength part of the gravitational field is accentuated because spatial derivatives of the acceleration are measured. In the rotating gradiometer which measures a combination of gradients, this accentuation is further amplified. Still another advantage of satellite gradiometry is insensitivity to atmospheric drag effects. While drag results in orbital decay and influences mission duration, the effect on the gradiometer sensors (proof masses) is essentially uniform and thus the observed gradients are unchanged. This is not the case with other satellite methods where atmospheric drag constitutes a significant source of error. However, this error source can be controlled by use of drag-free satellites.

1.2 Satellite Gradiometer Mission Parameters

Here we will summarize the pertinent considerations for an orbiting gradiometer mission based on the JPL Gravity Gradiometer Study (Gardner, et al., 1972, Section III B and IV C). That study demonstrates the desirability of placing the satellite in a nominal circular polar orbit at nominal altitude of 300 kilometers. Placing the satellite carrying the gradiometer in polar orbit allows for complete global latitude coverage. Further, this also permits using the earth's poles as calibration points as the satellite will pass over both poles in each revolution. A circular orbit, or perhaps more practically, an orbit of small eccentricity, permits uniform sampling of the gravitational field. This should yield data of near uniform accuracy and thus eliminate complex weighting schemes in the data reduction. The altitude is a trade-off

between gradiometer signal resolution and mission life. Gradiometer resolution is discussed further in Chapter 4. The JPL evaluation indicates that the orbital life at a nominal altitude of 300 kilometers will be approximately 15 to 40 days duration. Satellite tracking and orbit determination for a gradiometer mission was determined by JPL to be adequate with current state-of-the-art methods. The required 1σ position accuracy specified is 20-25 meters for gradient measurements accurate to 0.01E.

The simulation experiments described in Chapter 7 were guided by the JPL mission analysis. To the greatest extent possible, the experiments were designed by using parameters which conform to actual conditions expected.

2. GRAVITY FIELD REPRESENTATION

In recent years there has been extensive study of alternatives to the spherical harmonic representation of the gravity field. The spherical harmonics are ideally suited to depicting the long-wavelength components of the field, which makes them compatible with the resolution of satellite perturbation analysis. While Kaula (1969) advocates continued use of spherical harmonics for satellite geodesy, he acknowledges that the new satellite-borne systems, altimetry, gradiometry, etc., will require more appropriate representations for the fine structure of the field. Various alternatives have been proposed. Koch (1968) developed a spherical harmonic representation with a superimposed variable density layer. This procedure has been implemented by Koch and Morrison (1970) to calculate a density layer model fixed over $30^\circ \times 30^\circ$ blocks. Witte (1970) formulated the computational procedures for applying the density layer model to solutions using Doppler observations. The same concept was also applied to satellite-to-satellite Doppler tracking simulation studies by Schwarz (1971) using $2^\circ \times 2^\circ$ and $5^\circ \times 5^\circ$ density blocks. Lundquist et al., (1969) proposed using a set of periodic functions that have the property of being effectively zero except at a particular location. Needham (1970) demonstrated the formation of a geopotential model based on fitting point masses to mean gravity anomalies referred to a high order spherop. A significant feature of the point mass model is the detail that can be represented by superimposing

mass arrays of varying distribution and depth. Arnold (1967) was largely responsible for the concept of obtaining gravity anomalies directly from satellite orbit analysis. A direct simulated solution for $15^{\circ} \times 15^{\circ}$ mean anomalies was carried out by Obenson (1970).

As noted previously, the spherical harmonic representation has been the only representation considered to date in connection with satellite gradiometry. The reason for this apparent fixation on spherical harmonics comes from nearly exclusive consideration of satellite gradiometry by orbit analyst. However, there are several agruments against the use of a spherical harmonic representation in connection with satellite gradiometry. Because each harmonic coefficient represents an integral over the total mass distribution of the earth, gradient observations over the entire earth must be included in each solution. That is each solution is necessarily a global solution. Since the spherical harmonic representation is global in nature, the fact that some features of gravity field are better known in some regions cannot be reflected, e.g., land masses vs. oceanic areas. The logical alternative is to use some local representation which can be discretely expressed in terms of the anomalous gravity field in some appropriately sized blocks on the earth's surface or on the geoid. Additionally, arrays of point masses beneath the surface are another possible representation.

For this investigation, two geopotential representations were considered:

(1) Mean gravity anomalies referred to a high order spherop.

(2) Point masses fitted to the gravity anomalies

As is well known, gravity anomalies have long played a significant role in geodesy for use in the geodetic boundary value problem and in the determination of absolute positions of points on the earth's surface. Additionally, they are extensively used in geophysical exploration and, perhaps to a lesser extent, in trajectory computations. The lack of adequate global coverage has long been a shortfall in geodesy. Various geophysical and statistical methods have been applied to fill in gravimetrically unsurveyed areas. Uotila (1962, 1967) developed model anomalies by geophysical analyses and by least squares fitting of surfaces through known values. Rapp (1964), Moritz (1964), Obenson (1968) applied statistical methods of interpolation and extrapolation.

As demonstrated by Needham (1970), the point mass representation is considerably simpler and more efficient in computations similar to those based directly on gravity anomalies. Further, for the purpose of this study, the point mass concept had two appealing features. First of all, masses fitted to the gravity anomalies produce a somewhat smoothed field which was thought likely to be more consistent with the resolving capability of an orbiting gradiometer. Secondly, simulation experiments with point masses might give an indication of the capacity of satellite gradiometry in discrete mass detection for geophysical analysis and military intelligence applications. Unfortunately, these expectations were not attainable due to reasons which will be explained.

2.1 The Spherop Reference Field

The concept of a spherop or high order reference field has been discussed by Molodenski (1962), DeWitte (1966), Wong and Gore (1969) and Needham (1970). In essence, the usual level ellipsoid whose gravitational potential is described in terms of zonal harmonic coefficients by:

$$U = \frac{kM}{r}\left[1 + \sum_{n=2}^{\infty}\left(\frac{a}{r}\right)^{2n} C_{2no}\, P_{2no}(\sin\varphi)\right] \qquad (2.1)$$

where $C_{2no} = f(C_{2o})$, is replaced by complex undulating surface. The potential of this surface is given in spherical harmonic form by:

$$U_S = \frac{kM}{r}\left[1 + \sum_{n=2}^{N}\sum_{m=0}^{n}\left(\frac{a}{r}\right)^{n}(C_{nm}\cos m\lambda + S_{nm}\sin m\lambda)P_{nm}(\sin\varphi)\right] \qquad (2.2)$$

In equations 3.1 and 3.2 the notation has the following meaning:

U = Spheropotential of level ellipsoid

U_S = Spheropotential of spherop

kM = Product of the gravitational constant, k, and the mass of the earth, M

a = Equatorial radius of the earth

r = Geocentric radius to computation point

φ = Geocentric latitude of computation point

λ = Geocentric longitude of computation point

C_{nm}, S_{nm} = Conventional spherical harmonic coefficients

$P_{nm}(\sin\varphi)$ = Ordinary associated Legendre functions

N = Degree and/or order at which the series is truncated.

The spherop reference gravity field used in this study is identical

to the shperop 14 system described by Needham (1970, Chapter 3). The parameters of the reference field are based on the Geodetic Reference System of 1967 and a set of 14th degree and order spherical harmonic coefficients developed by Rapp (1969). The defined parameters for the GRS 67 (IAG, 1967) in equations (2.1) and (2.2) are:

$$a = 6378160 \text{ meters}$$

$$J_2 = -C_{20} = 1082.7 \times 10^{-6}$$

$$kM = 3.98603 \times 10^{20} \text{cm}^3/\text{sec}^2$$

2.2 The Anomalous Potential

Both gravity field representations for the anomalous potential used in this study are dependent on a set of mean residual[1] gravity anomalies referred to the spherop reference field. The models formed used the $1^\circ \times 1^\circ$ mean residual anomaly set developed by Needham (1970). This set covers most of the United States. However, since the models are used in a simulation study of gradiometry, the specifics of the anomaly set used is relatively unimportant. In fact, any number of reasonable arbitrary anomaly sets could have been used; although simulation models based on real data do have certain ascetic appeal.

2.2.1 The External Anomalous Potential in Terms of Gravity Anomalies

The anomalous potential T, at any point above the surface of the

---

[1] A residual gravity anomaly is defined as the difference between a gravity measurement, reduced to the geoid, and the spherop normal gravity at the corresponding point on the spherop reference surface.

earth may be expressed by the familiar formula of Pizzetti:

$$T = \frac{R}{4\pi} \int_{\sigma}\int \Delta g \, S(r,\psi) \, d\sigma \qquad (2.3)$$

In this expression, Δg normally represents free air gravity anomalies. Here the Δg are residual anomalies referred to the (14,14) spherop. DeWitte (1969) has shown that this substitution is valid and has the effect of reducing the truncation errors associated with the Stokes' kernel of the integral. The integration surface is a mean earth sphere of radius R = 6371000 meters; $d\sigma$ is an elemental area on the surface; $S(r,\psi)$ in the generalized Stokes' kernel or function given by Heiskanen and Moritz (1967, p. 235) in the form:

$$S(r,\psi) = t\left[\frac{2}{D} + 1 - 3D - t\cos\psi\,(5 + 3\ell n \frac{1 - t\cos\psi + D}{2})\right] \qquad (2.4)$$

where ψ is the angular distance between the computation point P and the variable point P' at the center of the mean anomaly block defined by geocentric latitude and longitude (φ,λ') is given by

$$\psi = \cos^{-1}\left[\sin\varphi \sin\varphi' + \cos\varphi\cos\varphi'\cos(\lambda' - \lambda)\right] \qquad (2.5)$$

$$t = \frac{R}{r} \qquad (2.6)$$

$$D = (1 - 2t\cos\psi + t^2)^{\frac{1}{2}} \qquad (2.7)$$

where r is the geocentric radial distance to the computation point.

2.2.2 The External Anomalous Potential in Terms of Point Masses

Given a set of point masses in places of gravity anomalies, the

anomalous potential at an external point P_i can be computed by the simple summation formula (Needham, 1970):

$$T_i = \sum \frac{km_j}{\ell_{ij}} \tag{2.8}$$

where: ℓ_{ij} = the distance between the computation point P and the point mass m

k = the gravitational constant ($6.673 \times 10^{8} cm^3/g\ sec^2$)

m_j = the jth point mass.

3. SPATIAL PARTIAL DERIVATIVES OF A POTENTIAL FUNCTION

Normally a gravitational potential function is related to position in terms of spherical coordinates (λ, φ, r). Geometrically, the function, if set equal to constants, defines a family of equipotential surfaces or 2-dimensional Riemannian manifolds imbedded in a 3-dimensional flat space. Since we are dealing with a gravitational potential function, the function is harmonic and thus will be restricted to satisfy the Laplace equation. This is also essentially a geometric consideration, analogous to Einstein's law of gravitation obtained by contracting the curvature tensor of 4-space, (Moritz, 1967). In fact, the Laplacian of the potential is simply a contraction of the gravity gradient tensor.

The spatial derivatives of interest in connection with the output from a satellite gradiometer (or for that matter any gradiometer) are the second partial derivatives with respect to a local Cartesian coordinate system at an arbitrary point in near earth space. The first partial derivatives of a gravitational potential function are the covariant components of the gravitational acceleration vector, a first order tensor. The gravitational gradients, the second partial derivatives of the potential with respect to Cartesian coordinates, are the components of a covariant second order tensor. The latter is obtained by absolute or covariant differentiation of the acceleration vector components.

3.1 Transformations Between Coordinate Systems

As the derivatives of the potential are tensor components, the required transformations are conveniently derived by the methods of tensor calculus. In Figure 1 the geocentric system is represented by $x^p = (x, y, z)$ and the spherical coordinates by $u^p = (\lambda, \varphi, r)$. The geocentric system is further described by the unit vector triad $(\hat{i}_1, \hat{i}_2, \hat{i}_3)$ designated as the basis i_p. Similarly, the local space coordinate system is described by the basis e_p. Note that the vectors in the triad (e_1, e_2, e_3) are not, in general, unit vectors. Adopting the notation of Moritz (1971), we introduce the local rectangular coordinate system (η, ξ, ζ) defined by the e_p basis.

First, let us consider the position vector of an arbitrary point P in space given in terms of the geocentric Cartesian coordinates by:

$$r = x^p i_p = x\hat{i}_1 + y\hat{i}_2 + z\hat{i}_3 \tag{3.1}$$

From the geometry of the figure the geocentric coordinates are functionally related to the spherical coordinates by:

$$x^p = x^p(u^p) \tag{3.2}$$

which is specifically given by:

$$\begin{aligned} x &= r\cos\varphi\cos\lambda \\ y &= r\cos\varphi\sin\lambda \\ z &= r\sin\varphi \end{aligned} \tag{3.3}$$

---

[1] The summation convention illustrated in equation (3.1) is used throughout this chapter.

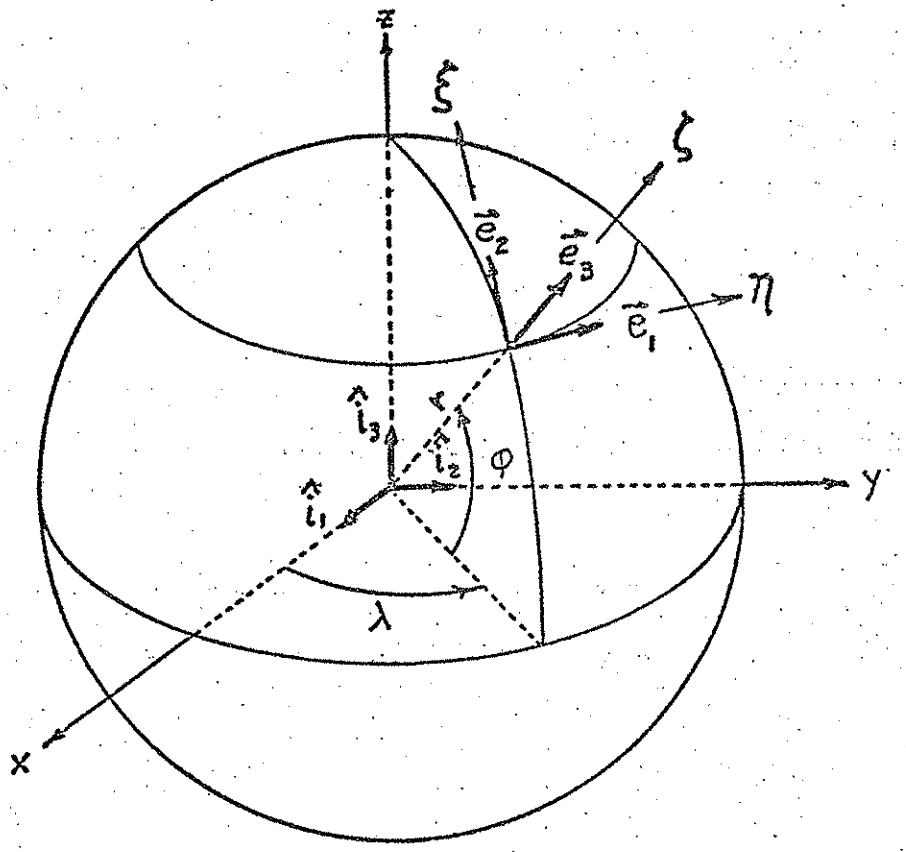

Figure 1. Coordinate Systems and Basis Vectors

The covariant basis e_p of the local coordinate system at the point P is given by:

$$e_q = i_p \frac{\partial x^p}{\partial u^q} \tag{3.4}$$

Using equation (3.3) the partial derivatives $\partial x^p / \partial u^p$ can be readily obtained. These terms arranged in matrix form are:

$$\frac{\partial(x,y,z)}{\partial(\lambda,\varphi,r)} = \begin{bmatrix} -r\cos\varphi\sin\lambda & -r\sin\varphi\cos\lambda & \cos\varphi\cos\lambda \\ r\cos\varphi\cos\lambda & -r\sin\varphi\sin\lambda & \cos\varphi\sin\lambda \\ 0 & r\cos\varphi & \sin\varphi \end{bmatrix} \tag{3.5}$$

Similarly, the geocentric basis i_p in terms of the local basis e_p is obtained by:

$$i_p = e_s \frac{\partial u^s}{\partial x_p} \tag{3.6}$$

Substituting (3.4) into (3.6), then:

$$i_p = i_p \frac{\partial x^p}{\partial u^q} \frac{\partial u^s}{\partial x^p}$$

which is true only if:

$$\frac{\partial x^p}{\partial u^p} \frac{\partial u^s}{\partial x^p} = \delta^s_q = \begin{cases} 1 & s = q \\ 0 & s \neq q \end{cases}$$

Thus the matrix of partial derivatives $\partial u^s/\partial x^p$ is the inverse of (3.5),

$$\frac{\partial(\lambda,\varphi,r)}{\partial(x,y,z)} = \begin{bmatrix} -\frac{\sin\lambda}{r\cos\varphi} & \frac{\cos\lambda}{r\cos\varphi} & 0 \\ -\frac{\sin\varphi\cos\lambda}{r} & -\frac{\sin\varphi\sin\lambda}{r} & -\frac{\cos\lambda}{r} \\ \cos\varphi\cos\lambda & \cos\varphi\sin\lambda & \sin\varphi \end{bmatrix} \tag{3.7}$$

Now by taking the inner products:

$$g_{pq} = e_p \cdot e_q$$

we obtain the covariant metric tensor of the surface described by the vector function $\bar{r} = \bar{r}(\lambda, \varphi, r)$:

$$g_{pq} = \begin{bmatrix} r^2\cos^2\varphi & 0 & 0 \\ 0 & r^2 & 0 \\ 0 & 0 & 1 \end{bmatrix} \tag{3.8}$$

Inverting (3.8) yields the contravariant metric tensor:

$$g^{pq} = \begin{bmatrix} \frac{1}{r^2\cos^2\varphi} & 0 & 0 \\ 0 & \frac{1}{r^2} & 0 \\ 0 & 0 & 1 \end{bmatrix} \tag{3.9}$$

To complete the mathematical preliminaries we must introduce the Christoffel symbols of the second kind which are defined by:

$$\left\{ \begin{matrix} s \\ pq \end{matrix} \right\} = \frac{1}{2} g^{st} \left(\frac{\partial g_{qt}}{\partial u^p} + \frac{\partial g_{pt}}{\partial u^q} - \frac{\partial g_{pq}}{\partial u^t} \right) \tag{3.10}$$

Equation (3.10) yields 27 values of which only 9 are non-zero. Thus

$$\left\{ \begin{matrix} 1 \\ p\ q \end{matrix} \right\} = \begin{bmatrix} 0 & -\tan\varphi & \frac{1}{r} \\ -\tan\varphi & 0 & 0 \\ \frac{1}{r} & 0 & 0 \end{bmatrix}$$

$$\left\{ \begin{matrix} 2 \\ p\ q \end{matrix} \right\} = \begin{bmatrix} \sin\varphi\cos\varphi & 0 & 0 \\ 0 & 0 & \frac{1}{r} \\ 0 & \frac{1}{r} & 0 \end{bmatrix} \tag{3.11}$$

$$\left\{ \begin{matrix} 3 \\ p\ q \end{matrix} \right\} = \begin{bmatrix} -r\cos^2\varphi & 0 & 0 \\ 0 & -r & 0 \\ 0 & 0 & 0 \end{bmatrix}$$

By making use of the Christoffel symbols and equations (3.4) and (3.5) we find that the derivatives of the e_p basis vectors are given by:

$$\frac{\partial e_p}{\partial u^q} = \left\{ \begin{matrix} s \\ p\ q \end{matrix} \right\} e_s \tag{3.12}$$

Similarly for the contravariant components e^p defined by:

$$e^p = g^{pq} e_p \tag{3.13}$$

we get

$$\frac{\partial e^p}{\partial u^q} = - \left\{ \begin{matrix} p \\ s\ q \end{matrix} \right\} e^s \tag{3.14}$$

Let us now consider a potential function

$$V = V(u^p) = V(\lambda, \varphi, r)$$

The gradient of V is defined in the (x, y, z) or (η, ξ, ζ) cartesian coordinate systems. Since V is defined in terms of spherical coordinates, we have

$$\bar{\nabla} V = \frac{\partial V}{\partial u^p} e^p \tag{3.15}$$

or using (3.13)

$$\bar{\nabla} V = \frac{\partial V}{\partial u^p} g^{pp} e_p \tag{3.16}$$

which yields for ∇V in the local coordinate system:

$$\bar{\nabla} V = \frac{1}{r^2 \cos^2\varphi} V_\lambda e_1 + \frac{1}{r^2} V_\varphi e_2 + V_r e_3 \tag{3.17}$$

Using (3.4) and (3.5), V is transformed to the geocentric system by:

$$\begin{aligned} \bar{\nabla} V = & \left(\frac{\sin\lambda}{r \cos\varphi} V_\lambda - \frac{\sin\varphi \cos\lambda}{r} V_\varphi + \cos\varphi \cos\lambda V_r \right) \hat{i}_1 \\ & + \left(\frac{\cos\lambda}{r \cos\varphi} V_\lambda - \frac{\sin\varphi \sin\lambda}{r} V_\varphi + \cos\varphi \sin\lambda V_r \right) \hat{i}_2 \\ & + \left(\frac{\cos\varphi}{r} V_\varphi + \sin\varphi V_r \right) \hat{i}_3 \end{aligned} \tag{3.18}$$

Recalling equation (3.7) the first partial derivatives of V (λ, φ, r) in the geocentric system is given by:

$$\begin{bmatrix} V_x \\ V_y \\ V_z \end{bmatrix} = \left[\frac{\partial (\lambda, \varphi, r)}{\partial (x, y, z)} \right]^T \begin{bmatrix} V_\lambda \\ V_\varphi \\ V_r \end{bmatrix} \tag{3.19}$$

Consider equation (3.16) in view of the fact that the vector triad defining the e_p basis are not all unit vectors. The obtain the correct physical components in the local coordinate system the e_p basis must be normalized to a unit vector basis, $\hat{e}_p$. Thus the normalized vectors are:

$$\hat{e}_1 = \frac{1}{r \cos \varphi} e_1 , \hat{e}_2 = \frac{1}{r} e_2 , \hat{e}_3 = e_3$$

Equation (3.16) rewritten in the normalized basis is then:

$$\nabla V = \frac{1}{r \cos \varphi} V_\lambda \hat{e}_1 + \frac{1}{r} V_\varphi \hat{e}_2 + V_r \hat{e}_3 \tag{3.20}$$

Therefore the first derivatives in the local (η, ξ, ζ) system are:

$$\begin{aligned} V_\eta &= \frac{1}{r \cos \varphi} V_\lambda \\ V_\xi &= \frac{1}{r} V_\varphi \\ V_\zeta &= V_r \end{aligned} \tag{3.21}$$

Substituting (3.21) into (3.19), we get the transformations of the first derivatives or gravitational acceleration components between the geocentric and local coordinate system:

$$\begin{bmatrix} V_x \\ V_y \\ V_z \end{bmatrix} = \left[\frac{\partial(\lambda, \varphi, r)}{\partial(x, y, z)}\right] (r\cos\varphi,\ r,\ 1) \begin{bmatrix} V_\eta \\ V_\xi \\ V_\zeta \end{bmatrix} = \begin{bmatrix} -\sin\lambda & -\sin\varphi\cos\lambda & \cos\varphi\cos\lambda \\ \cos\lambda & -\sin\varphi\sin\lambda & \cos\varphi\sin\lambda \\ 0 & \cos\varphi & \sin\varphi \end{bmatrix} \begin{bmatrix} V_\eta \\ V_\xi \\ V_\zeta \end{bmatrix} \tag{3.22}$$

If we let

$$A = \begin{bmatrix} -\sin\lambda & -\sin\varphi\cos\lambda & \cos\varphi\cos\lambda \\ \cos\lambda & -\sin\varphi\sin\lambda & \cos\varphi\sin\lambda \\ 0 & \cos\varphi & \sin\varphi \end{bmatrix} \tag{3.23}$$

then

$$\begin{bmatrix} V_\eta \\ V_\xi \\ V_\zeta \end{bmatrix} = A^T \begin{bmatrix} V_x \\ V_y \\ V_z \end{bmatrix} \tag{3.24}$$

The next step is to obtain the second partial derivatives of the potential function $V(\lambda, \varphi, r)$. Recall equation (3.15):

$$\bar{\nabla} V = \frac{\partial V}{\partial u^p} e^p \tag{3.15}$$

To form the second derivatives we make use of the dyadic notation where the $\bar{\nabla}$ operator is applied in a more general sense. That is we will use the notation $\bar{\nabla}\bar{\nabla} V$ to distinguish the computation for the Laplacian $\bar{\nabla}^2 V$. In general the operator $\bar{\nabla}$ can be expressed in terms of the contravariant basis e^p and spherical coordinates by:

$$\bar{\nabla} = e^p \frac{\partial}{\partial u^p}$$

Then

$$\begin{aligned} \bar{\nabla}\bar{\nabla} V &= e^p \frac{\partial}{\partial u^p}\left(\frac{\partial V}{\partial u^q} e^q\right) \\ &= e^p\left(\frac{\partial^2 V}{\partial u^p \partial u^q} + \frac{\partial V}{\partial u^q}\frac{\partial e^q}{\partial u^p}\right) \end{aligned} \tag{3.25}$$

Using (3.14) for $\partial e^q / \partial u^p$ (3.25) takes the form:

$$\bar{\nabla}\bar{\nabla} V = \left(\frac{\partial^2 V}{\partial u^p \partial u^q} - \frac{\partial V}{\partial u^s}\left\{ {s \atop pq} \right\}\right) e^p e^q \tag{3.26}$$

where the term inside the parenthesis is the covariant derivative of the acceleration vector. Again the basis vectors must be normalized to give

the proper physical components in the local Cartesian system. Using the normalized basis $\hat{e}_p$ from (3.20) and the Christoffel symbols from (3.11) in equation (3.25) we obtain the dyadic equation (3.27) in the dyad basis, $\hat{e}_p\ \hat{e}_q$:

$$\begin{aligned}
\bar{\bar{\nabla}}\nabla V &= \frac{1}{r^2\cos^2\varphi}(V_{\lambda\lambda} - \sin\varphi\cos\varphi V_{\varphi} + r\cos^2\varphi V_r)\,\hat{e}_1\hat{e}_1 \\
&+ \frac{1}{r^2\cos\varphi}(V_{\lambda\varphi} + \tan\varphi V_{\lambda})\hat{e}_1\hat{e}_2 + \frac{1}{r\cos\varphi}(V_{\lambda r} - \frac{1}{r}V_{\lambda})\hat{e}_1\hat{e}_3 \\
&+ \frac{1}{r^2\cos\varphi}(V_{\lambda\varphi} + \tan\varphi V_{\lambda})\hat{e}_2\hat{e}_1 + \frac{1}{r^2}(V_{\varphi\varphi} + r V_r)\hat{e}_2\hat{e}_2 \\
&+ \frac{1}{r}(V_{\varphi r} - \frac{1}{r}V_{\varphi})\hat{e}_2\hat{e}_3 + \frac{1}{r\cos\varphi}(V_{\lambda r} - \frac{1}{r}V_{\lambda})\hat{e}_3\hat{e}_1 \\
&+ \frac{1}{r}(V_{\varphi r} - \frac{1}{r}V_{\varphi})\hat{e}_3\hat{e}_2 + V_{rr}\,\hat{e}_3\hat{e}_3
\end{aligned} \tag{3.27}$$

Thus the second derivatives of the potential or gravitational gradients in the (η, ξ, ζ) system from (3.27) are:

$$\begin{aligned}
V_{\eta\eta} &= \frac{1}{r^2\cos^2\varphi}V_{\lambda\lambda} - \frac{\tan\varphi}{r^2}V_{\varphi} + \frac{1}{r}V_r \\
V_{\xi\xi} &= \frac{1}{r^2}V_{\varphi\varphi} + \frac{1}{r}V_r \\
V_{\zeta\zeta} &= V_{rr}
\end{aligned} \tag{3.28}$$

(3.28) - continued

$$V_{\xi\eta} = V_{\eta\xi} = \frac{1}{r^2\cos\varphi} V_{\lambda\varphi} + \frac{\sin\varphi}{r^2\cos\varphi} V_{\lambda}$$

$$V_{\zeta\eta} = V_{\eta\zeta} = \frac{1}{r\cos\varphi} V_{\lambda r} - \frac{1}{r^2\cos\varphi} V_{\lambda}$$

$$V_{\zeta\xi} = V_{\xi\zeta} = \frac{1}{r} V_{\varphi r} - \frac{1}{r^2} V_{\varphi}$$

By the law for transformation of tensors and using (3.23)

$$\begin{bmatrix} V_{xx} & V_{xy} & V_{xz} \\ V_{yx} & V_{yy} & V_{yz} \\ V_{zx} & V_{yy} & V_{zz} \end{bmatrix} = A \begin{bmatrix} V_{\eta\eta} & V_{\eta z} & V_{\eta\zeta} \\ V_{\xi\eta} & V_{\xi\xi} & V_{\xi\zeta} \\ V_{\zeta\eta} & V_{\zeta\xi} & V_{\zeta\zeta} \end{bmatrix} A^T \qquad (3.29)$$

By performing the mulitplications indicated on the right-hand side of (3.29) and using the relationships in (3.28) the second partial derivatives of the spherical coordinates with respect to the geocentric coordinates can be determined. The resulting partial derivatives are given in Chapter 5 in a form suitable for computer programming.

3.2 Specialization to the Potential in Spherical Harmonics

From equation (0.1) the spherical harmonic expansion of the potential is:

$$V(\lambda,\varphi,r) = \frac{kM}{r}\left[1 + \sum_{n=2}^{\infty}\sum_{m=0}^{n}\left(\frac{a}{r}\right)^n (C_{nm}\cos m\lambda + S_{nm}\sin m\lambda) P_{nm}(\sin\varphi)\right] \qquad (0.1)$$

Using equation (0.1) and (3.21) one obtains the acceleration vector components in the local system:

$$V_\eta = -\frac{kM}{r^2}\sum_{n=2}^{\infty}\sum_{m=0}^{n}\left(\frac{a}{r}\right)^n (C_{nm}\sin m\lambda - S_{nm}\cos m\lambda)\, P_{nm}^{\eta}(\sin\varphi)$$

$$V_\xi = \frac{kM}{r^2}\sum_{n=2}^{\infty}\sum_{m=0}^{n}\left(\frac{a}{r}\right)^n (C_{nm}\cos m\lambda + S_{nm}\sin m\lambda)\, P_{nm}^{\xi}(\sin\varphi) \qquad (3.30)$$

$$V_\zeta = \frac{kM}{r^2}\left[1 + \sum_{n=2}^{\infty}\sum_{m=0}^{n}\left(\frac{a}{r}\right)^n (C_{nm}\cos m\lambda + S_{nm}\sin m\lambda)\, P_{nm}^{\zeta}(\sin\varphi)\right]$$

where the polynomial terms are:

$$\begin{aligned} P_{nm}^{\eta}(\sin\varphi) &= \frac{m}{\cos\varphi} P_{nm}(\sin\varphi) \\ P_{nm}^{\xi}(\sin\varphi) &= P_{n,m+1}(\sin\varphi) - m\tan\varphi\, P_{nm}(\sin\varphi) \\ P_{nm}^{\zeta}(\sin\varphi) &= (n+1) P_{nm}(\sin\varphi) \end{aligned} \qquad (3.31)$$

Similarly, using equation (2.28) we obtain the second partial derivatives

$$V_{\eta\eta} = \frac{kM}{r^3}\left[-1 + \sum_{n=2}^{\infty}\sum_{m=0}^{n}\left(\frac{a}{r}\right)^n (C_{nm}\cos m\lambda + S_{nm}\sin m\lambda)\, P_{nm}^{\eta\eta}(\sin\varphi)\right]$$

$$V_{\xi\xi} = \frac{kM}{r^3}\left[-1 + \sum_{n=2}^{\infty}\sum_{m=0}^{n}\left(\frac{a}{r}\right)^n (C_{nm}\cos m\lambda + S_{nm}\sin m\lambda)\, P_{nm}^{\xi\xi}(\sin\varphi)\right] \qquad (3.32)$$

$$V_{\zeta\zeta} = \frac{2kM}{r^3}\left[1 + \frac{1}{2}\sum_{n=2}^{\infty}\sum_{m=0}^{n}\left(\frac{a}{r}\right)^n (C_{nm}\cos m\lambda + S_{nm}\sin m\lambda)\, P_{nm}^{\zeta\zeta}(\sin\varphi)\right.$$

(3.32) - continued

$$V_{\xi\eta} = \frac{kM}{r^3}\sum_{n=2}^{\infty}\sum_{m=0}^{n}\left(\frac{a}{r}\right)^n (C_{nm}\sin m\lambda - S_{nm}\cos m\lambda)\, P^{\xi\eta}(\sin\varphi)$$

$$V_{\eta\zeta} = \frac{kM}{r^3}\sum_{n=2}^{\infty}\sum_{m=0}^{n}\left(\frac{a}{r}\right)^n (C_{nm}\sin m\lambda - S_{nm}\cos m\lambda)\, P^{\eta\zeta}_{nm}(\sin\varphi)$$

$$V_{\xi\zeta} = \frac{kM}{r^3}\sum_{m=2}^{\infty}\sum_{m=0}^{n}\left(\frac{a}{r}\right)^n (C_{nm}\cos m\lambda + S_{nm}\sin m\lambda)\, P^{\xi\zeta}_{nm}(\sin\varphi)$$

The polynomial terms in (3.31) are:

$$P^{\eta\eta}_{nm}(\sin\varphi) = \left[\frac{m\sin^2\varphi - m^2}{\cos^2\varphi} - (n+1)\right]P_{nm}(\sin\varphi) - \tan\varphi\, P_{n,m+1}(\sin\varphi)$$

$$P^{\xi\xi}_{nm}(\sin\varphi) = \left[\frac{m^2 - m\sin^2\varphi}{\cos^2\varphi} - (n+1)^2\right]P_{nm}(\sin\varphi) + \tan\varphi\, P_{n,m+1}(\sin\varphi)$$

$$P^{\zeta\zeta}_{nm}(\sin\varphi) = (n+1)(n+2)\,P_{nm}(\sin\varphi)$$

$$P^{\xi\eta}_{nm}(\sin\varphi) = \frac{-m(m-1)\sin\varphi}{\cos^2\varphi}P_{nm}(\sin\varphi) + \frac{m}{\cos\varphi}P_{n,m+1}(\sin\varphi) \qquad (3.33)$$

$$P^{\eta\zeta}_{nm}(\sin\varphi) = -\frac{m(n+2)}{\cos\varphi}P_{nm}(\sin\varphi)$$

$$P^{\xi\zeta}_{nm}(\sin\varphi) = m(n+2)\tan\varphi\, P_{nm}(\sin\varphi) - (n+2)\,P_{n,m+1}(\sin\varphi)$$

In the next chapter the polynomial expressions in (3.33) will be discussed in connection with the estimation of the harmonic degree root mean square gravitational gradients. In Chapter 5, computationally more practical expressions for the gravitational gradients will be presented.

4. GRAVITY GRADIENTS AT ALTITUDE AND GRADIOMETER RESOLUTION

Concurrent with on-going development of satellite gradiometers there has been keen interest in studying the nature of gravity gradients at orbital altitudes. Such studies have a direct bearing on sensitivity and error budget parameters governing the development of an operational satellite gradiometer system. Various investigators have taken different approaches in evaluating the gradient contribution from the short wavelength, high order terms of the external gravitational field.

Chovitz, et al. (1972) performed an analysis of gravity gradients along simulated 300 kilometer altitude orbit trajectories over selected regions of dense $1^\circ \times 1^\circ$ anomalies. Rather than using the anomalies directly, spherical harmonic coefficients through degree and order 75 were computed from a set of several thousand gravity anomalies in 1° blocks covering more than 30 per cent of the earth and 5° blocks over the remainder.

The results of Chovitz's investigation indicate a gradiometer sensitivity of better than 0.01E is necessary to resolve the harmonics of a single degree in the range of degrees 60 to 70. In order to resolve the total band of harmonics between degrees 60 to 70, a required sensitivity of 0.02 E was indicated.

In another study by Sandson and Strange (1972) the anomalous vertical gradients were evaluated at an altitude of 300 kilometers above the North

Atlantic Ocean. Using a (12, 12) spherop reference field and 1° x 1° mean anomalies referred to the spherop, the gravity disturbances and the anomalous vertical gradients at altitude were computed. The conclusions of the investigation indicated that gradiometer information would require accuracies better than 0.1E to recover 1° or 2° surface block values. The maximum amplitude of the anomalous gradient was found to be 0.5E. Over the study area, the rate of change of gradient was on the order of 0.1E per degree of ground trace. Of particular interest in that study were the short wavelength variations detected by the gradients but smoothed over by the gravity disturbances. This latter effect can also be seen in Figure 11, Chapter 7 of this report.

Various investigators have made quantitative extimates of the gravity gradient spectrum based on Kaula's "rule of thumb", (Kaula, 1966b):

$$\bar{C}_{nm} \approx \bar{S}_{nm} \approx 10^{-5}/n^2 \tag{4.1}$$

where n is the spherical harmonic degree. Equation (4.1) expresses the power spectrum of the normalized spherical harmonic coefficients. From this power spectrum, one obtains the contribution of the (2n + 1) terms to each degree by:

$$\left[\sum_{m=0}^{n} (\bar{C}_{nm}^2 + \bar{S}_{nm}^2)\right]^{\frac{1}{2}} = (2n+1)^{\frac{1}{2}}\, 10^{-5}/n^2 \tag{4.2}$$

This latter form is also attributed to Kaula. Using this model the spherical harmonic expansion of various spectral responses of the gravity field may be

estimated. In the case of gravity gradients such estimates have been made by Forward (1971a), Kaula (1971a, 1971c), Glaser and Sherry (1972), and the JPL Gradiometer Study (Gardner, et al., 1972).

Forward has estimated the contribution of all harmonics of degree 75 to the radial component of the gravity gradient tensor to be about 0.01E at 250 kilometers, which is the threshold sensitivity proposed for the rotating gradiometer. However, from equation (1.6) we see that the amplitude of the rotating gradiometer signal contains more than just the radial gradient. Essentially equivalent results were obtained by the JPL Study.

Kaula in a similar analysis estimated the contribution at degree 75 to be roughly half that estimated by Forward. An aspect of Kaula's analysis which surely disturbed some proponents of satellite gradiometry was his estimate that an accuracy of 0.03 E.U. at 260 kilometers would only yield resolution of the gravity field to about harmonic degree 23. This corresponds to a half-wavelength of 870 kilometers. It should be noted that in arriving at his estimates of degree contribution and resolution, Kaula stated that he conservatively assumed a 10:1 ratio for the error contribution of any one harmonic coefficient to the total error. Kaula compares this resolution of a gradiometer to equivalent resolution for satellite-to-satellite tracking accurate to 0.5 mm/sec and satellite altimetry accurate to 1.0 m. In addition, he states that 0.05 mm/sec satellite-to-satellite tracking and 0.015E gradiometry have a common resolution of 400 kilometers at 200 kilometers altitude. Certain aspects of Kaula's analysis are not clear. In particular,

the meaning of the 10:1 error ratio and his method of computing the gravity gradient spectrum are obscure. In any case, Kaula's estimates markedly differ from results obtained by other investigators.

In the Glaser and Sherry paper, root mean square (RMS) amplitudes remaining by harmonic degree at various altitudes were estimated from a spherical harmonic expansion of the linearized rotating gradiometer signal. Their results indicate that a rotating gradiometer signal at 0.01E would have a resolution of about 300 kilometers (n = 120) at 300 kilometers altitude. They compare this to 0.05 mm/sec satellite-to-satellite tracking estimated to have resolution to degree n = 60 at the same altitude. However, certain assumptions were made in deriving the expressions for the RMS gradiometer signal which are questionable. We will discuss this in the next section and propose an alternative approach.

In addition to the analytical investigations, laboratory experiments were carried out by Hughes Research Laboratories using a prototype gradiometer (Bell, et al., 1970; Forward, 1971a). The noise level of the sensor was 1.0E (1 σ at 10 seconds integration time). Using this sensor real time gradient signals were observed in an experiment which simulated the magnitude and time variation of gravity gradient signals which would be expected in a lunar orbit. Forward concluded from the laboratory results that the limiting resolution is the altitude at which the gradiometer is flown. For example, a gradiometer at 300 kilometers can resolve a wavelength of not less that 300 kilometers at the earth's surface. In other words the maximum

degree resolution of a gradiometer can be expressed empirically by:

$$n \approx \frac{2\pi R}{h} \tag{4.3}$$

where: R = radius of the earth

h = altitude

n = harmonic degree to the nearest integer.

Thus at 300 kilometers altitude, the maximum possible degree resolution is about 120, which agrees with the analytical results by Glaser and Sherry.

Other factors to be considered in assessing resolution are the effect of gradiometer sensitivity and integration time on signal response. Savet (1967) discussed the trade-offs between sensitivity and integration time for various candidate gradiometers. In general, sensitivity may be improved by lengthening integration time. It should be obvious that as integration time increases, regardless of sensitivity, the signal response will be smoothed out over a longer path. As a result, the shorter wavelengths will be lost in the measurements. Considering the various factors that influence resolution, A. B. Whitehead in (Loomis, et al., 1972), concluded that a satellite gradiometer with a sensitivity of 0.01E can provide useful measurements over a wavelength region between 400 to 1500 kilometers. Whitehead used a planar approximation and assumed a series of sine waves to represent the gravitational field, which is a solution of the Laplace equation, $\nabla^2 V = 0$, in Cartesian coordinates.

4.1 Estimation of Gravity Gradients at Altitude

Estimation of the spectrum of anomalous gravimetric quantities relies on the assumption that such quantities are stochastic processes over a surface (Meissl, 1971). This simply means that we may apply expectation operators to the signals of the anomalous gravity field. In the usual statistical sense, the expectation of a random variable X is given by:

$$E(X) = \int_{-\infty}^{\infty} Xp(X)dX \tag{4.4}$$

where p(X) is a probability density function which has the characterisitics:

$$\int_{-\infty}^{\infty} p(X)dX = 1 \tag{4.5}$$

Unfortunately, the probability structure of gravimetric quantities is essentially unknown. To overcome this difficulty, the probability structure is assumed to be adequately represented by areal weights. We see that the integral

$$\frac{1}{\sigma} \iint_{\sigma} d\sigma = 1 \tag{4.6}$$

where σ is the total surface area and $d\sigma$ a differential element of surface area. Thus, if X(P) represents some quantity such as gravity anomalies or

gravity gradients then the expected value is given by:

$$E[X(P)] = \bar{X}(P) = \frac{1}{\sigma}\int_{\sigma}\int X(P)d\sigma \tag{4.7}$$

where $\bar{X}(P)$ is the mean value of the signal over the surface area σ. If the quantities X(P) are a true smoothed representation of the actual gravity field and contain no term of degree zero in the harmonic expansion of the quantity, the integral over the entire earth yields:

$$\bar{X}(P) = 0$$

Clearly $\bar{X}(P)$ provides no information with which to characterize the magnitude of the quantities X(P). Fortunately, we may consider the mean square of X(P) by applying the variance operator, thus

$$\text{var}\,[X(P)] = E[X^2(P)] - E[X(P)]^2,$$

but since $E[X(P)] = \bar{X}(P) = 0$,

$$\text{var}\,[X(P)] = E[X^2(P)] = \frac{1}{\sigma}\int_{\sigma}\int X^2(P)d\sigma. \tag{4.8}$$

Consequently the root mean square value of X(P) is:

$$\mathrm{RMS}[X(P)] = \left[\frac{1}{\sigma}\int_{\sigma}\int X^2(P)\,d\sigma\right]^{\frac{1}{2}} \tag{4.9}$$

In order to specialize equation (4.9) to obtain estimates one might consider the Cartesian derivatives of the Legendre functions in equation (3.33). This is essentially the procedure used by Glaser and Sherry (1972). In their development of RMS estimates for the **linearized** rotating gradiometer they neglected terms in equation (3.33) containing $P_{n\ m+1}(\sin\varphi)$ and the harmonic order, m. If this assumption were to be applied to all the Cartesian derivatives of the Legendre terms, only the diagonal components of the gravity gradient tensor would have non-zero RMS values. The Cartesian derivatives of the Legendre terms corresponding to the diagonal tensor component would be given approximately by:

$$P_{nm}^{\eta\eta}(\cos\varphi) \approx -(n+1)\,P_{nm}(\sin\varphi)$$

$$P_{nm}^{\xi\xi}(\sin\varphi) \approx -(n+1)^2 P_{nm}(\sin\varphi) \tag{4.10}$$

$$P_{nm}^{\zeta\zeta}(\sin\varphi) \approx (n+1)\,(n+2)\,P_{nm}(\sin\varphi)$$

Since the Legendre terms are harmonic, they must satisfy the condition:

$$\overset{\eta\eta}{P}_{n\,m}(\sin\varphi) + \overset{\xi\xi}{P}_{n\,m}(\sin\varphi) + \overset{\zeta\zeta}{P}_{n\,m}(\sin\varphi) = 0 \qquad (4.11)$$

Obviously this is true for the terms in both (3.33) and (4.10). What then does this imply? A probable explanation, one which would be tedious to demonstrate analytically, is that the terms in (4.10) are simply the eigenvalues of the Legendre terms in the gradient tensor since the trace of the tensor matrix has been preserved even though certain terms have been neglected. Which means that the η - axis and the ξ - axis have been rotated about the ζ -axis, thus changing the orientation of the coordinate system such that the horizontal axes no longer coincide with the direction of the parametric lines (parallels and meridians) on the (λ, φ, r) surface. Marussi (1949), Mueller (1960), and Hotine (1957, 1969) have shown that the gravity gradient tensor components are related to the curvature and torsion of the equipotential surface. Savet (1967) demonstrated that, if the horizontal coordinate axes are taken along the directions of maximum and minimum curvature (the principal directions) of the equipotential surface at a point, the off-diagonal components of the gradient tensor are zero. However, the orientation of the principal directions on a surface as complex as an equipotential surface in near earth space may vary considerably from point to point. Consequently, the validity of global integration of the first two polynomial expressions in equation (4.10) would seem to be suspect.

Clearly the integration of the terms in equation (3.33) would be extremely complex.. As an alternative method for the development of

expressions for RMS gradients consider the second cartesian derivatives of the potential derived by Hotine (1969, pp. 179-183).

Hotine's derivation is quite lengthy; hence, will not be repeated here. In general, his development of the Cartesian derivatives is based upon a power series expansion of the associated Legendre functions given by Hobson (1965), which is conformally mapped into isometric space using the theory of complex variable. By taking the pole of the harmonics along the local vertical, the resulting expression for the second derivatives in terms of fully normalized harmonics is:

$$\frac{\partial^2 V}{\partial X_i \partial X_j} = \frac{kM}{r^3} \sum_{n=0}^{\infty} \sum_{m=0}^{n} \left(\frac{a}{r}\right)^n (\bar{\bar{C}}_{nm} \cos m\lambda + \bar{\bar{S}}_{nm} \cos m\lambda) \bar{P}_{nm}(\sin\varphi) \qquad (4.11)$$

where $\bar{\bar{C}}_{nm}$ and $\bar{\bar{S}}_{nm}$ are modified coefficients which are functions of the fully normalized coefficients and $X_i = (\eta, \xi, \zeta)$. The modified coefficients for the components of the gravity gradient tensor are:

$$V_{\eta\eta}: \quad \bar{\bar{C}}_{nm} = 1/4\, \bar{C}_{n,m-2} - 1/2\,(n-m+1)(n-m+2)\, \bar{C}_{n,m} + 1/4(n-m-1)(n-m)(n-m+1)(n-m+2)\, C_{n,m+2}$$

$$\bar{\bar{S}}_{nm} = 1/4\, \bar{S}_{n,m-2} - 1/2(n-m+1)(n-m+2)\, \bar{S}_{n,m} + 1/4\,(n-m-1)(n-m)(n-m+1)(n-m+2) S_{n,m+2} \qquad (4.12)$$

$$V_{\xi\xi}: \overline{\overline{C}}_{n\,m} = -1/4\,\overline{C}_{n,\,m-2} - 1/2\,(n-m+1)(n-m+2)\overline{C}_{n,\,m}$$

$$-1/4(n-m+1)(n-m)(n-m+1)(n-m+2)\overline{\overline{C}}_{n,\,m+2}$$

$$\overline{\overline{S}}_{n\,m} = -1/4\,\overline{S}_{n,\,m-2} - 1/2(n-m+1)(n-m+2)\overline{C}_{n,\,m} \qquad (4.13)$$

$$-1/4\,(n-m-1)(n-m)(n-m+1)(n-m+2)S_{n,\,m+2}$$

$$V_{\zeta\zeta}: \overline{\overline{\overline{C}}}_{n\,m} = (n-m+1)(n-m+2)\overline{C}_{n,\,m}$$

$$\qquad (4.14)$$

$$\overline{\overline{\overline{S}}}_{n\,m} = (n-m+1)(n-m+2)\overline{S}_{n,\,m}$$

$$V_{\eta\,\xi}: \overline{\overline{C}}_{n\,m} = -1/4\,\overline{S}_{n,\,m-2} - 1/4(n-m-1)(n-m)(n-m+1)\overline{S}_{n,\,m+2} \qquad (4.15)$$

$$\overline{\overline{S}}_{n\,m} = 1/4\,\overline{C}_{n,\,m-2} -1/4(n-m+1)(n)(n-m+1)(n-m+2)\overline{C}_{n,\,m+2}$$

$$V_{\xi\,\zeta}: \overline{\overline{\overline{C}}}_{n\,m} = -1/2(n-m+2)\overline{S}_{n,\,m-1} - 1/2(n-m)(n-m+1)(n-m+2)\overline{S}_{n,\,m+1} \qquad (4.16)$$

$$\overline{\overline{\overline{S}}}_{n\,m} = 1/2\,(n-m+2)\overline{C}_{n,\,m-1} + 1/2(n-m)(n-m+1)(n-m+2)\overline{C}_{n,\,m+1}$$

$$V_{\eta\zeta} : \bar{\bar{C}}_{nm} = 1/2\,(n-m+2)\,\bar{C}_{n,m-1} - 1/2\,(n-m)\,(n-m+1)\,(n-m+2)\,\bar{C}_{n-2,m+1} \tag{4.17}$$

$$\bar{\bar{S}}_{nm} = 1/2(n-m+2)\,\bar{S}_{n,m-1} - 1/2(n-m)(n-m+1)(n-m+2)\,\bar{S}_{n,m-1}$$

The local coordinate system of the derivatives in equation (4.11) is in a astronomic basis which is nonintegrable (Grafarend, 1972b). Hence, we see that the $V_{\zeta\zeta}$ component is now dependent upon the harmonic order m (see equation 4.14). However, if we neglect m, the factor terms on the right hand side of (4.14) reduce to:

$$(n+1) \quad (n+2)$$

which is exactly the factors for the second radial derivative of the potential referred to a spherical orthogonal coordinate system. We would like to eliminate the order m from all the factors in equations (4.12) through (4.17) so that we can perform the integration of the gravity gradients implied by equation (4.9).

The usual practice in estimation theory as applied to Physical Geodesy is to assume that stochastic processes of the gravity field are isotropic. This means that the covariance functions for gravimetric quantities are independent of direction and hence independent of the harmonic order m. Although the assumption of isotropy may not be a physical reality, it reduces the problem of estimation to a manageable level which appears to yield satisfactory results. Using the assumption of isotropy the coefficients in the harmonic expansion

may be replaced by a power spectrum:

$$\psi_n = \sigma_n / \sqrt{2n+1} \tag{4.18}$$

where σ_n is obtained from the square root of the degree variance which is defined by Kaula (1966b, 1967) as:

$$\sigma_n^2 = \sum_{m=0}^{n} (\bar{C}_{nm}^2 + \bar{S}_{nm}^2). \tag{4.19}$$

Thus the power spectrum implied by Kaula's "rule of thumb", equation (4.1), may be used . Considering the altitude attenuation of the higher degree terms, say n>1000, the error in computing RMS gradients due to truncation at some finite value of n will be relatively insignificant.

Specializing the assumptions discussed in this section to equations (4.9), and (4.11), and using the orthogonality properties of the spherical harmonics, we obtain the following expressions for the RMS gravity gradients for n>2:

$$RMS_{22} = RMS_{\eta\eta} = \frac{kM}{r^3}\sqrt{\sum_{n=3}^{\infty}\left(\frac{a}{r}\right)^{2n}\left[\tfrac{1}{2} - \tfrac{1}{2}(n+1)(n+2)\right]^2(2n+1)10^{-10}/n^4} \tag{4.20}$$

$$RMS_{11} = RMS_{\xi\xi} = \frac{kM}{r^3}\sqrt{\sum_{n=3}^{\infty}\left(\frac{a}{r}\right)^{2n}\left[-\tfrac{1}{2} - \tfrac{1}{2}(n+1)(n+2)\right]^2(2n+1)10^{-10}/n^4} \tag{4.21}$$

$$RMS_{33} = RMS_{\zeta\zeta} = \frac{kM}{r^3}\sqrt{\sum_{n=3}^{\infty}\left(\frac{a}{r}\right)^{2n}(n+1)^2(n+2)^2(2n+1)10^{-10}/n^4} \qquad (4.22)$$

$$RMS_{12} = RMS_{\eta\xi} = \frac{kM}{r^3}\sqrt{\sum_{n=3}^{\infty}\left(\frac{a}{r}\right)^{2n}10^{-10}/4n^4} \qquad (4.23)$$

$$\begin{Bmatrix} RMS_{13} \\ \\ RMS_{23} \end{Bmatrix} = \begin{Bmatrix} RMS_{\eta\zeta} \\ \\ RMS_{\xi\zeta} \end{Bmatrix} = \frac{kM}{r^3}\sqrt{\sum_{n=3}^{\infty}\left(\frac{a}{r}\right)^{2n}(n+1)^2\ 10^{-10}/n^4} \qquad (4.24)$$

In a similar fashion the RMS amplitude of a rotating gradiometer may be obtained. Using the previous results of this section and equation (1.6) we get:

$$RMS_{ampl} = \frac{kM}{r^3}\sqrt{\sum_{n=3}^{\infty}\left(\frac{a}{r}\right)^{2n}\left[(1/2 + 3/2\,(n+1)(n+2))^2 + 4\,(n+1)^2\right](2n+1)10^{-10}/n^4} \qquad (4.25)$$

Glaser and Sherry (1972) and Glaser (1972) suggest a meaningful way to plot RMS results derived from equations of the type given above. What is done is to plot the contribution of each degree to the RMS value and the sum

of the higher degree terms above and including the harmonic degree n as a function of n. In Figure 2, the RMS values of the gravity tensor components summed to n = 1000 are plotted in this manner. Similarly the RMS signal amplitudes of a rotating gradiometer are plotted in Figure 3. In both cases the altitude is 300 kilometers and the values of the scale factor, kM, and the radius of the Earth, a, are the GRS 67 values given in section 2.1.

Care must be taken not to over interpret the results in Figures 2 and 3. A reasonable interpretation would be to view the plot of RMS value remaining by harmonic degree as a measure of the minimum gradiometer sensitivity required to resolve the harmonics up to and including degree n. On the other hand the RMS value by degree gives a measure of the upper limit of degree resolution, which is the degree where the curve becomes approximately asymptotic. For example, the curves in Figure 2 for the radial (3,3) tensor component indicate a sensitivity of about 0.01E required to resolve harmonic terms to degree 90, while the upper limit of resolution is about degree 120. The latter limit of resolution thus tends to confirm equation (4.3), which is based upon Forward's laboratory results (see page 41). Using the same reasoning for the remaining tensor component curves in Figure 2, we can see that the hard-mounted gradiometer system would require sensors of considerably better sensitivity to obtain resolution to degree 90. At 0.01E, sensitivity a gradiometer measuring only the horizontal components (1,1) and (2,2) have a possible resolution of about degree 75. The other components measurable with a hard-mounted system appear to give very little information

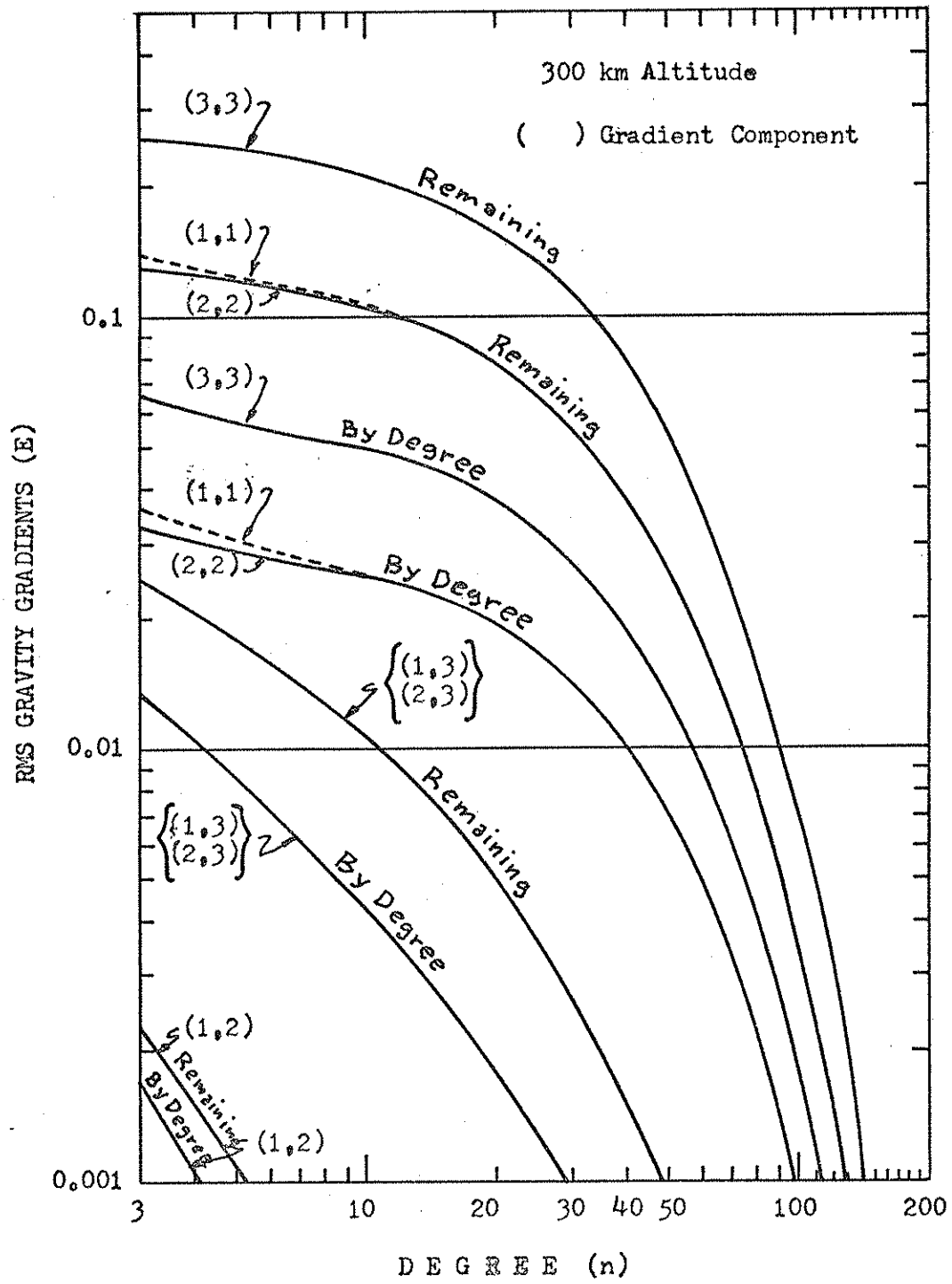

Figure 2. RMS Gravity Gradients

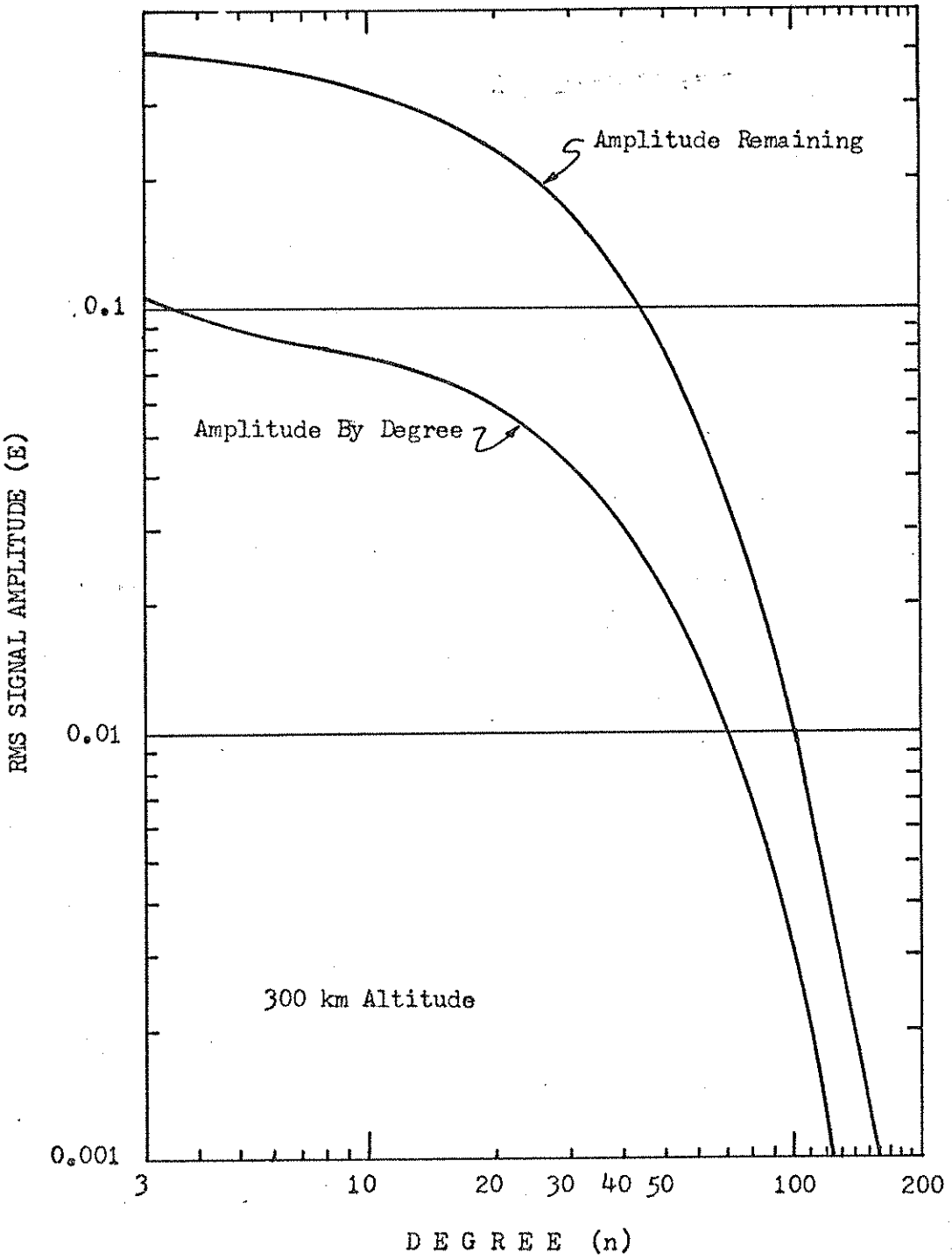

Figure 3. RMS Signal Amplitudes (Rotating Gradiometer)

in the range of harmonics necessary to make the system competitive with other satellite-borne hybrid gravimetric systems.

To further illustrate the difficulty that may arise with the hard-mounted gradiometer, the RMS gravity gradient tensor components for various harmonic degree summations and altitudes are given in Table 1. Assuming a threshold sensitivity of 0.01E, it is clear that the off-diagonal or cross-gradients will provide little or no information for the short wavelength components of the gravity field. This is true even at altitudes impractically too low for a reasonable orbital life expectancy of the satellite. The diagonal tensor components with the exception of the radial (3,3) component are marginal at 300 kilometers for degree 75. Other computed results, not shown here, indicate that useful information to degree 90 from the (1,1) and (2,2) components would require a maximum altitude in the neighborhood of 250 kilometers.

Table 2 shows the same information given in Table 1, but for the signal amplitude of the rotating gradiometer. These results along with the data plotted in Figure 3 indicate that we have no difficulty in resolving wavelength corresponding to harmonic degree 90 at 0.01E sensitivity. The corresponding surface block size that we can expect to resolve at 300 kilometers is given by $180^\circ/n$, which yields $2^\circ \times 2^\circ$ squares. Numerical results of the simulations discussed in Chapter 7 of this report tend to confirm this upper limit of resolution.

Table 1

RMS Gravity Gradients at Altitude

Altitude (km)	Gravity Gradients (E)					
400		n>2			n>14	
	0.1016	0.0021	0.0217	0.0590	0.0001	0.0050
		0.0988	0.0217		0.0588	0.0050
			0.2004			0.1177
		n≥75			n≥90	
	0.0025	0.0000	0.0000	0.0011	0.0000	0.0000
		0.0025	0.0000		0.0011	0.0000
			0.0050			0.0022
300		n>2			n>14	
	0.1332	0.0023	0.0250	0.0917	0.0002	0.0072
		0.1304	0.0250		0.0914	0.0072
			0.2636			0.1831
		n≥75			n≥90	
	0.0094	0.0000	0.0002	0.0053	0.0000	0.0001
		0.0094	0.0002		0.0053	0.0001
			0.0188			0.0106
200		n>2			n>14	
	0.1938	0.0025	0.0292	0.1569	0.0002	0.0107
		0.1912	0.0292		0.1565	0.0107
			0.3849			0.3134
		n≥75			n≥90	
	0.0394	0.0000	0.0008	0.0259	0.0000	0.0005
		0.0394	0.0008		0.0259	0.0005
			0.0768			0.0518
100		n>2			n>14	
	0.3693	0.0028	0.0356	0.3438	0.0004	0.0172
		0.3673	0.0356		0.3433	0.0172
			0.7366			0.6871
		n≥75			n≥90	
	0.1942	0.0000	0.0037	0.1654	0.0000	0.0027
		0.1941	0.0037		0.1654	0.0027
			0.3883			0.3308

Table 2

RMS Signal Amplitudes at Altitude (Rotating Gradiometer)

	100 km.	200 km.	300 km.	400 km.
	(RMS amplitudes in Eotvos Units)			
$n > 2$	1.1083	0.5816	0.3999	0.3050
$n > 14$	1.0315	0.4708	0.2752	0.1770
$n \geq 75$	0.5825	0.0778	0.0281	0.0075
$n \geq 90$	0.4963	0.1152	0.0152	0.0033

Table 3

Maximum Degree Resolution of Gravity Gradients At Altitude for

Measuring Sensitivity of 0.01E

Gradient Term	100 km	200 km	300 km	400 km
(1, 1)	301	126	74	50
(1, 2)	---	---	---	---
(1, 3)	32	16	10	8
(2, 2)	301	126	74	50
(2, 3)	32	16	10	8
(3, 3)	350	151	91	63
Ampl.	378	164	101	70

Table 3 shows the maximum degree resolution at 0.01E sensitivity for each component of the gravity gradient tensor and the rotating gradiometer signal amplitude. This further demonstrates the apparent lack of significant information in the cross-gradient terms.

4.2 Altitude Attenuation of Gravity Gradients

As is known the second derivatives of the potential are altitude attenuated by a factor $(a/r)^{n+3}$. Figure 4 graphically illustrates altitude attenuation of the anomalous gravity gradient tensor components. The values plotted were computed using the superimposed point mass set described in Tables 17 and 18 of Needham (1970). For convenience those tables are reproduced in Appendix A. These point mass sets were formed by least squares solutions using as observed data gravity anomalies residual to the (14,14) spherop described in Chapter 2. The local (1,2,3) coordinates to which the anomalous gradients are referred are defined as follows: The 3-axis is taken positive outward along the normal to the GRS 67 ellipsoid (IAG, 1967), 1-axis points North, 2-axis points West. The footpoint of the normal is located in the central United States at $\varphi = 37^\circ$, $\lambda = 260.5^\circ$. Typical values from which the plot was drawn are given in Table 4, along with the gradients of the reference field and the total gradients. Although, it is difficult to draw specific inferences from such localized values, certain aspects of the altitude variation of the gravity gradients do stand out. It is evident that the anomalous part of the gradients are considerably less sensitive to altitude attenuation than the gradients arising from the (14,14) field. Simple calculations using Table 4

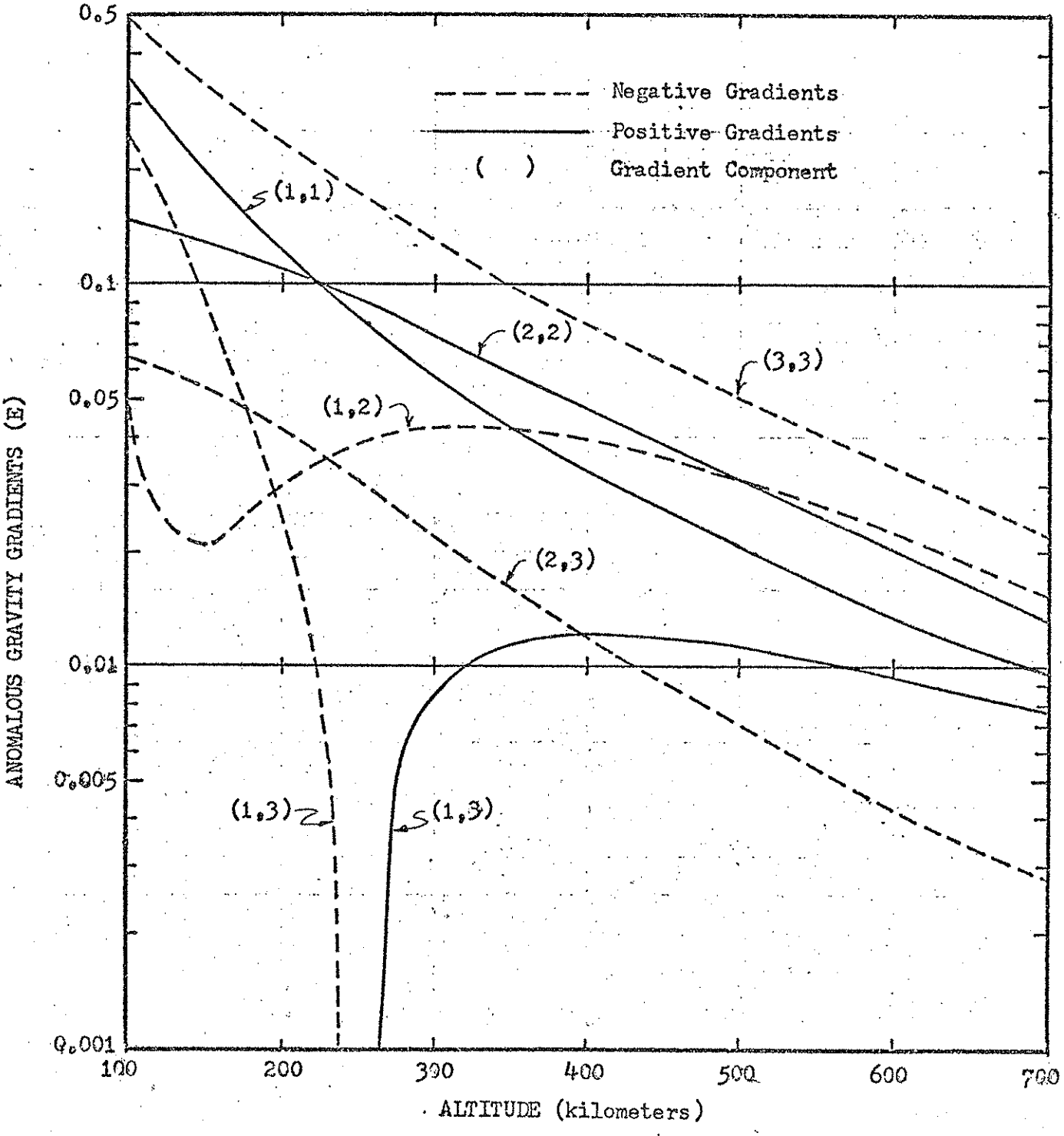

Figure 4. Variation of Anomalous Gravity Gradients With Altitude

Table 4

Gravity Gradients at Altitude
$\varphi = 37^\circ$, $\lambda = 260.5^\circ$

Altitude (km)	(14,14)	Field Gradient (E)		Anomalous Gradients (E)			Total Gradients (E)		
250	-1372.5241	-0.0800	-20.7301	0.0839	-0.0388	-0.0001	-1372.4402	-0.1188	-20.7302
		-1375.3402	0.0716		0.0901	-0.0303		-1375.2502	0.0413
			2747.8644			-0.1740			2747.6904
275	-1357.1031	-0.0759	-20.3890	0.0701	-0.0413	-0.0053	-1357.0330	-0.1172	-20.3837
		-1359.8648	0.0669		0.0816	-0.0259		-1359.7832	0.0410
			2716.9679			-0.1517			2716.8163
300	-1341.9122	-0.0720	-20.0550	0.0593	-0.0425	0.0086	-1341.8529	-0.1145	-20.0464
		-1344.6206	0.0626		0.0737	-0.0222		-1344.5469	0.0403
			2686.5328			-0.1330			2686.3997
325	-1326.9469	-0.0684	-19.7278	0.0507	-0.0427	0.0105	-1326.8962	-0.1111	-19.7173
		-1329.6033	0.0585		0.0665	-0.0191		-1329.5368	0.0394
			2656.5502			-0.1172			2656.4330

indicate that the rate of change of total gradients in the 275 to 300 kilometer altitude region, is on the order of 10^{-3} E/meter. Similarly for the anomalous gradients we find 10^{-7} E/meter. The variation of the total gradient is significant as it implies a tolerance of about 10 meters in determining the radial position of the satellite carrying the gradiometer for 0.01E accuracy in measuring the gradients. This was confirmed by more detailed computations where the altitude was varied ± 20 meters about a 300 kilometer altitude in one meter steps. The maximum variation in the total gradients over this range was about 0.03E for computation points varied up to ± 15 minutes in latitude and longitude about $\varphi = 37^{\circ}$, $\lambda = 260.5^{\circ}$ over the point mass model described on page 57. Additionally, these computations indicated that cross-track and along-track variations of position of about 100 meters have a negligible effect on the total gradients. These results clearly indicate that orbit determination should not be a critical factor in satellite gradiometry.

5. SIMULATION OF SATELLITE GRADIOMETER DATA

This chapter describes the algorithm for the generation of simulated satellite gradiometer observations. The simulations are developed for two distinct gradiometer and satellite configurations.

(1) A strap-down or hard-mounted gradiometer in a satellite using gradient torque stabilization and active attitude control.

(2) A rotating gradiometer in a cylindrical satellite using spin stabilization.

5.1 Generation of Satellite Orbits

In order to be consistent with proposed gradiometer mission profiles, selected orbital passes over the model region were generated in polar, near circular orbits. The orbital parameters were generated using the Rapp (14,14) geopotential model (Appendix B) in a modified version of the Cowell orbit generation program (Cigarski, et al., 1967). This program uses an eighth order Runge-Kutta starting integration followed by a variable option step and order Cowell predictor-corrector and optional force functions (drag, luni-solar, solar radiation). For this study an eleventh order integration with a fixed time step size was used. The force model used

included only the earth's geopotential effects.

Pertinent data generated for subsequent gradient computations and analysis included:

(1) The pass and observation point number and time from initial epoch

(2) The Greenwich Apparent Sidereal time

(3) The satellite state vector

$$\bar{r}_{st} = \begin{bmatrix} x \\ y \\ z \\ \dot{x} \\ \dot{y} \\ \dot{z} \end{bmatrix} = \left[\bar{r} , \dot{\bar{r}} \right]^T$$

(4) The satellite subpoint and altitude.

5.2 Computation of Gradients in the Inertial Coordinate System

As a preliminary to computing the simulated gradiometer observations, the first and second derivatives of the potential were computed with respect to the inertial coordinate system. This facilitated transformation of the gradients into the gradiometer fixed coordinate axes.

From equation (1.3) the following partial derivatives are required:

$$V_{xx}, V_{xy}, V_{xz}, V_{yy}, V_{yz}, V_{zz}.$$

In addition, to define the local vertical at the satellite the partial derivatives

$$V_x, V_y, V_z$$

are also required. Since the potential is divided into a reference potential

defined by the (14,14) spherop and an anomalous potential due to the residual gravity anomalies or point masses, the total derivatives have the form:

$$V_{xx} = U_{xx} + T_{xx}$$

The algorithm for computing these derivatives is based upon the chain rule method derived by Gulick (1970). With this approach the derivatives are first taken with respect to the spherical coordinates (λ, φ, r). The spherical derivatives are then transformed to the inertial Cartesian system as follows:

$$V_x = \frac{\partial V}{\partial r}\frac{\partial r}{\partial x} + \frac{\partial V}{\partial \varphi}\frac{\partial \varphi}{\partial x} + \frac{\partial V}{\partial \lambda}\frac{\partial \lambda}{\partial x} \tag{5.1}$$

and

$$\begin{aligned} V_{xx} = {} & \frac{\partial V}{\partial r}\frac{\partial^2 r}{\partial x^2} + \frac{\partial r}{\partial x}\left[\frac{\partial^2 V}{\partial r^2}\frac{\partial r}{\partial x} + \frac{\partial^2 V}{\partial r \partial \varphi}\frac{\partial \varphi}{\partial x} + \frac{\partial^2 V}{\partial r \partial \lambda}\frac{\partial \lambda}{\partial x}\right] \\ & + \frac{\partial V}{\partial \varphi}\frac{\partial^2 \varphi}{\partial x^2} + \frac{\partial \varphi}{\partial x}\left[\frac{\partial^2 V}{\partial r \partial \varphi}\frac{\partial r}{\partial x} + \frac{\partial^2 V}{\partial \varphi^2}\frac{\partial \varphi}{\partial x} + \frac{\partial^2 V}{\partial \varphi \partial \lambda}\frac{\partial \lambda}{\partial x}\right] \\ & + \frac{\partial V}{\partial \lambda}\frac{\partial^2 \lambda}{\partial x^2} + \frac{\partial \lambda}{\partial x}\left[\frac{\partial^2 V}{\partial r \partial \lambda}\frac{\partial r}{\partial x} + \frac{\partial^2 V}{\partial \varphi \partial \lambda}\frac{\partial \varphi}{\partial x} + \frac{\partial^2 V}{\partial \lambda^2}\frac{\partial \lambda}{\partial x}\right] \end{aligned}$$

$$\begin{aligned} V_{xy} = {} & \frac{\partial V}{\partial r}\frac{\partial^2 r}{\partial x \partial y} + \frac{\partial r}{\partial x}\left[\frac{\partial^2 V}{\partial r^2}\frac{\partial r}{\partial y} + \frac{\partial^2 V}{\partial r \partial \varphi}\frac{\partial \varphi}{\partial y} + \frac{\partial^2 V}{\partial r \partial \lambda}\frac{\partial \lambda}{\partial y}\right] \\ & + \frac{\partial V}{\partial \varphi}\frac{\partial^2 \varphi}{\partial x \partial y} + \frac{\partial \varphi}{\partial x}\left[\frac{\partial^2 V}{\partial r \partial \varphi}\frac{\partial r}{\partial y} + \frac{\partial^2 V}{\partial \varphi^2}\frac{\partial \varphi}{\partial y} + \frac{\partial^2 V}{\partial \varphi \partial \lambda}\frac{\partial \lambda}{\partial y}\right] \\ & + \frac{\partial V}{\partial \lambda}\frac{\partial^2 \lambda}{\partial x \partial y} + \frac{\partial \lambda}{\partial x}\left[\frac{\partial^2 V}{\partial r \partial \lambda}\frac{\partial r}{\partial y} + \frac{\partial^2 V}{\partial \varphi \partial \lambda}\frac{\partial \varphi}{\partial y} + \frac{\partial^2 V}{\partial \lambda^2}\frac{\partial \lambda}{\partial y}\right] \end{aligned} \tag{5.2}$$

and similarly for the remaining derivatives.

The partial derivatives of the spherical coordinates with respect to the inertial Cartesian coordinates can be derived from the following relationships:

$$r = (x^2 + y^2 + z^2)^{\frac{1}{2}}$$
$$\alpha = \lambda + \theta$$

where α is the right ascension of the satellite and θ the Greenwich apparent sidereal time. The longitude λ is taken positive eastward.

$$\tan \alpha = y/x$$

$$\sin \varphi = z/r$$

$$\cos \varphi = (x^2 + y^2)^{\frac{1}{2}}/r = P/r$$

Using equations (3.23), (3.28) and (3.29) as explained on page 27, we obtain:

$$\frac{\partial r}{\partial x} = \frac{x}{r} \; ; \quad \frac{\partial \varphi}{\partial x} = -\frac{xz}{r^2 P} \; ; \quad \frac{\partial \lambda}{\partial x} = -\frac{y}{P^2} \tag{5.3}$$

$$\frac{\partial r}{\partial y} = \frac{y}{r} \; ; \quad \frac{\partial \varphi}{\partial y} = -\frac{yz}{r^2 P} \; ; \quad \frac{\partial \lambda}{\partial y} = \frac{x}{P^2} \tag{5.4}$$

$$\frac{\partial r}{\partial z} = \frac{z}{r} \; ; \quad \frac{\partial \varphi}{\partial z} = \frac{P}{r^2} \; ; \quad \frac{\partial \lambda}{\partial z} = 0 \tag{5.5}$$

$$\frac{\partial^2 r}{\partial x^2} = \frac{r^2 - x^2}{r^3} \; ; \quad \frac{\partial^2 \varphi}{\partial x^2} = -\frac{z(r^2 y + 2x^2 P^2)}{r^4 P^3} \; ; \quad \frac{\partial^2 \lambda}{\partial x^2} = \frac{2xy}{P^4} \tag{5.6}$$

$$\frac{\partial^2 r}{\partial x \partial y} = -\frac{xy}{r^3} \; ; \quad \frac{\partial^2 \varphi}{\partial x \partial y} = \frac{xyz(2P^2 + r^2)}{r^4 P^3} \; ; \quad \frac{\partial^2 \lambda}{\partial x \partial y} = \frac{y^2 - x^2}{P^4} \tag{5.7}$$

$$\frac{\partial^2 r}{\partial x \partial z} = -\frac{xz}{r^3} \; ; \quad \frac{\partial^2 \varphi}{\partial x \partial z} = -\frac{x(2z^2 - r^2)}{r^4 P} \; ; \quad \frac{\partial^2 \lambda}{\partial x \partial z} = 0 \tag{5.8}$$

$$\frac{\partial^2 r}{\partial y^2} = \frac{r^2 - y^2}{r^3}\ ;\ \frac{\partial^2 \varphi}{\partial y^2} = \frac{z\,(2y^2 P^2 - r^2 x^2)}{r^4\, p^3}\ ;\ \frac{\partial^2 \lambda}{\partial y^2} = -\frac{2xy}{p^4} \qquad (5.9)$$

$$\frac{\partial^2 r}{\partial y \partial z} = -\frac{y\,z}{r^3}\ ;\ \frac{\partial^2 \varphi}{\partial y \partial z} = -\frac{y\,(r^2 - 2z^2)}{r^4\, P}\ ;\ \frac{\partial^2 \lambda}{\partial y \partial z} = 0 \qquad (5.10)$$

$$\frac{\partial^2 r}{\partial z^2} = \frac{r^2 - z^2}{r^3}\ ;\ \frac{\partial^2 \varphi}{\partial z^2} = -\frac{2zP}{r^4}\ ;\ \frac{\partial^2 \lambda}{\partial z^2} = 0 \qquad (5.11)$$

It can be shown that the chain rule method is identical to the tensor transformation technique presented in Chapter 2. From a programming point of view the method shown here appears to be simpler.

5.3 Spherical Partial Derivatives of the Harmonic Reference Potential

Upon differentiation of equation (2.2) for N = 14, with respect to the spherical coordinates we obtain:

$$\frac{\partial U}{\partial r} = -\frac{kM}{r^2}\left[1 + \sum_{n=2}^{14}\sum_{m=0}^{n}(n+1)\left(\frac{a}{r}\right)^n (C_{nm}\cos m\lambda + S_{nm}\sin m\lambda)\, P_{nm}(\sin\varphi)\right] \qquad (5.12)$$

$$\frac{\partial U}{\partial \varphi} = -\frac{kM}{r}\left[\sum_{n=2}^{14}\sum_{m=0}^{n}\left(\frac{a}{r}\right)^n (C_{nm}\cos m\lambda + S_{nm}\sin m\lambda)(m\tan\varphi\, P_{nm}(\sin\varphi) - P_{n\,m+1}(\sin\varphi))\right] \qquad (5.13)$$

$$\frac{\partial U}{\partial \lambda} = -\frac{kM}{r}\left[\sum_{n=2}^{14}\sum_{m=0}^{n}\left(\frac{a}{r}\right)^n (C_{nm}\sin m\lambda - S_{nm}\cos m\lambda)\, mP_{nm}(\sin\varphi)\right] \tag{5.14}$$

Differentiating equations (5.12), (5.13) and (5.14) again with respect to the spherical coordinates yields

$$\frac{\partial^2 U}{\partial r^2} = \frac{2kM}{r^3}\left[1+\tfrac{1}{2}\sum_{n=2}^{14}\sum_{m=0}^{n}\left(\frac{a}{r}\right)^n (n+1)(n+2)(C_{nm}\cos m\lambda + S_{nm}\sin m\lambda)P_{nm}(\sin\varphi)\right] \tag{5.15}$$

$$\frac{\partial^2 U}{\partial \varphi^2} = -\frac{kM}{r}\left[\sum_{n=2}^{14}\sum_{m=0}^{n}\left(\frac{a}{r}\right)^n (C_{nm}\cos m\lambda + S_{nm}\sin m\lambda)\right.$$
$$\times\left(\frac{m}{\cos^2\varphi}P_{nm}(\sin\varphi) + m\tan\varphi\,(P_{n,m+1}(\sin\varphi) - m\tan\varphi\, P_{nm}(\sin\varphi))\right.$$
$$\left.\left.+ (m+1)\tan\varphi P_{n,m+1}(\sin\varphi) - P_{n,m+2}(\sin\varphi)\right)\right] \tag{5.16}$$

$$\frac{\partial^2 U}{\partial \lambda^2} = -\frac{kM}{r}\left[\sum_{n=2}^{14}\sum_{m=0}^{n}\left(\frac{a}{r}\right)^n (C_{nm}\cos m\lambda + S_{nm}\sin m\lambda)m^2 P_{nm}(\sin\varphi)\right] \tag{5.17}$$

and the cross partials

$$\frac{\partial^2 U}{\partial r\partial \varphi} = -\frac{kM}{r^2}\left[\sum_{n=2}^{14}\sum_{m=0}^{n}(n+1)\left(\frac{a}{r}\right)^n (C_{nm}\cos m\lambda + S_{nm}\sin m\lambda)\right.$$
$$\left.\times\left(P_{n,m+1}(\sin\varphi) - m\tan\varphi P_{nm}(\sin\varphi)\right)\right] \tag{5.18}$$

$$\frac{\partial^2 U}{\partial r \partial \lambda} = -\frac{kM}{r^2}\left[\sum_{n=0}^{14}\sum_{m=0}^{n}(n+1)(-C_{nm}\sin m\lambda + S_{nm}\cos m\lambda)\,P_{nm}(\sin\varphi)\right] \tag{5.19}$$

$$\frac{\partial^2 U}{\partial \varphi \partial \lambda} = -\frac{kM}{r^2}\left[\sum_{n=2}^{14}\sum_{m=0}^{n}\left(\frac{a}{r}\right)^n(-C_{nm}\sin m\lambda + S_{nm}\cos m\lambda) \times m(m\tan\varphi\, P_{nm}(\sin\varphi) - P_{n,m+1}(\sin\varphi)\right] \tag{5.20}$$

To evaluate the Legendre functions in the partial derivatives, the recursion formula is given by Hobson (1965) as:

$$P_{no}(\sin\varphi) = \left[(2n+1)\sin\varphi\, P_{n-1,o}(\sin\varphi) - (n-1)P_{n-2,o}(\sin\varphi)\right] \Big/ n,\ n \geq 2 \tag{5.21}$$

The associated Legendre functions are evaluated by:

$$P_{nm}(\sin\varphi) = \left[P_{n-2,m}(\sin\varphi) + (2n+1)\cos\varphi\, P_{n-1,m-1}(\sin\varphi)\right],\ n \geq 2,\ m \geq 1 \tag{5.22}$$

where the term $P_{n-2,m}(\sin\varphi) = 0$, for $m > n-2$. In equations (5.13), (5.16) and (5.20); the term $P_{n,m-1}(\sin\varphi) = 0$, for $m > n-1$. The required initial values are:

$$\begin{aligned} P_{oo}(\sin\varphi) &= 1 \\ P_{1o}(\sin\varphi) &= \sin\varphi \\ P_{11}(\sin\varphi) &= \cos\varphi \end{aligned}$$

$$P_{20}(\sin\varphi) = 1.5\sin^2\varphi - 0.5$$

$$P_{21}(\sin\varphi) = 3\sin\varphi\cos\varphi$$

$$P_{22}(\sin\varphi) = 3\cos^2\varphi$$

The contribution of the spherical harmonic reference field to the acceleration vector and gravity gradients in the inertial system may now be computed by the method given in section 5.2.

5.4 Partial Derivatives of the Anomalous Potential in Terms of Gravity Anomalies

If the anomalous potential is represented by mean gravity anomalies in blocks, the integration of equation (2.3) may be expressed as a finite summation:

$$T = \frac{R}{4\pi}\sum_k \Delta g_k\, S(r,\psi)\,\Delta s_k \qquad (5.23)$$

where ΔS_k denotes the area of the $k^{\underline{th}}$ block in solid angle. The partial derivatives analogous to those in section 5.3 are:

$$\frac{\partial T}{\partial r} = \frac{R}{4\pi}\sum_k \Delta g_k \frac{\partial S(r,\psi)}{\partial r}\Delta s_k \qquad (5.24)$$

$$\frac{\partial T}{\partial \varphi} = \frac{R}{4\pi}\sum_k \Delta g_k \frac{\partial S(r,\psi)}{\partial \psi}\frac{\partial \psi}{\partial \varphi}\Delta s_k \qquad (5.25)$$

$$\frac{\partial T}{\partial \lambda} = \frac{R}{4\pi}\sum_k \Delta g_k \frac{\partial S(r,\psi)}{\partial \psi}\frac{\partial \psi}{\partial \lambda}\Delta s_k \qquad (5.26)$$

$$\frac{\partial^2 T}{\partial r^2} = \frac{R}{4\pi} \sum_k \Delta g_k \frac{\partial^2 S(r,\psi)}{\partial r^2} \Delta s_k \qquad (5.27)$$

$$\frac{\partial^2 T}{\partial \varphi^2} = \frac{R}{4\pi} \sum_k \Delta g_k \left[\frac{\partial^2 S(r,\psi)}{\partial \psi^2} \left(\frac{\partial \psi}{\partial \varphi} \right)^2 + \frac{\partial S(r,\psi)}{\partial \psi} \frac{\partial^2 \psi}{\partial \varphi^2} \right] \Delta s_k \qquad (5.28)$$

$$\frac{\partial^2 T}{\partial \lambda^2} = \frac{R}{4\pi} \sum_k \Delta g_k \left[\frac{\partial^2 S(r,\psi)}{\partial \psi^2} \left(\frac{\partial \psi}{\partial \lambda} \right)^2 + \frac{\partial S(r,\psi)}{\partial \psi} \frac{\partial^2 \psi}{\partial \lambda^2} \right] \Delta s_k \qquad (5.29)$$

$$\frac{\partial^2 T}{\partial \varphi \partial \lambda} = \frac{R}{4\pi} \sum_k \Delta g_k \left[\frac{\partial^2 S(r,\psi)}{\partial \psi^2} \frac{\partial \psi}{\partial \varphi} \frac{\partial \psi}{\partial \lambda} + \frac{\partial S(r,\psi)}{\partial \psi} \frac{\partial^2 \psi}{\partial \varphi \partial \lambda} \right] \Delta s_k \qquad (5.30)$$

$$\frac{\partial^2 T}{\partial r \partial \varphi} = \frac{R}{4\pi} \sum_k \Delta g_k \frac{\partial^2 S(r,\psi)}{\partial r \partial \psi} \frac{\partial \psi}{\partial \varphi} \Delta s_k \qquad (5.31)$$

$$\frac{\partial^2 T}{\partial r \partial \lambda} = \frac{R}{4\pi} \sum_k \Delta g_k \frac{\partial^2 S(r,\psi)}{\partial r \partial \psi} \frac{\partial \psi}{\partial \lambda} \Delta s_k \qquad (5.32)$$

The derivatives $\frac{\partial S(r,\psi)}{\partial r}$ and $\frac{\partial S(r,\psi)}{\partial \psi}$ are given in Heiskanen and Moritz (1967) as:

$$\frac{\partial S(r,\psi)}{\partial r} = -\frac{t^2}{R}\left[\frac{1-t^2}{D^3} + \frac{4}{D} + 1 - 6D - t\cos\psi\left(13 + 6\ell n \frac{1-t\cos\psi+D}{2}\right)\right] \quad (5.33)$$

$$\frac{\partial S(r,\psi)}{\partial \psi} = -t^2 \sin\psi\left[\frac{2}{D^3} + \frac{6}{D} - 8 - 3\frac{1-t\cos\psi-D}{D\sin^2\psi} - 3\ell n \frac{1-t\cos\psi+D}{2}\right] \quad (5.34)$$

Recalling from equation (2.6), $t = \frac{R}{r}$, we find

$$\frac{\partial t}{\partial r} = -\frac{R}{r^2} = -\frac{t^2}{R}$$

$$\frac{\partial t}{\partial \psi} = 0$$

and from equation (2.7), $D = (1-2t\cos\psi + t^2)^{\frac{1}{2}}$,

$$\frac{\partial D}{\partial r} = \frac{\partial D}{\partial t}\frac{\partial t}{\partial r} = \frac{t^2(\cos\psi - t)}{DR}$$

$$\frac{\partial D}{\partial \psi} = \frac{t\sin\psi}{D}$$

Using the above differentials the second partials of $S(r,\psi)$ may be computed. Differentiating equation (5.33) again with respect to the radial distance r yields

$$\frac{\partial^2 S(r,\psi)}{\partial r^2} = \frac{t^3}{R^2}\left[(1-t\cos\psi)\left(\frac{3(1-t^2)}{D^5} - \frac{4}{D^3}\right) - \frac{(1+t^2)}{D^3} - \frac{10}{D} - 18D + 2 - 3t\cos\psi\,(15 + 6\ell n\,\frac{1-t\cos\psi+D}{2})\right] \quad (5.35)$$

This derivative was originally derived by Witte (1970a) in another form. As a check on the derivation of equation (5.35), an attempt was made to convert Witte's equation (4):

$$\frac{\partial^2 S(r,\psi)}{\partial r^2} = \frac{R^2}{r^2}\left[\frac{3r(r-R\cos\psi)(r^2-R^2) - \ell^2(r^2+R^2)}{R\ell^5} + \frac{4R^2(\ell^2 + r(r-R\cos\psi)) + 2R\ell^3 - 6\ell^2(3\ell^2 - r(r-R\cos\psi))}{r^2 R \ell^3} - \frac{3\cos\psi}{r^2}\,13 + 6\ell n\,\frac{r-R\cos\psi+\ell}{2r} - \frac{2(r-\ell)}{\ell}\right]$$

where $\ell = (r^2 + R^2 - 2Rr\cos\psi)^{\frac{1}{2}}$, into the same form. It became apparent that Witte's derivation has a probable printing error. The last line of Witte's form should be

$$-\frac{3\cos\psi}{r^2}\left(13 + 6\ell n\,\frac{r-R\cos\psi+\ell}{2r} - \frac{2(r-\ell)}{\ell}\right)\Bigg]$$

The mixed partial of S (r, ψ) is obtained by differentiating equation (5.33) with respect to the spherical distance ψ:

$$\frac{\partial^2 S(r,\psi)}{\partial r \partial \psi} = \frac{t^3 \sin\psi}{R}\left[\frac{3(1-t^2)}{D^5} + \frac{4}{D^3} + \frac{6}{D} - 13 - 6\ell n\,\frac{1-t\cos\psi+D}{2} + \frac{t\cos t\,(D+1)}{D(1-t\cos\psi+D)}\right] \tag{5.36}$$

This derivative agrees with the derivation by Witte (1970b). Differentiating equation (5.34) with respect to the spherical distance yields

$$\frac{\partial^2 S(r,\psi)}{\partial^2 \psi} = -t^2\cos\psi\left[\frac{2}{D^3} + \frac{6}{D} - 8 - 3\,\frac{1-t\cos\psi-D}{D\sin^2\psi} - 3\ell n\,\frac{1-t\cos\psi+D}{2}\right] + t^3\sin^2\psi\left[\frac{6}{D^5} + \frac{6}{D^3} + 3\,\frac{(D-1)}{D^2\sin^2\psi} + 3\,\frac{(D+1)}{D(1-t\cos\psi+D)} - 3\,\frac{1-t\cos\psi-D}{D\sin^2\psi}\left(\frac{2\cos\psi}{t\sin^2\psi} + \frac{1}{D^2}\right)\right] \tag{5.37}$$

As an independent check on equation (5.37), the surface form of the Stokes' function:

$$S(\psi) = \frac{1}{\sin\frac{\psi}{2}} - 6\sin\frac{\psi}{2} + 1 - 5\cos\psi - 3\cos\psi\,\ell n\left(\sin\frac{\psi}{2} + \sin^2\frac{\psi}{2}\right)$$

was differentiated twice to obtain

$$\frac{\partial^2 S(r,\psi)}{\partial \psi^2} = \frac{1}{4}\,\frac{2 + 5\sin\frac{\psi}{2} + 2\sin^2\frac{\psi}{2} - 4\sin^3\frac{\psi}{2}}{\sin^3\frac{\psi}{2}\,(1+\sin\frac{\psi}{2})} + 6\sin\frac{\psi}{2} - 22\sin^2\frac{\psi}{2} + 3\cos\psi\,\ell n\left(\sin\frac{\psi}{2} + \sin^2\frac{\psi}{2}\right)$$

By letting $t = 1$ and $D = (2 - 2\cos\psi)^{\frac{1}{2}} = 2\sin\frac{\psi}{2}$, and after tedious algebraic and trigonometric manipulations, equation (5.37) was reduced to this form.

To obtain the partial derivatives of the spherical distance with respect to geocentric latitude and longitude, we recall the well-known spherical triangle relationships:

$$\cos\psi = \sin\varphi \sin\varphi_k + \cos\varphi\cos\varphi_k \cos(\lambda_k - \lambda) \tag{5.38}$$

$$\sin\psi = \frac{\cos\varphi_k \sin(\lambda_k - \lambda)}{\sin\psi} \tag{5.39}$$

$$\cos\alpha_k = \frac{\cos\varphi \sin\varphi_k - \sin\varphi\cos\varphi_k\cos(\lambda_k - \lambda)}{\sin\lambda} \tag{5.40}$$

where α_k is the azimuth from the satellite subpoint to the center of any mean anomaly block. Differentiating equation (5.38) and using equations (5.39) and (5.40) gives

$$\frac{\partial\psi}{\partial\varphi} = -\frac{\cos\varphi\sin\varphi_k + \sin\varphi\cos\varphi_k\cos(\lambda_k - \lambda)}{\sin\psi} \tag{5.41}$$

$$= -\cos\alpha_k$$

$$\frac{\partial \psi}{\partial \lambda} = - \frac{\cos\varphi \cos\varphi_k \sin(\lambda_k - \lambda)}{\sin\psi} \tag{5.42}$$

$$= - \cos\varphi \sin\alpha_k$$

Differentiating equations (5.41) and (5.42):

$$\frac{\partial^2 \psi}{\partial \varphi^2} = \sin\alpha_k \frac{\partial \alpha_k}{\partial \varphi} \tag{5.43}$$

$$\frac{\partial^2 \psi}{\partial \lambda^2} = - \cos\varphi \cos\alpha_k \frac{\partial \alpha_k}{\partial \lambda} \tag{5.44}$$

From equation (5.39):

$$\frac{\partial \alpha_k}{\partial \varphi} = \sin\alpha_k \cot\psi \tag{5.45}$$

$$\frac{\partial \alpha_k}{\partial \lambda} = - \frac{\cos\varphi_k \cos(\lambda_k - \lambda) - \cos\varphi \sin^2\alpha_k \cos\psi}{\cos\alpha_k \sin\psi} \tag{5.46}$$

Substituting these differentials into equations (5.43) and (5.44):

$$\frac{\partial^2 \psi}{\partial \varphi^2} = \sin^2\alpha_k \cot\psi \tag{5.47}$$

$$\frac{\partial^2 \psi}{\partial \lambda^2} = \frac{\cos\varphi}{\sin\psi} \left[\cos\varphi_k \cos(\lambda_k - \lambda) - \cos\varphi \sin^2\alpha_k \cos\alpha_k \right] \tag{5.48}$$

The mixed partial of ψ from equation (5.41):

$$\frac{\partial^2\psi}{\partial\varphi\partial\lambda} = \frac{\partial}{\partial\lambda}\left(\frac{\partial\psi}{\partial\varphi}\right) = -\frac{\partial\cos\alpha_k}{\partial\lambda}$$

which is simply minus the derivative of the right hand side of equation (5.40) with respect to λ. Thus

$$\frac{\partial^2\psi}{\partial\varphi\partial\lambda} = \sin\alpha_k\,(\sin\varphi - \cos\varphi\cos\alpha_k\cot\psi) \tag{5.49}$$

With the equations given in this section, the anomalous part of the acceleration vector and the gravity gradients in the inertial system may be computed by the previously described chain rule method.

5.5 Partial Derivatives of the Anomalous Potential in Terms of Point Masses.

In the case of the point mass representation as used in this study the position of a mass element is defined by earth-fixed Cartesian coordinates (X, Y, Z). This system has the Z - axis along the mean rotation axis of the earth, positive North, the X- axis positive through the Greenwich meridian, and is right handed. The relationship between the computation point in earth-fixed system and the inertial system is

$$\begin{Bmatrix} X_1 \\ Y_1 \\ Z_1 \end{Bmatrix} = R_3(\theta) \begin{Bmatrix} x_1 \\ y_1 \\ z_1 \end{Bmatrix} \tag{5.50}$$

where θ is the Greenwich Apparent Sidereal Time.

Rigorously the above transformation should include the effects of polar motion. For the purpose of simplifying the simulations, polar motion is neglected.

The gravitational acceleration components are computed by differentiating equation (2.8) with respect to the earth fixed coordinates. For example,

$$\frac{\partial T_i}{\partial X_i} \quad -\sum_j \frac{\frac{\partial \ell_{ij}}{\partial X_i}}{\ell_{ij}^2} \text{ km}_j \tag{5.51}$$

where

$$\ell_{ij} = \left[\left(X_i - X_j\right)^2 + \left(Y_i - Y_j\right)^2 + \left(Z_i - Z_j\right)^2\right]^{\frac{1}{2}} \tag{5.52}$$

Differentiating (5.52) we obtain:

$$\frac{\partial \ell_{ij}}{\partial X_i} = \frac{X_i - X_j}{\ell_{ij}} = \frac{\Delta X_{ij}}{\ell_{ij}} \tag{5.53}$$

Thus

$$\frac{\partial T_i}{\partial X_i} = -\sum_j \frac{\Delta X_{ij}}{\ell_{ij}^3} \text{ km}_j \tag{5.54}$$

Similarly for the other components we get

$$\frac{\partial T_i}{\partial Y_i} = -\sum_j \frac{\Delta Y_{ij}}{\ell_{ij}^3} \text{ km}_j \tag{5.55}$$

$$\frac{\partial T_i}{\partial Z_i} = -\sum_j \frac{\Delta Z_{ij}}{\ell_{ij}^3} \text{ km}_j \tag{5.56}$$

Now the acceleration vector T_R in the earth fixed system may be transformed to T_r in the inertial system by

$$\overline{T_r} = R_3(-\theta)\ \overline{T_R} \tag{5.57}$$

where as before θ is the Greenwich apparent sidereal time.

Differentiating (5.54) again yields

$$\frac{\partial^2 T_i}{\partial X_i^2} = \sum_j \left(\frac{3\Delta X_{ij}^2 - \ell_{ij}^2}{\ell_{ij}^5} \right) km_j \tag{5.58}$$

Similiarly from (5.55) and (5.56) we get

$$\frac{\partial^2 T_i}{\partial Y_i^2} = \sum_j \left(\frac{3\Delta Y_{ij}^2 - \ell_{ij}^2}{\ell_{ij}^5} \right) km_j \tag{5.59}$$

$$\frac{\partial^2 T_i}{\partial Z_i^2} = \sum_j \left(\frac{3\Delta Z_{ij}^2 - \ell_{ij}^2}{\ell_{ij}^5} \right) km_j \tag{5.60}$$

The mixed partials are given by

$$\frac{\partial^2 T_i}{\partial X_i \partial Y_i} = \sum_j \left(\frac{3\Delta X_{ij}\Delta Y_{ij}}{\ell_{ij}^5} \right) km_j \tag{5.61}$$

$$\frac{\partial^2 T_i}{\partial X_i \partial Z_i} = \sum_j \left(\frac{3\Delta X_{ij}\Delta Z_{ij}}{\ell_{ij}^5} \right) km_j \tag{5.62}$$

$$\frac{\partial^2 T_i}{\partial Y_i \partial Z_i} = \sum_j \left(\frac{3\Delta Y_{ij}\Delta Z_{ij}}{\ell_{ij}^5} \right) km_j \tag{5.63}$$

At any instant of time the derivatives (5.58) through (5.63) are the components of a second-order gravity gradient tensor. Hence, the usual rules for change of basis may be applied to transform the earth-fixed gravity gradients into the inertial system. If we define the earth-fixed tensor as T_{RS} and T_{rs} as the tensor in the inertial system, then

$$T_{rs} = R_3 (-\theta) T_{RS} R_3 (\theta) \qquad (5.64)$$

5.6 Transformation of Gravitational Gradient Tensor to the Satellite Coordinate System.

Up to this point a method has been shown for computing the gravitational acceleration vector and gradient components in the inertial coordinate system. In this section, the transformation of the gradients into a satellite-fixed system will be derived.

It should be noted that Glaser (1972) used a transformation from a local (φ, λ, r) coordinate system to the satellite system using the Keplerian orbital elements. The transformation derived here used the Cartesian elements defined by the satellite state vector and the gravitational acceleration vector. The pervasive difference arises from the definition of the orientation of the gradiometer output axes. Since a gradiometer operates in a gravitational field, the output is influenced by the variation of the field strength along the direction of the local vertical. The direction of the local vertical is the negative direction of the gravitational acceleration vector

(outward from the earth).

Basically the transformation between two coordinate systems may be expressed by

$$\begin{Bmatrix} x \\ y \\ z \end{Bmatrix} = A \begin{Bmatrix} x' \\ y' \\ z' \end{Bmatrix}, \quad \begin{Bmatrix} x' \\ y' \\ z' \end{Bmatrix} = A^T \begin{Bmatrix} x \\ y \\ z \end{Bmatrix} \tag{5.65}$$

where

$$A = \begin{Bmatrix} a_{11} & a_{21} & a_{31} \\ a_{12} & a_{22} & a_{32} \\ a_{13} & a_{23} & a_{33} \end{Bmatrix} \tag{5.66}$$

is an orthogonal matrix of direction cosines and A^T is its transpose. The corresponding gradient tensor transformations would be

$$\begin{aligned} V_{RS} &= A\, V_{rs}\, A^T \\ V_{rs} &= A^T V_{RS}\, A \end{aligned} \tag{5.67}$$

What we are seeking here is a change of basis. In figure 5, the unit vector triad ($\hat{\iota}_1$, $\hat{\iota}_2$, $\hat{\iota}_3$) is defined at point such that $\hat{\iota}_1$, $\hat{\iota}_2$, and $\hat{\iota}_3$ are parallel to the geocentric inertial coordinate axes x, y and z, respectively. If we define the directions of the satellite-fixed axes by the orthogonal basis unit vectors $\hat{e}_1$, $\hat{e}_2$, $\hat{e}_3$ it can be shown that the relationship between the ($\hat{\iota}_1$, $\hat{\iota}_2$, $\hat{\iota}_3$) basis and the ($\hat{e}_1$, $\hat{e}_2$, $\hat{e}_3$) basis is

$$e_p = \sum_{q=1}^{3} a_{pq}\, i_q, \quad p = 1, 2, 3 \tag{5.68}$$

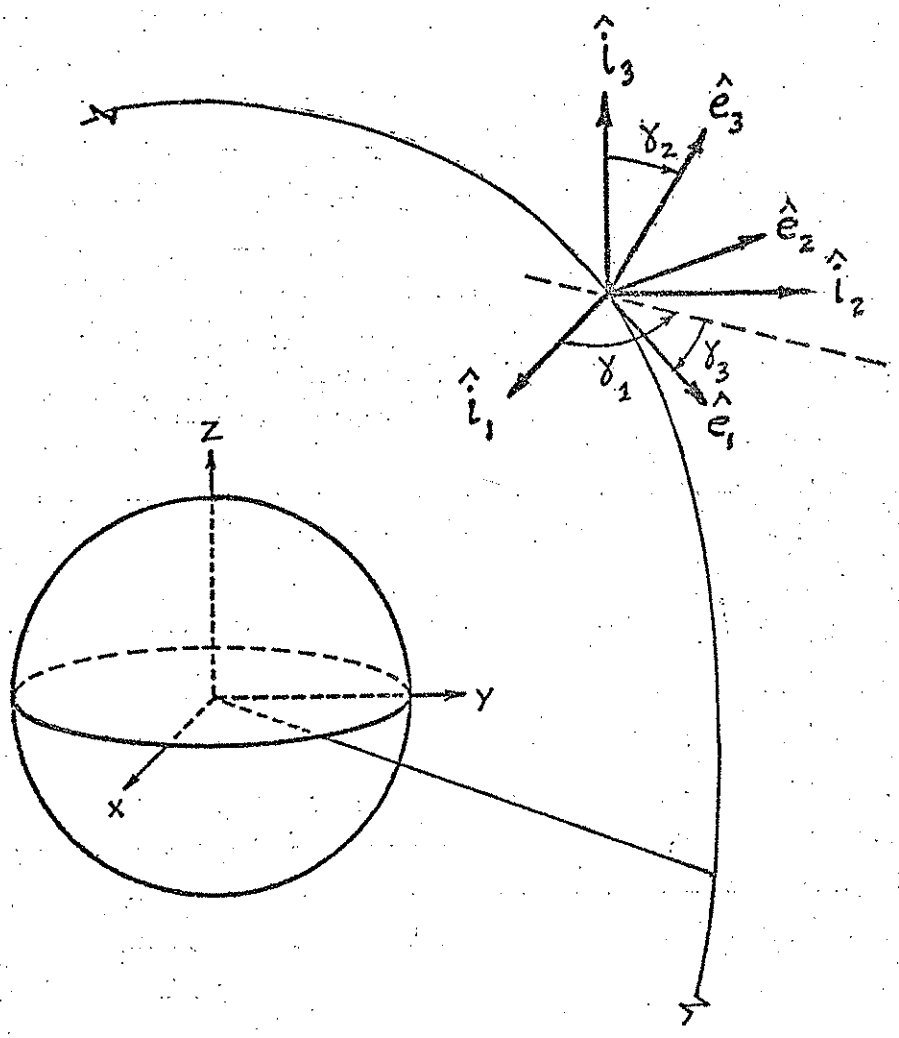

Figure 5. Gradiometer Coordinate System, Basis Vectors and Euler Angles

where $(a_{pq})^T = A$, the transformation matrix desired.

5.6.1 Orientation of the Hard-Mounted Gradiometer Satellite

For the hard-mounted gradiometer system, it is assumed that active attitude control maintains, at least approximately so, the orientation of the satellite. In this case the satellite is in what we choose to call a "gravitational" coordinate system.

The 3 - axis is defined by the local vertical:

$$\hat{e}_3 = -\bar{g}/g \tag{5.69}$$

where

$$\bar{g} = \begin{Bmatrix} g_x \\ g_y \\ g_z \end{Bmatrix} = \begin{Bmatrix} V_x \\ V_y \\ V_z \end{Bmatrix} \tag{5.70}$$

is the gravitational acceleration vector defined by its component in the inertial coordinate system. The 2 - axis is defined by the projection of the angular momentum vector.

$$\bar{h} = \bar{r} \times \dot{\bar{r}} \tag{5.71}$$

onto the 1 - 2 plane. Thus the 1 - axis is defined by the cross-product

$$\hat{e}_1 = \bar{h}/h \times \hat{e}_3 \tag{5.72}$$

and the 2 - axis by

$$\hat{e}_2 = \hat{e}_3 \times \hat{e}_1 \tag{5.73}$$

Using (5.68), (5.69), (5.72) and (5.73) the direction cosines for the transformation may be computed:

$$\begin{aligned} a_{11} &= -(h_y/h)\,(g_z/g) + (g_y/g)\,(h_z/h) \\ a_{12} &= -(h_z/h)\,(g_x/g) + (g_z/g)\,(h_x/h) \\ a_{13} &= -(h_x/h)\,(g_y/g) + (g_x/g)\,(h_y/h) \end{aligned} \tag{5.74}$$

$$\begin{aligned} a_{31} &= -g_x/g \\ a_{32} &= -g_y/g \\ a_{33} &= -g_z/g \end{aligned} \tag{5.75}$$

$$\begin{aligned} a_{21} &= a_{13}\,a_{32} - a_{12}\,a_{33} \\ a_{22} &= a_{11}\,a_{33} - a_{13}\,a_{31} \\ a_{23} &= a_{12}\,a_{31} - a_{11}\,a_{32} \end{aligned} \tag{5.76}$$

5.6.2 Orientation of the Rotating Gradiometer Satellite

Since the rotating gradiometer is required to be spun, attitude control by spin stabilization has been proposed by JPL (Gardner et al, 1972). In effect, the spinning satellite acts like a gyroscope. If the angular rate is sufficient, the spin axis will, in the absence of external torque, tend to maintain its orientation in space. This phenomena arises from the well

known principle of conservation of angular momentum. Thus it is reasonable to define the plane of rotation as the plane of the orbit. In this case we say that the satellite is in an "orbital" coordinate system.

The 2 - axis is defined by the angular momentum vector given in equation (5.71). Thus

$$\hat{e}_2 = \bar{h}/h \tag{5.77}$$

$$\bar{h} = \begin{Bmatrix} h_x \\ h_y \\ h_z \end{Bmatrix} \tag{5.78}$$

in terms of components in the inertial coordinate system.

If we define a unit vector

$$\hat{k} = -\bar{g}/g \tag{5.79}$$

in the direction of the local vertical, the 1 - axis is given by the cross-product

$$\hat{e}_1 = \hat{e}_2 \times \hat{k} \tag{5.80}$$

The 3 - axis given by

$$\hat{e}_3 = \hat{e}_1 \times \hat{e}_2 \tag{5.81}$$

which is the projection of $-\bar{g}/g$ onto the 2-3 plane.

Using (5.68), (5.77), (5.79) and (5.80) the direction cosines for the

transformation may be obtained. Note that the orientation of the 1 - axis is identical to that given by equation (5.74). The orientations of the 2 and 3 axes are given by

$$\begin{aligned} a_{21} &= h_x/h \\ a_{22} &= h_y/h \\ a_{23} &= h_z/h \end{aligned} \qquad (5.82)$$

$$\begin{aligned} a_{31} &= a_{13}\,a_{23} - a_{13}\,a_{32} \\ a_{32} &= a_{13}\,a_{21} - a_{11}\,a_{33} \\ a_{33} &= a_{11}\,a_{22} - a_{12}\,a_{21} \end{aligned} \qquad (5.83)$$

5.6.3 Gradiometer Satellite Orientation in Terms of Euler Angles

In the previous two sections, the orientation matrix was shown to contain 9 elements. These elements, the direction cosines, however, depend upon only 3 independent quantities, the Euler angles, γ_1, γ_2, γ_3, (see figure 5). We will see in Chapter 6, that the hard-mounted gradiometer system provides the possibility of modeling for the orientation parameters in a least squares solution. On the assumption that on-broad sensors will provide orientation information along with the gradiometer output, the Euler angles may be treated as observables in the solution.

From figure 5 the orientation matrix expressed in terms of the Euler angles is given by

$$A = R_3(-\gamma_1)\, R_1(-\gamma_2)\, R_3(-\gamma_3) \tag{5.84}$$

Performing the indicated multiplications in (5.84) results in

$$A = \begin{Bmatrix} \cos\gamma_1\cos\gamma_3 - \sin\gamma_1\cos\gamma_2\sin\gamma_3 & -\cos\gamma_1\sin\gamma_3 - \sin\gamma_1\cos\gamma_2\cos\gamma_3 & \sin\gamma_1\sin\gamma_2 \\ \sin\gamma_1\cos\gamma_3 + \cos\gamma_1\cos\gamma_2\sin\gamma_3 & -\sin\gamma_1\sin\gamma_3 + \cos\gamma_1\cos\gamma_2\cos\gamma_3 & -\cos\gamma_1\sin\gamma_2 \\ \sin\gamma_2\sin\gamma_3 & \sin\gamma_2\cos\gamma_3 & \cos\gamma_2 \end{Bmatrix} \tag{5.85}$$

6. LEAST SQUARES ADJUSTMENT OF SATELLITE GRADIOMETER DATA

The algorithms presented in this chapter simulate the least squares solutions for parameters describing the Earth's gravity field from data collected with the hard-mounted and rotating types of satellite gradiometers. The adjustment models do not include uncertainties in the satellite orbit. Rather it has been assumed that any errors in the satellite position are directly reflected as errors in the gradiometer measurements. This assumption is based upon the fact that the measurements are taken directly and do not depend on perturbations of the satellite. Thus the position of the satellite at the time a gradiometer measurement is recorded may be assumed to be known from post-mission analysis. As noted in Section 1.2, the JPL Gradiometer Study (Gardner, et al, 1972) concludes from a simulation study that current orbit determination technology is adequate for a gradiometer mission. Results of gradient computations given in Section 4.2 confirm the JPL conclusion. However, Glaser (1972) has suggested an iterative procedure whereby the gradiometer data itself may be used to improve the orbit determination, and to remove positioning errors from the data. Glaser's procedure uses an integral curve fitting technique to obtain harmonic coefficients from the amplitude of a rotating gradiometer signal. Hence, the observed quantities are five independent components of the gravity gradient tensor in the case of the hard-mounted system, and the signal amplitude in the case of the rotating system. In addition, orientation

parameters of the hard-mounted system are assumed to be observed as noted in section 5.6.3. However, these are considered nuisance parameters of no particular interest.

As discusses in section 1.1, the gravitational potential is conveniently partitioned into normal and disturbing parts V = U + T. Here the normal part refers to the potential of a high order sherop. The gravity gradient tensor in the gradiometer fixed coordinate system may be similarly partitioned:

$$\left[V_{ij} \right] = \left[U_{ij} \right] + \left[T_{ij}(\Phi) \right], \quad i, j = 1,2,3. \tag{6.1}$$

where Φ is a parameter describing the anomalous gravity field. Alternately, (6.1) may be written in terms of the inertial coordinates:

$$\left[V_{ij} \right] = A^T \left[U_{pq} \right] A + A^T \left[T_{pq}(\Phi) \right] A, \quad p,q = x,y,z. \tag{6.2}$$

where A is the orientation matrix described in section 5.6. Since the principal unknowns of the least squares solutions are the parameters, Φ, describing mean residual anomalies (Δg) in some convenient sized blocks or an array of point masses (km), a value of zero may be used to approximate all of the mean anomalies or point masses. Therefore, if the resulting observation equations are sufficiently linear, the final adjusted values of the parameters may be obtained in a single iteration. This is a significant advantage since the parameters may be neglected in forming the observation equations.

In formulating the adjustments, the classical least squares method using the procedures and notation of Uotila (1967) will be followed. It should be mentioned that Moritz (1971) suggests the method of least squares collocation for solutions from observed gravity gradients. Collocation solutions are characterized by a minimum mean square error of estimation. This method is, in fact, a generalization of classical adjustment computations where the square sum of the residuals (adjusted values minus observed values) is a minimum. The pervasive difference in collocation arises from the inclusion of field covariances derived from an appropriate covariance function. These field covariances express the behavior of the anomalous gravity field as a stochastic process as compared to error covariances which express the statistical behavior of observational errors. While collocation provides, theoretically, an optimum method for geodetic application of gradiometer measurements the formation and inversion of the covariance matrix is analytically and computationally a formidable and expensive undertaking (Moritz, 1972).

6.1 Mathematical Model and Observation Equations (Hard-Mounted Gradiometer)

A mathematical model for a gravity gradient measured by the hard-mounted system could be written functionally as

$$V_{ij} = V_{ij}(x, y, z, t, U, \gamma_1, \gamma_2, \gamma_3, \Phi_1 \ldots \Phi_n) \qquad 6.3)$$

where (x, y, z) are the inertial coordinates of the point of observation at time t; U represents the parameters of the reference spherop; γ_1, γ_2, γ_3 are the Euler angles describing the orientation of the gradiometer at time t, and n the number of anomaly blocks or mass points. As discussed earlier, the satellite position, and consequently the time history of the observed gradients may be assumed known. The parameters U are defined to fixed. More appropriately the mathematical model should be expressed in terms of observations and unknowns, thus

$$F_t(V_{ij}, \gamma_1, \gamma_2, \gamma_3, \Phi_1 \ldots \Phi_n) = 0 \tag{6.4}$$

In the case of the hard-mounted gradiometer we actually have 5 equations of this form:

$$\begin{aligned}
&F_t(V_{11}, \gamma_1, \gamma_2, \gamma_3, \Phi_1 \ldots \Phi_n) = 0 \\
&F_t(V_{12}, \gamma_1 \gamma_2, \gamma_3, \Phi_1 \ldots \Phi_n) = 0 \\
&F_t(V_{13}, \gamma_1, \gamma_2, \gamma_3, \Phi_1 \ldots \Phi_n) = 0 \\
&F_t(V_{22}, \gamma_1, \gamma_2, \gamma_3, \Phi_1 \ldots \Phi_n) = 0 \\
&F_t(V_{23}, \gamma_1, \gamma_2, \gamma_3, \Phi_1 \ldots \Phi_n) = 0
\end{aligned} \tag{6.5}$$

Note that in (6.5) V_{33} could be used in place of either V_{11} or V_{22} since

$$V_{11} + V_{22} + V_{33} = 0$$

At any time t, the errors in the observed gradients are given in differential form as:

$$\begin{bmatrix} dV_{11} \\ dV_{12} \\ dV_{13} \\ dV_{22} \\ dV_{23} \end{bmatrix}_t = \left[\begin{array}{c:c} D_1 & D_2 \end{array}\right]_t \left[\begin{array}{c} d\Phi_1 \\ \cdot \\ \cdot \\ \cdot \\ d\Phi_n \\ \hdashline d\gamma_1 \\ d\gamma_2 \\ d\gamma_3 \end{array}\right]_t \qquad 6.6)$$

where

$$D_1 = \frac{\partial (V_{11}, V_{12}, V_{13}, V_{22}, V_{23})_t}{\partial (\Phi_1 \ldots\ldots\ldots\ldots\ldots \Phi_n)}$$

$$D_2 = \frac{\partial (V_{11}, V_{12}, V_{13}, V_{22}, V_{23})_t}{\partial (\gamma_1, \gamma_2, \gamma_3)_t}$$

Since U_{ij} is not a function of the parameters, Φ_k, the D_1 partition may be written in terms of the anomalous gradients as:

$$D_1 = \frac{\partial (T_{11}, T_{12}, T_{13}, T_{22}, T_{23})_t}{\partial (\Phi_1 \ldots\ldots\ldots\ldots\ldots \Phi n)} \qquad 6.7)$$

Approximating the differential quantities in equation (6.6) by finite differences, the left hand side can be obtained by taking the differences between the observed gravity gradients and the approximate gradients at time t. With the approximate values of the parameters, Φ_k, taken to be zero the approximate gradient tensor is first computed from the truncated harmonic series describing the external potential of the (14,14) spherop as described in sections 5.2 and 5.3. The approximate tensor is then transformed into the approximate gradiometer fixed coordinate system by

$$\left[U_{ij}\right]_t \qquad A_o^T \left[U_{pq}\right]_t A_o \tag{6.8}$$

where A_o is the approximate orientation matrix computed by the method given in section 5.6.1. In this case the local vertical (the 3-axis) is defined by the unit vector

$$e_3 = -\bar{g}_o/g_o \tag{6.9}$$

where

$$\bar{g}_o = \begin{Bmatrix} U_x \\ U_y \\ U_z \end{Bmatrix} \tag{6.10}$$

Note that although only 5 components of the gravity gradient tensor are required in equation (6.8), the computations are facilitated by using matrix operations on the full tensor. The desired components may then be extracted at any step of the computations. In addition, as shown in

section 1.1, if five independent components of the tensor are known all the components are known. This procedure will also be used in obtaining the partial derivatives required to form the observation equations for both types of gradiometer.

6.1.1 The Parameter Sensitivity Matrix

The matrix D_1 in equation (6.6) may be properly called a parameter sensitivity matrix which describes the effect of a differential variation in the parameters Φ_k on the gravity gradients. Considering equation (6.7) the partial derivative of the gravity gradient tensor with respect to the parameters is:

$$\left\{\frac{\partial V_{ij}}{\partial \Phi_k}\right\}_t = \left\{\frac{\partial T_{ij}}{\partial \Phi_k}\right\}_t = A^T \left\{\frac{\partial T_{pq}}{\partial \Phi_k}\right\}_t A \qquad 6.11)$$

If Φ_k represents mean residual gravity anomalies, equations (5.27) through (5.32) and the transformations given in Chapter 5 are used to form the partial derivatives in (6.11) by differentiating with respect to the anomalies, Δg_k. Similarly for point masses, equations (5.58) through (5.63) are differentiated with respect to the point masses, km_j.

6.1.2 Partial Derivatives with Respect to the Orientation Parameters

Recall that the orientation matrix A given in section 5.6 may be readily computed using vector operators on the unit basis vectors of the geocentric

inertial coordinate system and the gradiometer fixed coordinate system. From equation (5.66) the orientation matrix is given in terms of direction cosines as:

$$A = \begin{Bmatrix} a_{11} & a_{21} & a_{31} \\ a_{12} & a_{22} & a_{32} \\ a_{13} & a_{23} & a_{33} \end{Bmatrix}$$

In section 5.6.3, it was shown that (5.66) may also be given in terms of the Euler angles γ_1, γ_2, γ_3 (see equation 5.85).

Here we require the partial derivatives which go into the D_2 partition of equation (6.6). Development of a method of forming these partials presents an interesting problem in matrix calculus. First of all using equations (5.66) and (5.85) and taking the partial derivatives with respect to the Euler angles, we get in terms of direction cosines:

$$\frac{\partial A}{\partial \gamma_1} = \begin{Bmatrix} -a_{12} & -a_{22} & -a_{32} \\ a_{11} & a_{21} & a_{31} \\ 0 & 0 & 0 \end{Bmatrix} \tag{6.12}$$

$$\frac{\partial A}{\partial \gamma_2} = \frac{1}{\sqrt{1-a_{33}^2}} \begin{Bmatrix} a_{13}a_{31} & a_{23}a_{31} & a_{33}a_{31} \\ a_{13}a_{32} & a_{23}a_{32} & a_{33}a_{32} \\ a_{13}a_{33} & a_{23}a_{33} & -(1-a_{33})^2 \end{Bmatrix} \tag{6.13}$$

$$\frac{\partial A}{\partial \gamma_3} = \begin{Bmatrix} a_{21} & -a_{11} & 0 \\ a_{22} & -a_{12} & 0 \\ a_{23} & -a_{13} & 0 \end{Bmatrix} \qquad (6.14)$$

By considering the pattern of the element in (6.12) and (6.14) it can be shown that

$$\frac{\partial A}{\partial \gamma_1} = S\ A \qquad (6.15)$$

and

$$\frac{\partial A}{\partial \gamma_3} = A\ S \qquad (6.16)$$

where

$$S = \begin{Bmatrix} 0 & -1 & 0 \\ 1 & 0 & 0 \\ 0 & 0 & 0 \end{Bmatrix} \qquad (6.17)$$

We can see that the transpose of S is:

$$S^T = -S$$

Thus

$$\frac{\partial A^T}{\partial \gamma_1} = A^T S^T = -A^T S \qquad (6.18)$$

and

$$\frac{\partial A^T}{\partial \gamma_3} = S^T A^T = -S A^T \qquad (6.19)$$

Having established these properties for the derivatives of the orientation

matrix, the next step is to compute the partial derivatives of the gradient tensor with respect to the Euler angles. We have shown in equation (6.2) that the tensor in the gradiometer fixed coordinates can be expressed in terms of the tensor in the inertial system by

$$\left[V_{ij}\right]_t = A^T \left[V_{pq}\right]_t A \qquad (6.20)$$

The orthogonality of the A matrix requires that

$$A\,A^T = I$$

and (6.21)

$$A^T A = I$$

where I is an identity matrix. Hence, by pre-multiplying both sides of (6.20) by A we get

$$A\left[V_{ij}\right]_t = \left[V_{pq}\right]_t A \qquad (6.22)$$

Similarly, post-multiplying by A^T gives

$$\left[V_{ij}\right]_t A^T = A^T \left[V_{pq}\right]_t \qquad (6.23)$$

Now taking the derivative with respect to γ_1, and using the relationships in (6.15), (6.17), (6.22) and (6.23):

$$\begin{aligned}\left[\frac{\partial V_{ij}}{\partial \gamma_1}\right]_t &= \frac{\partial A^T}{\partial \gamma_1}\left[V_{pq}\right]_t A + A^T\left[V_{pq}\right]_t \frac{\partial A}{\partial \gamma_1} \\ &= -A^T S A\left[V_{ij}\right]_t + \left[V_{ij}\right]_t A^T S A\end{aligned} \qquad (6.24)$$

Differentiating the tensor with respect to γ_2 using (6.13), (6.22) and (6.23) we get

$$\left[\frac{\partial V_{ij}}{\partial \gamma_2}\right]_t = \frac{\partial A^T}{\partial \gamma_2}\left[V_{pq}\right]_t A + A^T\left[V_{pq}\right]_t \frac{\partial A}{\partial \gamma_2}$$
$$= \left[\frac{\partial A}{\partial \gamma_2}\right]^T A\left[V_{ij}\right]_t + \left[V_{ij}\right] A^T \frac{\partial A}{\partial \gamma_2} \qquad (6.25)$$

Now with respect to γ_3 using (6.16), (6.19), (6.20), (6.22) and (6.23) the partial derivatives are

$$\left[\frac{\partial V_{ij}}{\partial \gamma_3}\right]_t = \frac{\partial A^T}{\partial \gamma_3}\left[V_{pq}\right]_t A + A^T\left[V_{pq}\right]_t \frac{\partial A}{\partial \gamma_3}$$
$$= -SA^T A\left[V_{ij}\right]_t + \left[V_{ij}\right]_t A^T AS \qquad (6.26)$$
$$= -S\left[V_{ij}\right]_t + \left[V_{ij}\right]_t S$$

An interesting aspect of the results of this development is that the partial derivatives with respect to the orientation parameters can be computed completely by matrix operations on the orientation matrix and the observed gradients. The only exception is the formation of $\partial A/\partial \gamma_2$ in equation (6.12). Once these operations have been carried out, the components corresponding to the differentials on the left hand side of equation (6.6) can be extracted to form the D_1 partition in equation (6.6).

6.1.3 Formulation of the Adjustment Model

We now want to collect all of the data to be incorporated into the adjustment. The mathematical model in equation (6.4) may be represented by the matrix equation:

$$F(L^a, X^a) = 0 \tag{6.27}$$

where L denotes a vector of observations and X a vector of parameter, some of which are observables. Such a model may be solved by generalized least square models (Uotila, 1967). If we treat the gradients errors in equation (6.6) as finite differences, then we must replace dV_{11}, dV_{12}, dV_{13}, dV_{22}, and dV_{23} by $dV_{11} + v_{11}$, $dV_{12} + v_{12}$, $dV_{13} + v_{13}$, $dV_{22} + v_{22}$, $dV_{23} + v_{23}$ where the small v's are the observation residuals of the data. The linearized form of equation (6.27) is then

$$BV_\ell + AV_x + W = 0 \tag{6.28}$$

where

$$B = \frac{\partial F}{\partial L} = -I,\ A = \frac{\partial F}{\partial X},\ W = F(L^b, X^o) \tag{6.29}$$

Note that in equation (6.27) the superscript a indicates adjusted values, while in (6.29) the superscripts b and o denote observed and estimated values, respectively. It can be shown that the corrections V_x to the parameters may be obtained from the following:

$$V_x = -\left[A^T P_\ell A + P_x\right]^{-1} A^T P_\ell W \tag{6.30}$$

where P_ℓ is the weight matrix of the observations and P_x the weight matrix for the parameters. The values of the parameters weighted are taken as X^o. Weights were introduced for each observation equation by inverting the estimated variance for the observation. The P_ℓ matrix and the P_x matrix

are arranged in diagonal form for each set of 5 gradient measurements and each set of 3 Euler angles treated as observed parameters. However, the only parameters of interest are those pertaining to the anomalous gravity field. Hence, we want to eliminate the orientation parameters from the system of normal equations. Rewriting equation (6.28) in the form

$$-V_\ell + \overline{A}_j \delta \Phi_k + \overline{\overline{A}}_j \overline{\overline{X}}_j + W_j = 0 \qquad (6.31)$$

where the subscript j denotes the jth set of 5 gradient observations and

$$\overline{\overline{X}}_j = \begin{Bmatrix} \gamma_1 \\ \gamma_2 \\ \gamma_3 \end{Bmatrix}_j$$

The normal equation may be written in partitioned form as

$$\begin{bmatrix} N_{11} & N_{12} \\ & T \\ N_{12} & N_{22} \end{bmatrix} \begin{bmatrix} \delta \Phi_k \\ \overline{\overline{X}} \end{bmatrix} = \begin{bmatrix} -U_1 \\ -U_2 \end{bmatrix} \qquad (6.32)$$

The desired reduced normal equations are of the form:

$$\overline{N}\, \delta \Phi_k = -\overline{U} \qquad (6.33)$$

In order to economize on compute core storage each set of 5 gradient observation equations were output into a disk storage unit as temporary data sets. When all observation equations were formed the sets of 5 equations were reintroduced into core storage one set at a time. The following algorithm was used to form the reduced normal equation by iteratively adding the contribution of each set of 5 observation equations:

$$N_{11_j} = \overline{A}^T P_{\ell_j} \overline{A}_j$$

$$N_{12_j} = \overline{A}_j^T P_{\ell_j} \overline{\overline{A}}_j$$

$$N_{22_j} = \overline{\overline{A}}^T P_{\ell_j} + P_{x_j}$$

$$\overline{N} = \sum_j (N_{11_j} - N_{12_j} N_{22_j}^{-1} N_{12_j}^T)$$

(6.33.1)

$$U_{1_j} = \overline{A}^T{}_j P_{\ell_j} W_j$$

$$U_{2_j} = \overline{\overline{A}}^T{}_j P_{\ell_j} W_j$$

$$\overline{U} = \sum_j (U_{1_j} - N_{12_j}^{-1} U_{2_j})$$

6.2 Mathematical Model and Observation Equations (Rotating Gradiometer)

As discussed in section 1.1, the signal of the rotating satellite gradiometer, equation (1.5) may reduced to a signal amplitude,

$$\text{Amplitude} = \left[(V_{33} - V_{11})^2 + 4V_{13}^2 \right]^{\frac{1}{2}} \qquad (1.6)$$

which will be treated as the observed quantity to be adjusted. Letting G denote the amplitude, equation (1.6) may be written functionally as:

$$G = G(V_{11}, V_{13}, V_{33}) \qquad 6.34)$$

where V_{11}, V_{13} and V_{33} are functionally given in equation (6.3). However, in this case all the parameters of V_{ij} are assumed to be known with the exception of the gravity field parameters Φ_k. Thus the model in terms of

observations and unknowns is:

$$F_t (G, \Phi_1, \ldots \Phi_n) = 0 \qquad (6.35)$$

In differential form the error in the observed signal amplitude is

$$dG_t = \left[\frac{\partial G}{\partial \Phi_1} \cdots \frac{\partial G}{\partial \Phi_n} \right]_t \begin{bmatrix} d\Phi_1 \\ \cdot \\ \cdot \\ \cdot \\ d\Phi_n \end{bmatrix} \qquad (6.36)$$

The development of equation (6.36) into finite difference form for the observation equations will be, in principle, the same as in section 6.1.

6.2.1 The Parameter Sensitivity Matrix

The elements of the parameter sensitivity matrix for the rotating gradiometer are computed by

$$\left[\frac{\partial G}{\partial \Phi_k} \right] = \left[\frac{\partial G_1}{\partial V_{11}} \frac{\partial V_{11}}{\partial \Phi_k} + \frac{\partial G}{\partial V_{13}} \frac{\partial V_{13}}{\partial \Phi_k} + \frac{\partial G}{\partial V_{33}} \frac{\partial V_{33}}{\partial \Phi_k} \right]_t \qquad (6.37)$$

Recalling from equation (6.11) that

$$\left[\frac{\partial V_{ij}}{\partial \Phi_k} \right]_t = \left[\frac{\partial T_{ij}}{\partial \Phi_k} \right]_t = A^T \left[\frac{\partial T_{pq}}{\partial \Phi_k} \right]_t A$$

equation (6.37) becomes

$$\left[\frac{\partial G}{\partial \Phi_k} \right]_t = \left[\frac{\partial G}{\partial V_{11}} \frac{\partial T_{11}}{\partial \Phi_k} + \frac{\partial G}{\partial V_{13}} \frac{\partial T_{13}}{\partial \Phi_k} + \frac{\partial G}{\partial V_{33}} \frac{\partial T_{33}}{\partial \Phi_k} \right]_t \qquad (6.38)$$

Applying equation (6.38) to equation (1.7) we get

$$\left[\frac{\partial G}{\partial \Phi_k}\right] = \left[(V_{33} - V_{11})\left(\frac{\partial T_{33}}{\partial \Phi_k} - \frac{\partial T_{11}}{\partial \Phi_k}\right) + 4V_{13}\frac{\partial T_{13}}{\partial \Phi_k}\right] \qquad (6.39)$$

These are the only partial derivatives required in forming observation equations for the rotating satellite gradiometer. Clearly, we can never get sufficient equations to permit the inclusion of orientation parameters as in the model for the hard-mounted system.

6.2.2 Formulation of the Adjustment Model

Again collecting all of the data to be adjusted, the matrix form of the mathematical model is identical to equation (6.27):

$$F(L^a, X^a) = 0 \qquad (6.27)$$

Here we replace dG in equation (6.36) by $dG + v$, where v is the observed amplitude residual. The linearized form is again

$$BV_\ell + AV_x + W = 0 \qquad (6.28)$$

The solution for the correction vector is:

$$V_x = -(A^T PA)^{-1} A^T PW, \qquad (6.40)$$

where P is the weight matrix of the observed signal amplitudes. In this case there are no weights on the parameters.

The observation equation for the jth observation may be written in the form

$$-V_{\ell j} + A_j \delta\Phi_k + W_j = 0 \qquad (6.41)$$

Taking the general form of the normal equations to be

$$N\delta\Phi_k = -U \qquad (6.42)$$

the normal equations were formed by the algorithm:

$$\begin{aligned} N &= \sum_j A_j^T pA_j \\ U &= \sum_j A_j^T pW_j \end{aligned} \qquad (6.43)$$

where p is the weight or the inverse of the apriori estimate of the variance of the observed signal amplitude.

6.3 Constraints on the Least Squares Solutions

The principal purpose of the adjustments on satellite gradiometer data is to obtain estimates of the gravity field parameters Φ_k. In effect, what we are attempting is to determine, from some spectral response of the Earth's external potential (in this case gravity gradients), quantities on or beneath the Earth's surface which represent the causative factor of the observed response. The formulation of such solutions are called improperly posed problems of inverse potential theory (Krarup, 1969; Moritz, 1972; Grafarend, 1972a,b). What this means is that the distribution and magnitude of the causative factor is not unique. Generally the causative factor, which we may represent by mean gravity anomalies or point masses, referred to an equipotential surface approximating the figure of the earth, is the distribution and density of masses within the earth. Now this does not mean that our least square solutions are not unique, but rather there are a family of possible

solutions depending on the sampling of the external gravity field and the modeling of the earth's gravity field. Hence we must consider the conditions imposed on our model by the physical nature of the problem we are attempting to solve.

Obenson (1970), Rapp (1971), and Needham (1970) have suggested conditions which should be placed on the adjusted parameters. The purpose of such conditions is to form a gravity field model which maintains the total mass and moments of inertia of the earth. This means that constraints should be placed on the gravity parameters, Φ_k, in order to eliminate zero and first degree terms from the harmonic representation of the parameters. In addition we also want to eliminate terms of higher degree and order which define the normal gravity field.

6.3.1 Anomaly Constraints

To define the conditions to be imposed on the mean residual gravity anomalies, we may consider the representation of the anomalies in spherical harmonic form:

$$g = \sum_{n=0}^{n} \sum_{m=0} (A_{nm} \cos m\lambda + B_{nm} \sin m\lambda) P_{nm} (\sin \varphi) \qquad 6.44)$$

where

$$\begin{Bmatrix} A_{nm} \\ B_{nm} \end{Bmatrix} = \frac{1}{4\pi} \int_{\sigma} \int \Delta g \; P_{nm} (\sin \varphi) \begin{Bmatrix} \cos m\lambda \\ \sin m\lambda \end{Bmatrix} d\sigma \qquad 6.45)$$

Rapp (1971) gives the general form of the condition equations as follows:

$$G_1 \quad \left(\frac{1}{4\pi}\int_\sigma\int \Delta g\, P_{nm} \cos m\lambda\, d\sigma - A_{nm}\right) = 0$$

$$G_2 \quad \left(\frac{1}{4\pi}\int_\sigma\int \Delta g\, P_{nm} \sin m\lambda\, d\sigma - B_{nm}\right) = 0 \qquad (6.46)$$

These equations represent a possible $(n+1)^2$ linear constraints on the adjusted mean gravity anomalies assuming that the harmonic coefficients are perfectly known. That would mean up to 225 constraint equations for a normal field defined by a (14, 14) spherop. Certainly if our model contained several thousand anomalies, 225 constraints would not be unreasonable. However, as we will se in Chapter 6, the maximum anomalies in any solution is 64, thus the imposition of a large number of constraints would have completely overwhelmed the observational data. Therefore, the only constraint considered was elimination of the zero degree term:

$$A_{oo} = \Delta g_o$$

where Δg_o is the mean residual gravity anomaly over the model region. The condition equation for a limited region in finite summation form is

$$\frac{1}{S}\sum_k \Delta g_k\, \Delta S_k - \Delta g_o = 0 \qquad (6.47)$$

where ΔS_k is an element of surface area in solid angle and

$$S = \sum_k \Delta S_k$$

6.3.2 Point Mass Constraints

In using the point mass model, Needham (1970) demonstrated that at

least two conditions are necessary to constrain point mass solutions. These conditions require that the integral of the potential over the model region be zero and that sum of the point masses in the model be zero.

$$\sum_i \sum_j \frac{km_j}{\ell_{ij}} \cos\varphi \Delta\varphi \Delta\lambda = 0 \qquad 6.48)$$

Similarly the condition on the total mass is given by

$$\sum_j km_j = 0 \qquad 6.49)$$

The latter equation was the only condition used in the simulated gradiometer solutions for the point mass representation.

6.4 Modification of the Normal Equation for Constraints

The basic mathematical model for the conditions imposed on the parameters is

$$G(X^a) = 0 \qquad 6.50)$$

In linearized form the condition equation is

$$C X + W_o \qquad 6.51)$$

where

$$C = \frac{\partial G}{\partial X}, \qquad W_g = G(L_c^b, X^o) \qquad 6.52)$$

The condition modified normal equations from equation (6.33) or (6.42) will have the partitioned form:

$$\begin{bmatrix} N & C^T \\ C & 0 \end{bmatrix} \begin{bmatrix} \delta\Phi_k \\ -K \end{bmatrix} = \begin{bmatrix} -U \\ -Wg \end{bmatrix} \qquad 6.53)$$

where K is a vector of correlates associated with the conditions imposed on the parameters, Φ_k .

Equation (6.53) is solved for corrections to the approximate values of the gravity field parameters $\delta\Phi_k$. The inverse of the normal coefficients N modified by the condition equations is the variance-covariance matrix of the parameters. By analyzing the standard errors and correlations obtained from the normal inverse together with the numerical errors in the simulated solutions and indicators of conditioning of the normal coefficient matrix, conclusions may be drawn on the effectiveness of satellite gradiometer measurements in resolving either point masses and/or mean gravity anomalies.

7. SIMULATION EXPERIMENTS AND NUMERICAL RESULTS

The algorithms described in Chapters 4 and 5 were coded in FORTRAN IV language. Various versions of the algorithms were used to perform a series of simulated solutions. Computations were carried out on the IBM 370/165 of The Ohio State University Instructional and Research Computer Center. Double precision arithmetic (8 bytes per word) was used in all computations.

Gravity models were formed using as normal gravity the potential of the (14,14) spherop described in section 2.1. A set of 1000 1° x 1° anomalies derived from terrestrial observations which were transformed into the GRS 67 system and subsequently reconciled to be consistent with the set of coefficients defining the (14,14) spherop. Thus the 1° x 1° set which are used in this study to form selected gravity models may be regarded as the best estimate of a 1° x 1° field consistent with the harmonic coefficients.

The residual anomaly models formed consisted of 2° x 2° and 5° x 5° blocks over the bulk of the continental United States and Northern Mexico. The largest area considered in the simulated solution is described by 40 5° x 5° blocks. A smaller sub-area was used in solutions for 2° x 2° blocks. The anomalous gravity outside the model regions considered was assumed to be zero. To obtain some idea of the possible effect of neglecting distance anomalies, the second radial derivative of the generalized Stokes' function,

(5.4), was plotted against the spherical distance ψ as shown in Figure 6. Additionally, Table 5 gives select values of the function out to $\psi = 180^\circ$. If these values are multiplied by 10^4 they could be interpreted as the contribution to the vertical gradient in Eotvos Units from a 1 milligal gravity anomaly over a 1 radian solid angle at the spherical distances shown. It is interesting to note that the first zero in the function occurs in the region $\psi < 5^\circ$ as compared to a first zero at about 38° for the Stokes' function itself and about 30° for the first radial derivative (Rapp, 1966), while the second zero in all cases comes at about $\psi = 120^\circ$.

7.1 Gravity Field Models

Five assumed gravity fields were formed using the Rapp (14,14) field and the Needham $1^\circ \times 1^\circ$ residual anomaly set. The five models are described below.

A. A set of 40 $5^\circ \times 5^\circ$ residual anomalies were generated from the set of 1000 $1^\circ \times 1^\circ$ residual anomalies. The value of the anomalies in this set are shown in Figure 7.

B. A set of 240 $2^\circ \times 2^\circ$ residual anomalies generated from the $1^\circ \times 1^\circ$ set excluding 80 $1^\circ \times 1^\circ$ blocks along the Southern edge of the area. The area covered by this model is designated region B in Figure 8.

C. A subset of B consisting of 64 $2^\circ \times 2^\circ$ residual anomalies in the sub-area block designated region C in Figure 8. See also Figure 9.

D. A subset of 256 $1^\circ \times 1^\circ$ residual anomalies in region C.

E. A set of 152 point masses least squares fitted to set B using a slightly

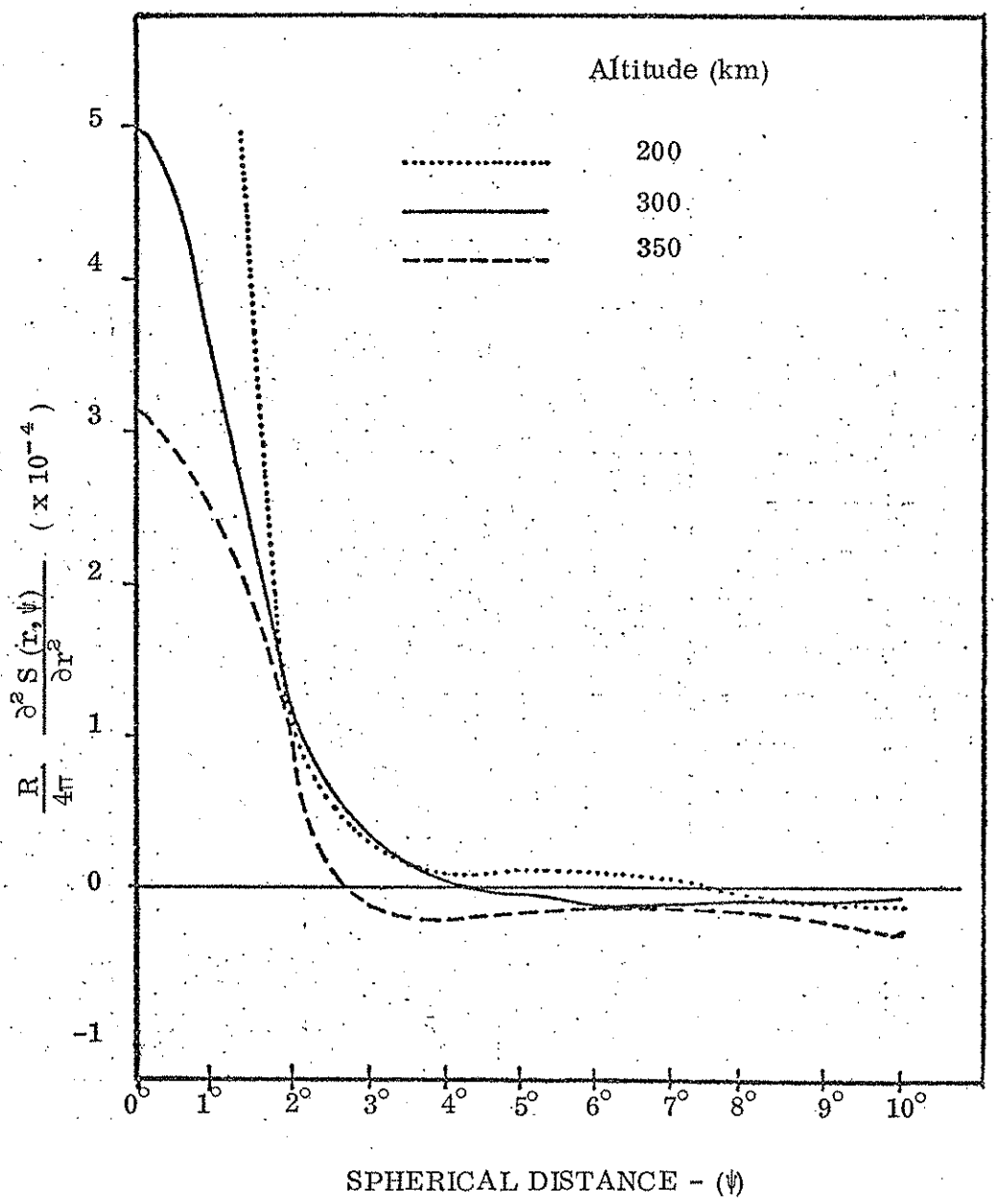

Figure 6. Behavior of the Second Radial Derivatives of Stokes Function at Altitude

Table 5

Representative Values of $\frac{R}{4\pi} \frac{\partial^2 S(r,\psi)}{\partial r^2}$ at 300 Kilometers Altitude

ψ	$\frac{R}{4\pi} \frac{\partial^2 S(r,\psi)}{\partial r^2}$ ($\times 10^{-4}$)
0	4.970
1'	4.969
15'	4.843
30'	4.488
1°	3.361
2°	1.255
3°	0.328
4°	0.043
5°	-0.029
10°	-0.018
15°	-0.006
30°	-0.002
60°	-0.003
90°	-0.002
120°	0.000
150°	0.002
180°	0.003

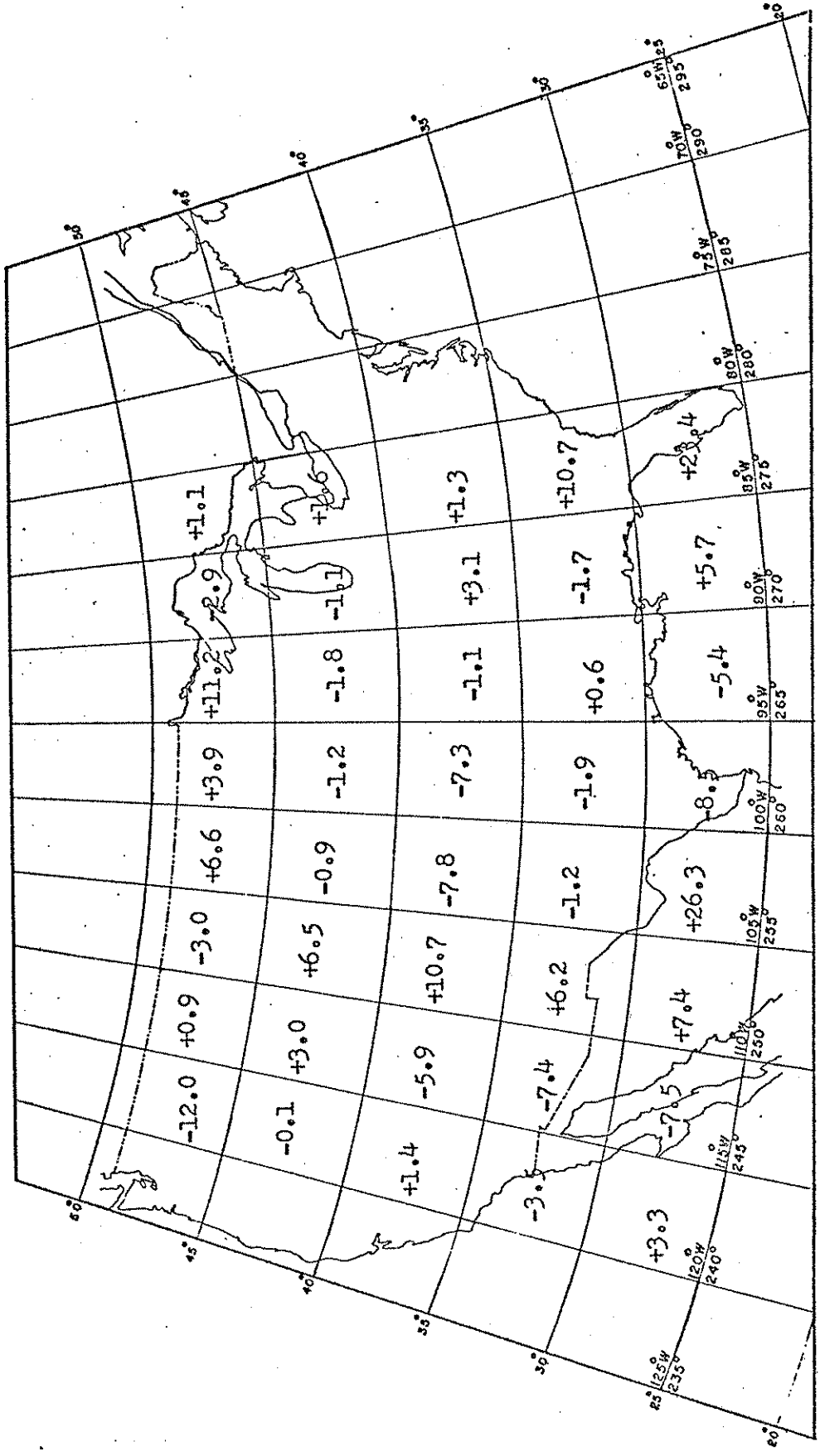

Figure 7. 5° x 5° Mean Gravity Anomalies Residual to the (14, 14) Sherop

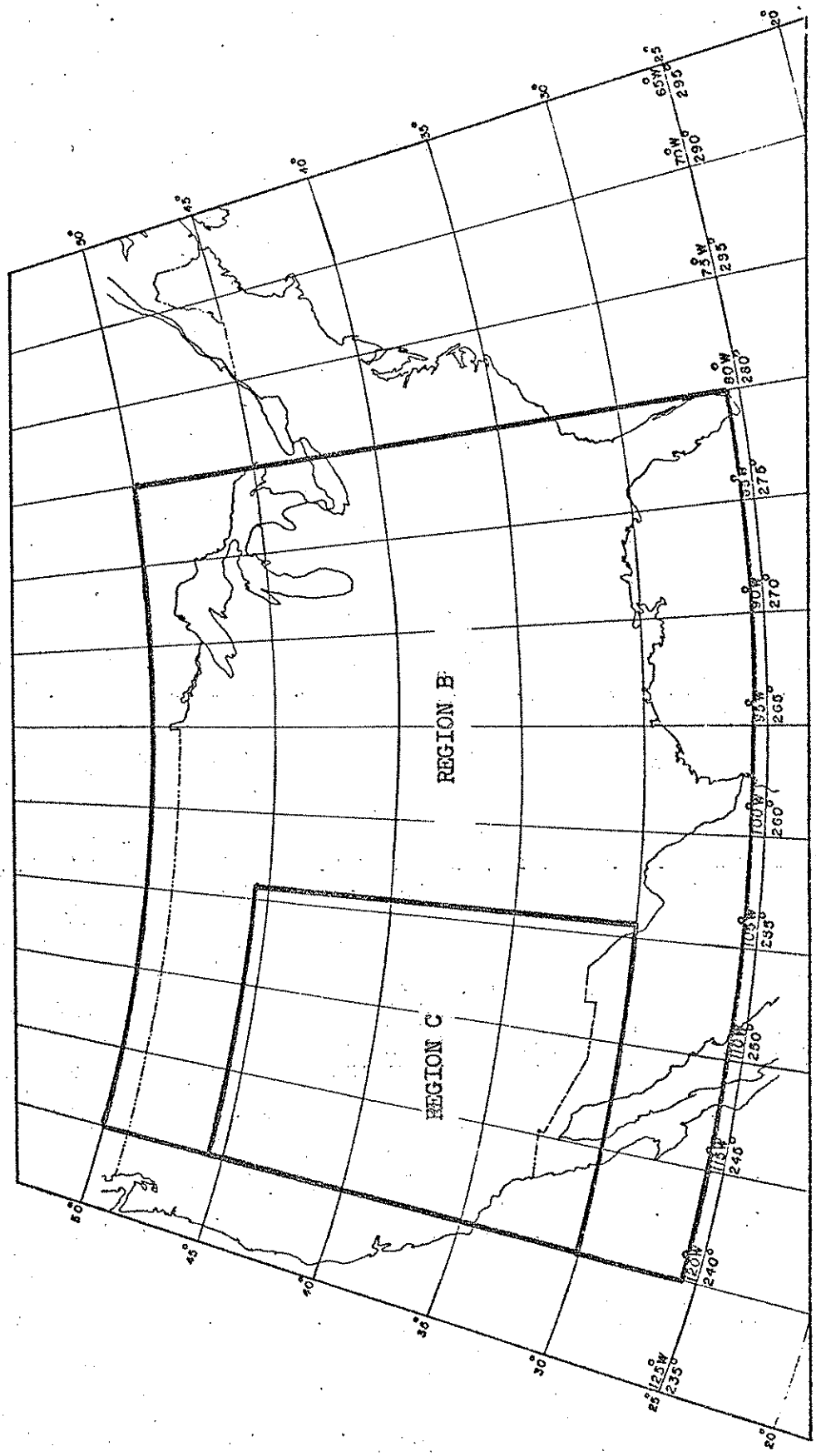

Figure 8. Gravity Model Regions

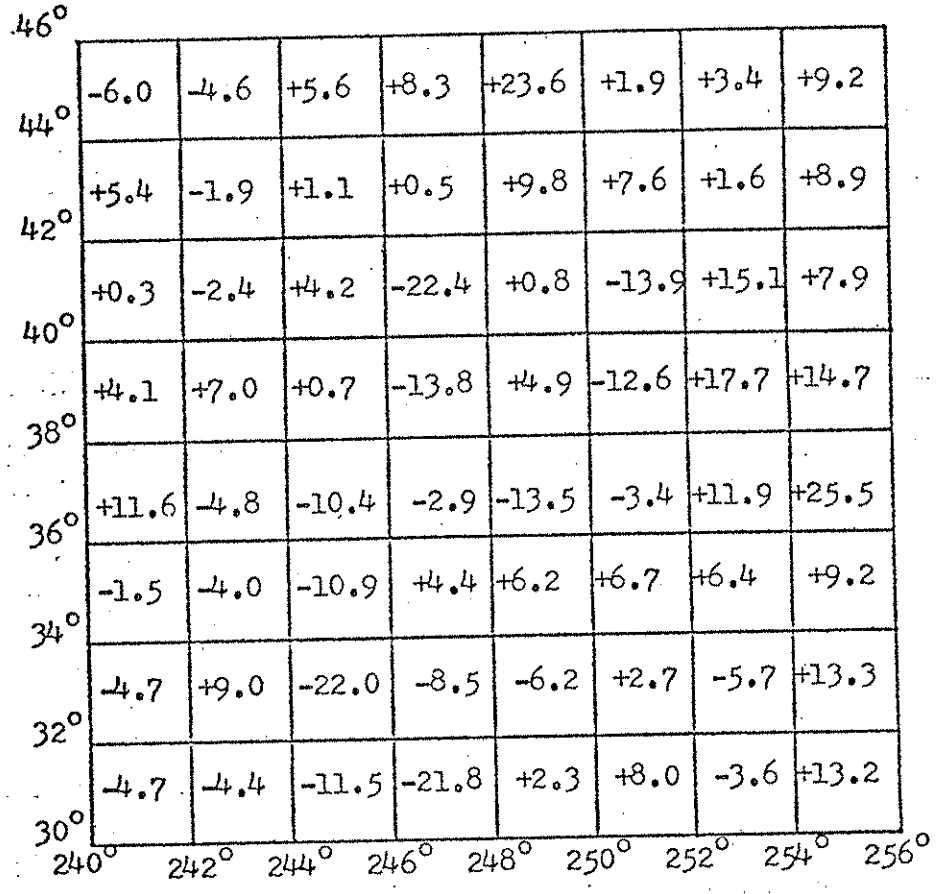

Figure 9. Mean Gravity Anomalies (mgal.) in 2° x 2° Blocks Residual to (14, 14) Spherop.

modified version of the point mass program developed by Needham (1970). The modifications were limited to reducing the amount of computer core storage required. The specifications for point mass models given by Needham require an over-determination ratio (anomalies/point masses) of about 1.6 and a mass depth to block side ratio of at least 0.8. The model formed here used a depth of 200 kilometers. The number of masses was determined from 3 possible solutions having over-determination ratios in the neighborhood of 1.6. The 152 mass solution was selected as the best fit to the $2^\circ \times 2^\circ$ anomalies on the basis of the mean and RMS residual anomaly after fitting the masses. The results of the point mass solution are summarized in Table 6.

Table 6

Point Mass Solution Using $2^\circ \times 2^\circ$ Mean Anomalies

Depth of masses (km)	200
Latitude limits	26° N - 50° N
Longitude limits	240° E - 280° D
No. of anomalies used in solution	240
No. of unknown masses determined	152
Mean input anomaly (mgal)	1.34
RMS input anomaly (mgal)	11.27
Mean residual anomaly after fitting masses (mgal)	0.30
RMS residual anomaly after fitting masses (mgal)	5.72

7.2 Sensitivity of Gravity Gradients to Gravity Model Representations

As pointed out by Schwarz (1970), the coefficients in observation equations provide a measure of the sensitivity of the measured quantity to the unknown parameters. In Figure 10, the partial derivatives of the rotating gradiometer signal amplitude with respect to the mean value of the gravity anomalies in the 40 5° x 5° blocks (Set A) were computed and plotted for a point near the Eastern edge of model region B at 300 kilometers altitude. The subpoint is located at latitude 37.5° N, longitude 278°. These sensitivity coefficients may be viewed as the effect on the gradiometer signal amplitude of a block in which the anomaly is 1 milligal. This illustrates that the gradients are most responsive to the features of the gravity field arising from crustal masses directly beneath the observation point. However, this also implies that observation points over the boundaries of the model blocks will produce high correlation between adjacent blocks, while points directly over the blocks should provide good separation. This suggests that it would be desirable to filter out data taken near the block boundaries. This was not done in the simulated solution, but should be considered in operational reduction of gradiometer data for solutions of the type given in this study. Examination of the coefficients at other points within the model region indicate that the pattern of sensitivity contours in Figure 10 is fairly constant and exhibits symmetry about the observation point.

In the case of the point mass model the coefficients of the observation equations are on the order of 10^{15} to 10^{18} E per/cm^3 /sec^2. The size of the

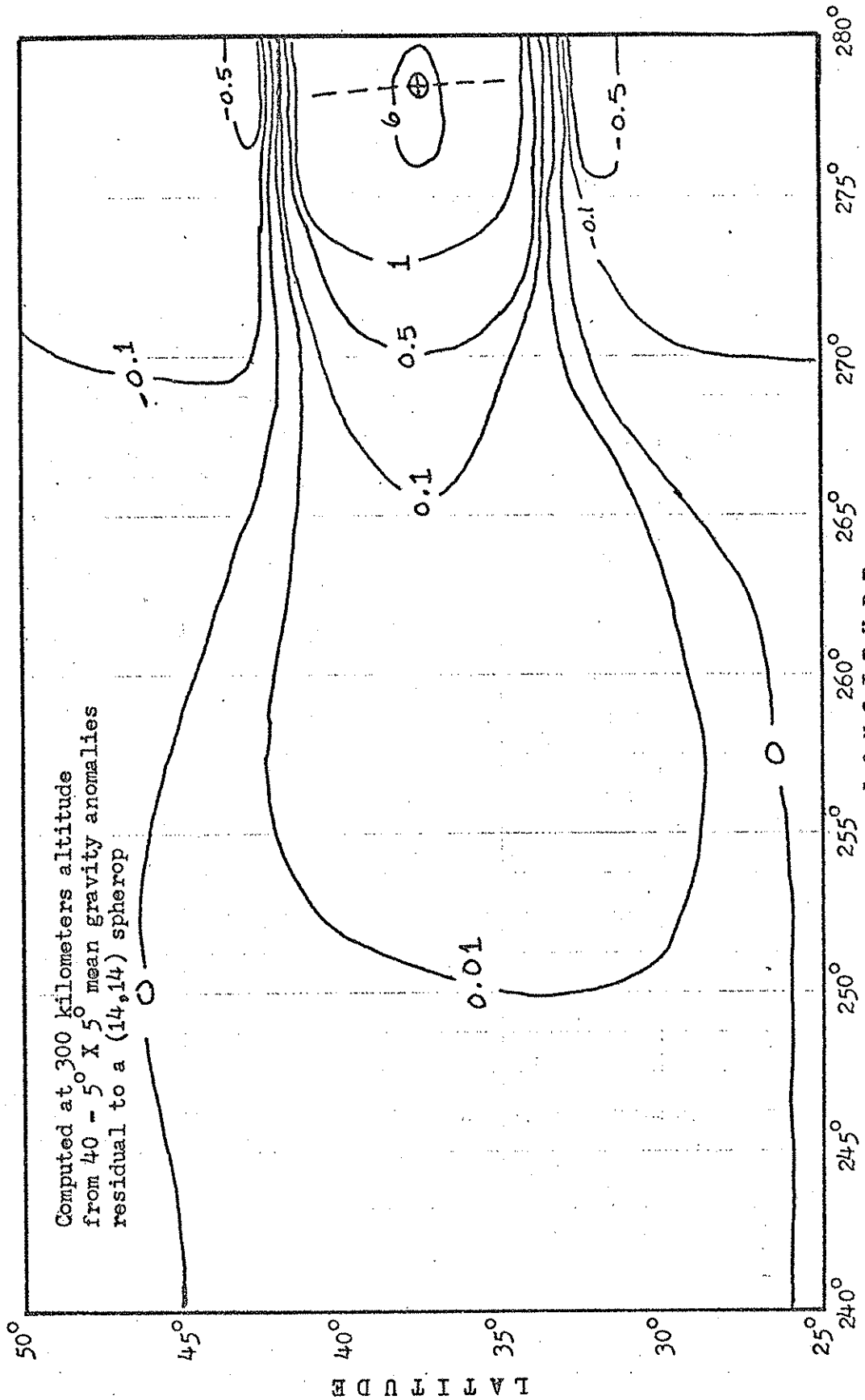

Figure 10. Sensitivity of Rotating Gradiometer Signal Amplitude in 10^{-2} Eotvos to Δg in Milligals at $\varphi = 37.5^{\circ}$, $\lambda = 278^{\circ}$

point masses in terms of km (see equ. 2.8) are on the order of 10^{14} cm^3/sec^2. This clearly indicates that the gradients are insensitive to this type of gravity representation. An explanation of this in addition to the sheet size of the masses arises from the fact that the masses are 200 kilometers beneath the earth's surface, and the coefficients are on the order of the inverse of the cubed sum of the altitude and the mass depth. The apparent lack of sensitivity seriously impacted on solutions attempted with the point mass model which are discussed later in this chapter.

7.3 Experimental Solutions Using Simulated Data

In this section we will describe the simulation experiments and the results of the simulated solutions. Several series of solutions were performed to evaluate the potential capabilities of satellite gradiometry. The solutions test the gradiometer configurations considering accuracy and sensitivity of the measurements and density of the observational data. In addition, the solutions evaluate the effect of the gravity model representation on the solutions.

7.3.1 Preliminary Considerations of Data Simulation

Attempts to conduct experiments which require generation of fictitious data simulating dynamic measuring systems presents certain difficulties in achieving a satisfactory degree of realism. Satellite gradiometers are dynamic systems whose signal output is associated with a threshold measuring sensitivity and finite time response. What this implies is that computing point values of the signals from some model will in all likelihood fail to be representative of the signals measured under dynamic conditions. In computing the fictitious

data it may seem desirable to have models which, in this case, represent the maximum possible spectrum of the external gravity field. Indeed this would be the case if accurate point values were being sought. We could theoretically compute a sufficient density of such point values and obtain some functional operator which would simulate the measuring systems dynamic integration of the point values over some finite period of time. In this manner, provided we have chosen the proper operator, smoothed values simulating the signal output could be obtained. Alternatively, consideration can be given to smoothing the model itself.

From the estimates given in Chapter 4, the upper limit of gradiometer resolutions at a nominal altitude of 300 kilometers is about degree 90 at a measuring sensitivity of 0.01 E. Assuming that a real gradiometer of this sensitivity would selectively filter out all wavelengths represented by degrees greater than 90, the model should not contain those wavelengths. To test this hypothesis, trial rotating gradiometer solutions were run to recover 64 2° x 2° gravity anomalies from point values of the gradiometer signal amplitude computed from 256 1° x 1° anomalies at 30 second intervals along the satellite trajectories generated at 300 kilometers over model region C (Figure 8). The resulting solutions produced large errors in the recovered anomalies. Only 8 of the recovered anomaly errors were less than 1 milligal while 23 errors were in excess of 5 milligals. Six errors were greater than 10 milligals with one over 20 milligals. These results indicate that the roughness of the point values computed from the 1° x 1° anomalies cannot be

adequately smoothed just through the adjustment itself.

To further illustrate the roughness of the signal amplitude point values, a single trajectory pass was generated at 300 kilometers over the approximate center of model region C using a 5 second step size. The point values of the rotating gradiometer anomalous signal amplitude were computed from $1^\circ \times 1^\circ$ anomalies (set D), and from $2^\circ \times 2^\circ$ anomalies (set C) using a center point quadrature and a 4 point quadrature of the $2^\circ \times 2^\circ$ blocks. The results are plotted in Figure 11. In addition the norm of the anomalous acceleration at each point was also computed from the $1^\circ \times 1^\circ$ anomalies and is plotted in Figure 11. Considering that a 30 second gradiometer integration time represents smoothing over about 2 degrees of the trajectory arc, it was judged that the point values computed from $2^\circ \times 2^\circ$ anomalies using the 4 point quadrature was adequately representative of the smoothed gradiometer signal amplitude.

7.3.2 Experiments Using the Point Mass Model

As discussed in section 7.2, the gradients at orbital altitude show poor sensitivity to the point mass representation. Experimental solutions using the 152 point masses (set E) for both the rotating system and the hard-mounted system were judged to be unsatisfactory. These solutions were characterized by uncertainties and errors of about the same magnitude as the true values. Solutions were initially attempted using orbital passes with a cross-track spacing of about 2°. Reducing the cross-track spacing to about 1° made no marked improvement in the solution. Attempts at scaling the normal equation proved fruitless. Although this was not attempted, a satisfactory solution might

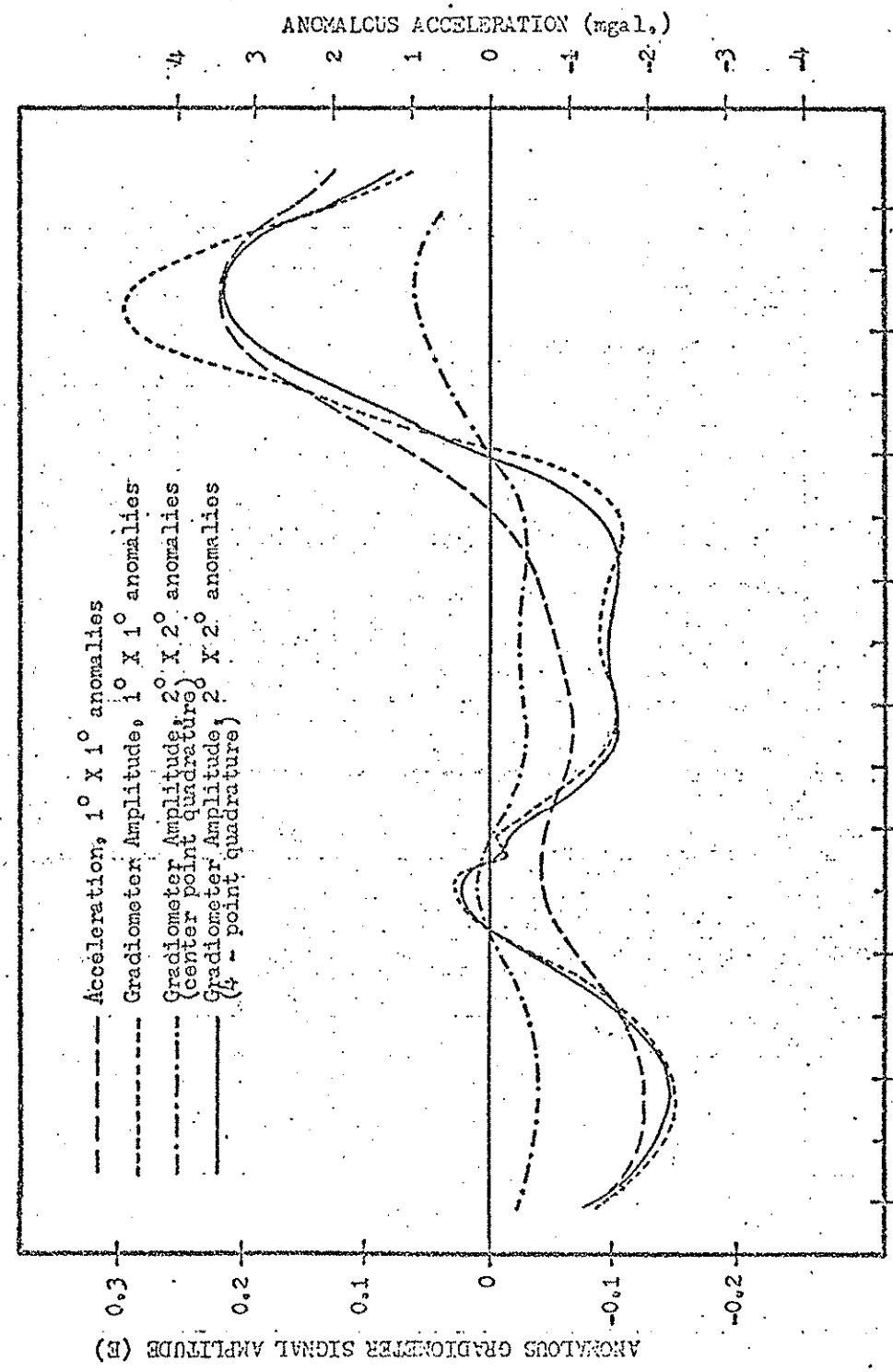

Figure 11. Variation of Anomalous Acceleration and Anomalous Signal Amplitude for a Rotating Gradiometer at 300 Kilometers Orbital Altitude.

be obtained if approximate values of parameters other than zero were used in forming the observation equations. However, the magnitude of the point mass values (km) are of the order 10^{14} cm^3/sec^2 and may be positive or negative. It would be unreasonable to expect such quantities to be estimated apriori.

All subsequent experiments discussed make use of the mean residual gravity anomaly representation.

7.3.3 Simulated Rotating Satellite Gradiometer Solutions

More emphasis has been placed on the rotating gradiometer system in the experiments because it is the most likely candidate system for real data collection.

7.3.3.1 Experiment with 300 Kilometer High Orbits

The initial series of solutions using the 64 2° x 2° residual gravity anomalies (set B), were designed to determine the density of orbital passes required to separate the 2° x 2°, and the effects of weights based on apriori estimates of the standard error of the observations. Based on the proposed design measuring sensitivity of 0.01 E, (Gardner, et al., 1972) it is reasonable that the standard error of the measurements should be compatible with the sensitivity. Whether or not this can be achieved in a real gradiometer system remains to be seen.

A solution was attempted using 14 orbital arcs of a polar circular orbit with 7 passes ascending and 7 descending. Correlation between adjacent blocks was found to be highly asymmetric; east and west through the center of

the model region. Examination of the locations of the data points showed that several data points were on or near the block boundaries with no points near the center of the blocks. Consequently, some blocks could not be adequately separated. Fourteen additional arcs were added so that there were at least two data points nearly over the center of each block. These arcs were also divided evenly between ascending and descending passes. This reduced the cross-track spacing of the passes to about 1°.

A series of 3 solutions were then run to evaluate the solutions considering the effect or random errors on the observations and truncation of the simulated data to simulate measuring sensitivity.[1] The first two solutions did not include conditions on the zeroth degree term (see page 103).

Solution 1.1 used untruncated data without simulated errors. The weights on the observations were generated using a standard error of 0.01 E. The errors in recovering the anomalies are shown in Figure 12. The mean of the differences (adjusted - true) or errors was -0.032 mgal. and the RMS difference of adjusted anomalies was 1.92 mgal. The mean anomaly recovered over the 16° x 16° block (Region C) was 0.09 mgal compared to the block mean of the true values of 1.00 mgal. While the individual anomalies are recovered fairly well, considering the regional mean indicates a need to constrain the solution as discussed in Chapter 6.

---

[1]Truncation here is defined to mean the rounding off of the computed gradients or signal amplitudes to a pre-determined number of significant digits consistent with the measuring sensitivity of a gradiometer.

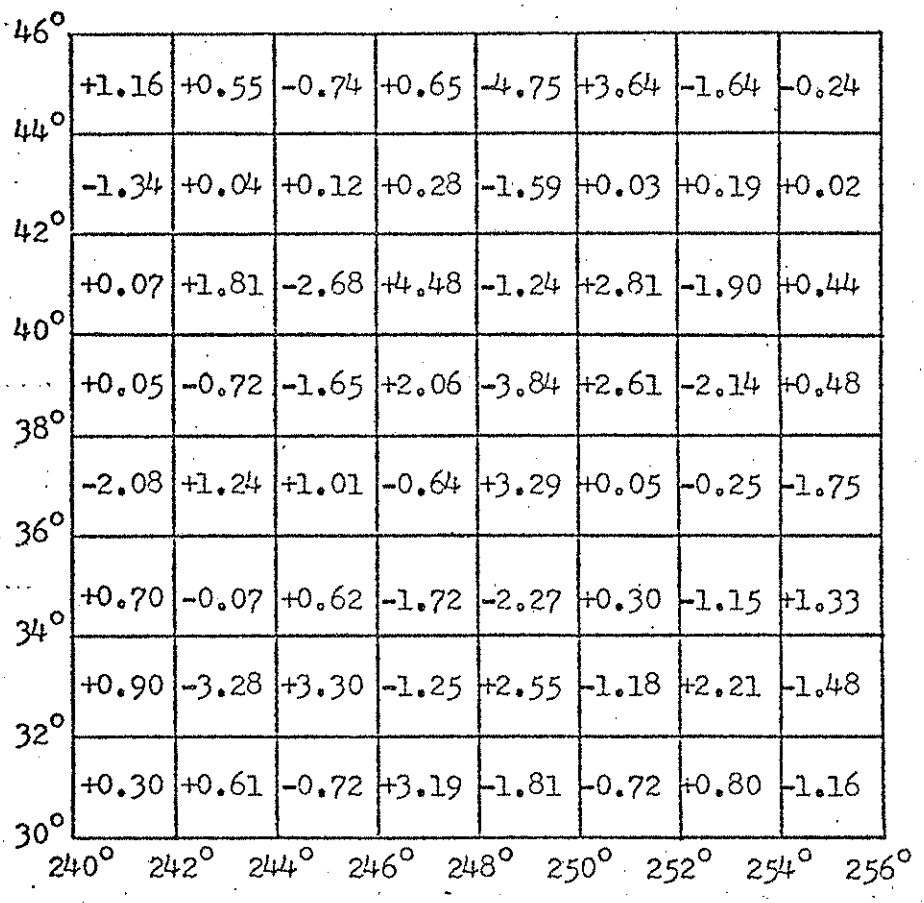

Figure 12. Errors in Recovery of Gravity Anomalies (mgal.) (Rotating Gradiometer, solution 1.1, No Errors, No Truncation, No Constraints, 300 kilometer Orbit)

Solution 1.2 was run with the same basic data as in solution 1.1. However, in this case the generated observations were truncated to 0.01 E. In addition, simulated normally distributed errors were generated for the observations using subroutine GAUSS which is a normal deviate generator available in IBM Scientific Subroutine Package (IBM, 1968). The errors were specified to have a mean of zero and a standard deviation of 0.01E. None of the generated errors exceeded 4 . Figure 13 shows the errors in recovering the anomalies. The mean error is -0.39 mgal. and the RMS error is 3.45 mgal. The recovered block mean is 0.61 mgal. From the standpoint of the anomaly errors, this solution is judged to be unsatisfactory. A probable reason for this is that the generated errors have in some of the data overwhelmed the truncated signal amplitude.

Solution 1.3 again used the same basic data as before. Truncation of the signal amplitude and generated errors were also applied. However, the condition on the zeroth degree term was included in this solution. The adjusted differences associated with this solution are in Figure 14. The pertinent statistics pertaining to the solution are summarized as follows:

16° x 16° adjusted mean anomaly	=	1.00 mgal.
Mean difference in adjusted anomalies	=	-0.001 mgal.
RMS difference in adjusted anomalies	=	1.13 mgal.
Mean error imposed on observations	=	-0.001 E
RMS error imposed on observations	=	0.01 E
Mean observation residual after adjustment	=	0.005 E

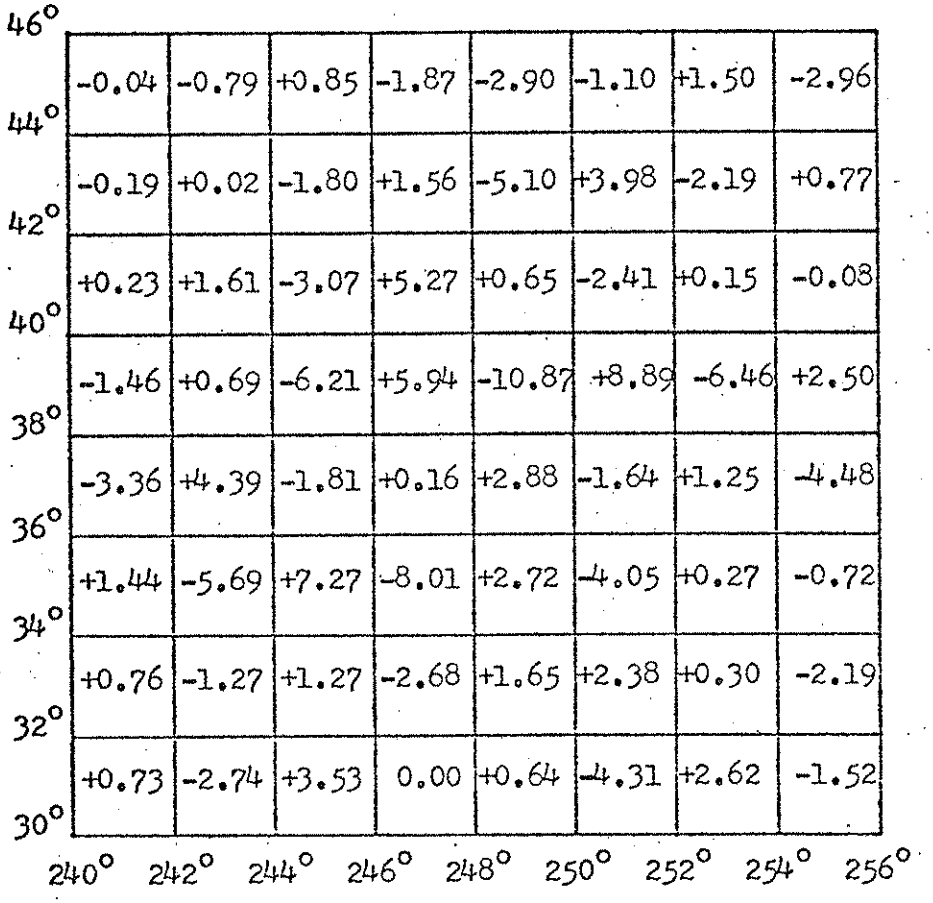

Figure 13. Errors in Recovery of Gravity Anomalies (mgal). (Rotating Gradiometer, Solution 1.2, Truncated at 0.01 E, Errors Imposed, No Constraint, 300 kilometer Orbit).

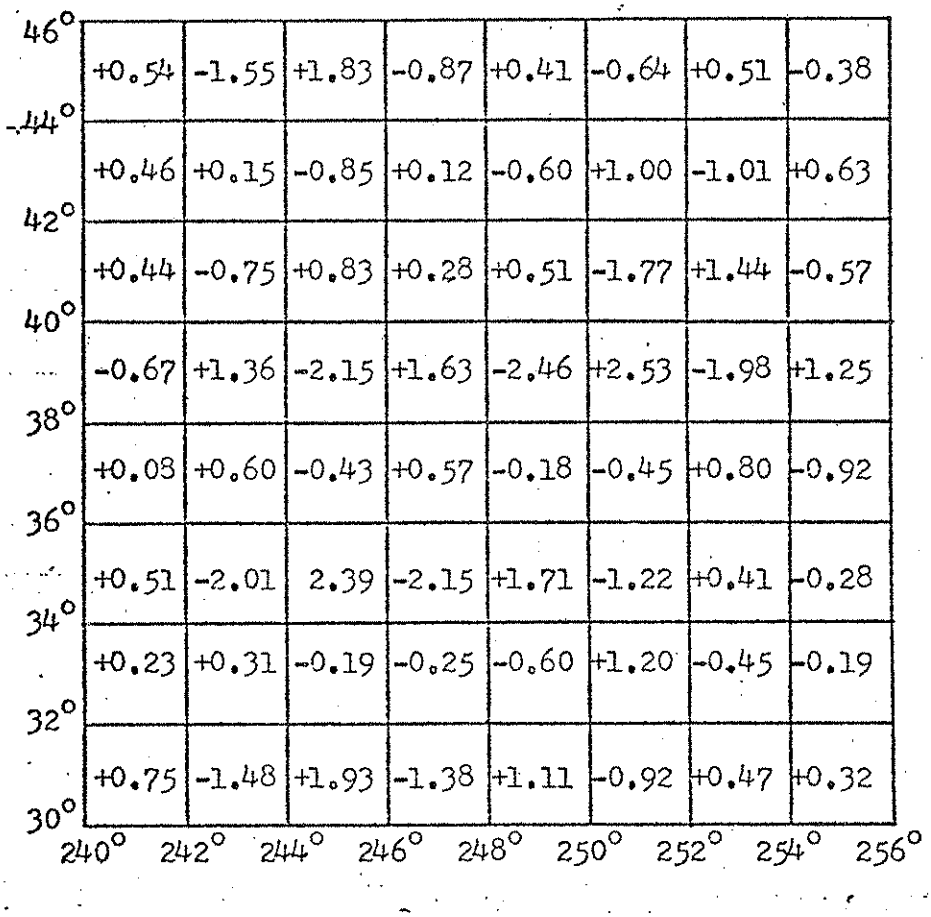

Figure 14. Errors in Recovery of Gravity Anomaly (mgal.) (Rotating Gradiometer, Solution 1.3, Truncation at 0.01 E, Errors Imposed, Zeroth Degree constraint, 300 kilometer Orbit).

RMS observational residual after adjustment	=	0.01 E
Standard Errors of Unit Weight after adjustment	=	1.22

The standard errors of the recovered anomalies are given in Figure 15. Although this figure is specifically associated with the last solution in the series, it is typical of the standard errors in solutions 1.1 and 1.2. The correlation between the recovered values in neighboring blocks is described by the typical correlation pattern below.

1.0	-0.80	+0.55	-0.30
-0.40	+0.35	-0.25	+0.15
+0.20	-0.15	+0.10	-0.05
-0.05	+0.05	-0.05	+0.00

This pattern is interpreted by imagining the number in the upper left-hand corner to be the correlation of the block with itself. The number in the second column of the first row is the correlation of a block with its immediate neighbor to the east or west. The third number in the first row is the correlation of a block with another block at the same latitude when a third block separates them, and similarly for the fourth number in the first when two blocks intervene between them. Going down the columns describes correlations of a block with other blocks to the north and south in the same manner. The actual correlation coefficients for any particular block may vary as much as ±0.05 from these values.

The pattern of the standard errors in this solution exhibit definite edge

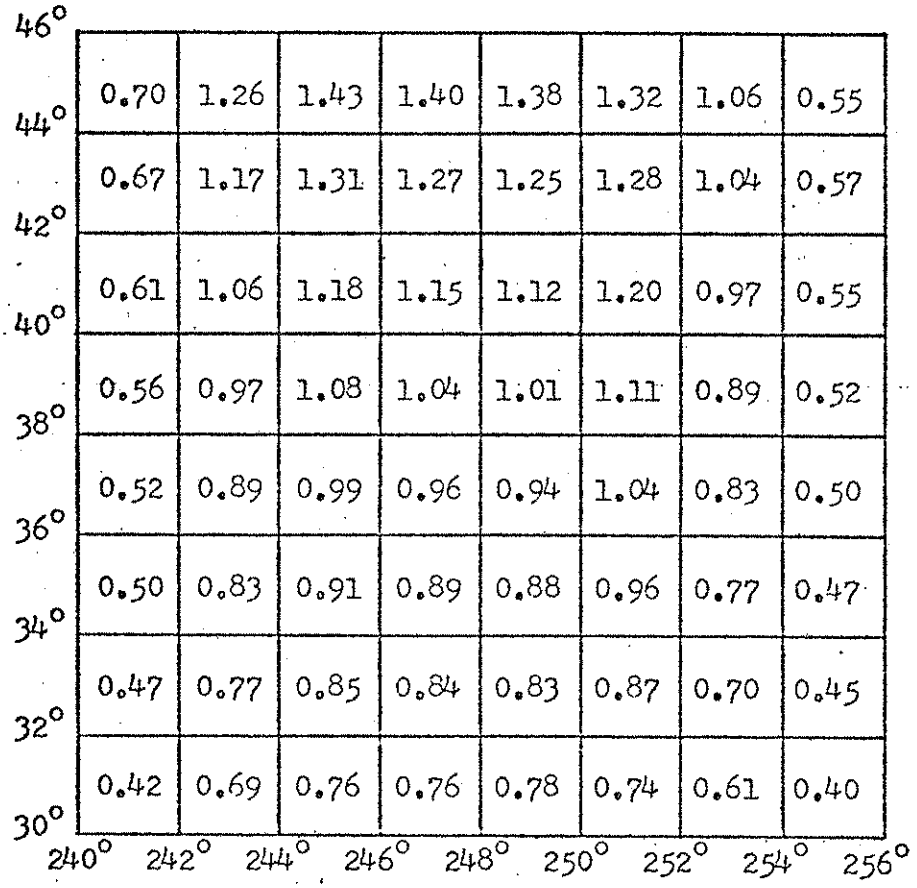

Figure 15. Standard Errors of Recovered Anomalies (mgal). (Rotating Gradiometer, Solution 1.3, 300 kilometer Orbit).

effects as the errors increase inward from the east and west sides. The systematic increase of standard errors from south to north are probably associated with the reduction of surface area toward the north.

It was encouraging to see that the adjustment model removed the errors in the observations as indicated by the mean and RMS of the signal amplitude residuals. Other than the fact that the separation of blocks in the east and west directions can only be considered fair, the overall solution results are satisfactory.

7.3.3.2 Experiment with 250 Kilometer High Orbits

In order to see if the block separation could be improved, 29 orbital arcs were generated over model region C at 250 kilometers altitude. The passes were divided between 14 ascending and 15 descending. Greater care was taken with these passes to have the data points fall as near as possible to the center of the blocks.

For sake of comparison, solution 2.1 was run using the same procedures previously described for solution 1.2, that is, truncation of signal, addition of errors and no conditions imposed. The resulting differences in the adjusted anomalies are given in Figure 16. These results show improvement over solution 1.2, since there are only 6 differences in excess of 4 milligals in solution 2.1 compared to 14 differences in solution 1.2. In solution 2.1, the mean difference is -0.53 mgal. and the RMS difference 2.64 mgal. The block mean recovered is 0.47 mgal.

A second experiment at 250 kilometers, solution 2.2, added the condition

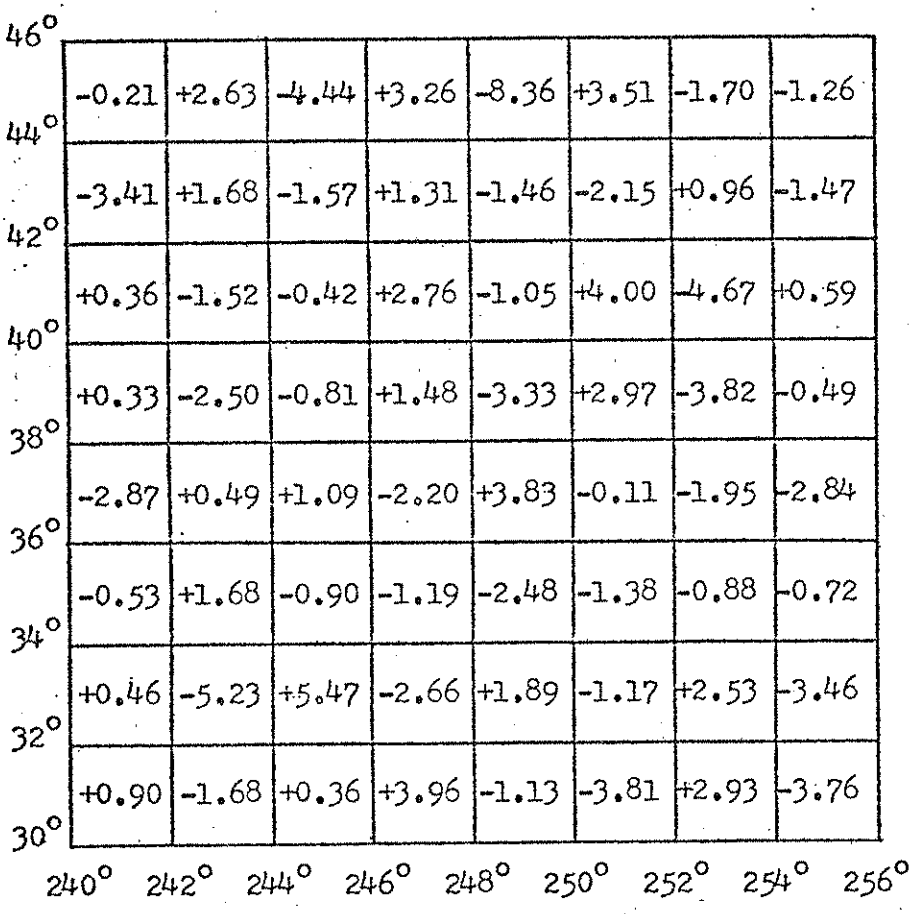

Figure 16. Errors in Recovery of Gravity Anomalies (mgal.) (Rotating Gradiometer, Solution 2.1, Truncation at 0.01 E, Errors Imposed, No Constraints, 250 kilometer Orbit).

on the zeroth degree harmonic. Anomaly errors are shown in Figure 17 and the standard errors in Figure 18. Statistical data for this solution is as follows:

16° x 16° adjusted mean anomaly	=	1.00 mgal.
Mean difference of adjusted anomalies	=	0.00 mgal.
RMS difference of adjusted anomalies	=	0.45 mgal.
Mean error imposed on observation	=	-0.001 E
RMS error imposed on observations	=	0.01 E
Mean observation residual after adjustment	=	0.007 E
RMS observation residual after adjustment	=	0.01 E
Standard error of unit weight after adjustment	=	1.36

The typical pattern of correlation coefficients for solution 2.2 shown below indicates some improvement in block separation cross-track and significant improvement along-track:

1	-0.75	+0.45	-0.25
-0.25	+0.15	-0.10	+0.05
+0.05	-0.05	+0.02	-0.01
-0.01	+0.01	-0.00	0.00

The actual pattern for any given block may vary about ± 0.05. While the uncertainties again show a definite edge effect and a tendency to increase to the north, the effect is somewhat less pronounced. In general one would be

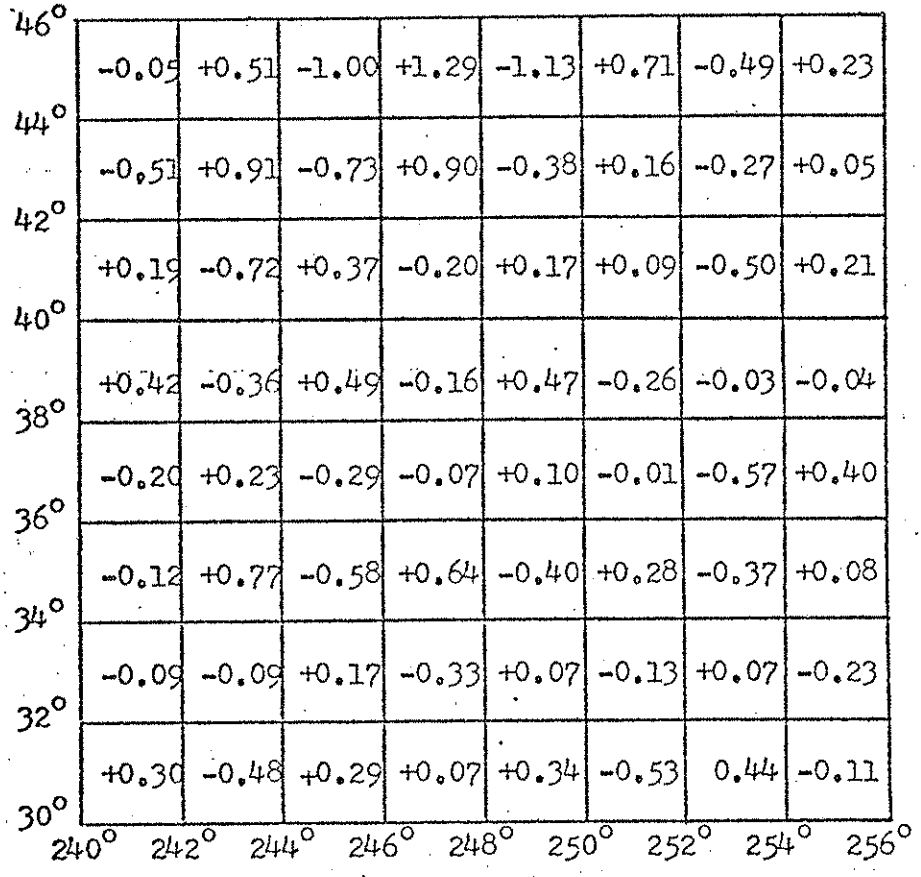

Figure 17 Errors in Recovery of Gravity Anomalies (mgal.) (Rotating Gradiometer, Solution 2.2, Truncation at 0.01 E, Errors Imposed, Zeroth Degree Constraint, 250 kilometer Orbit).

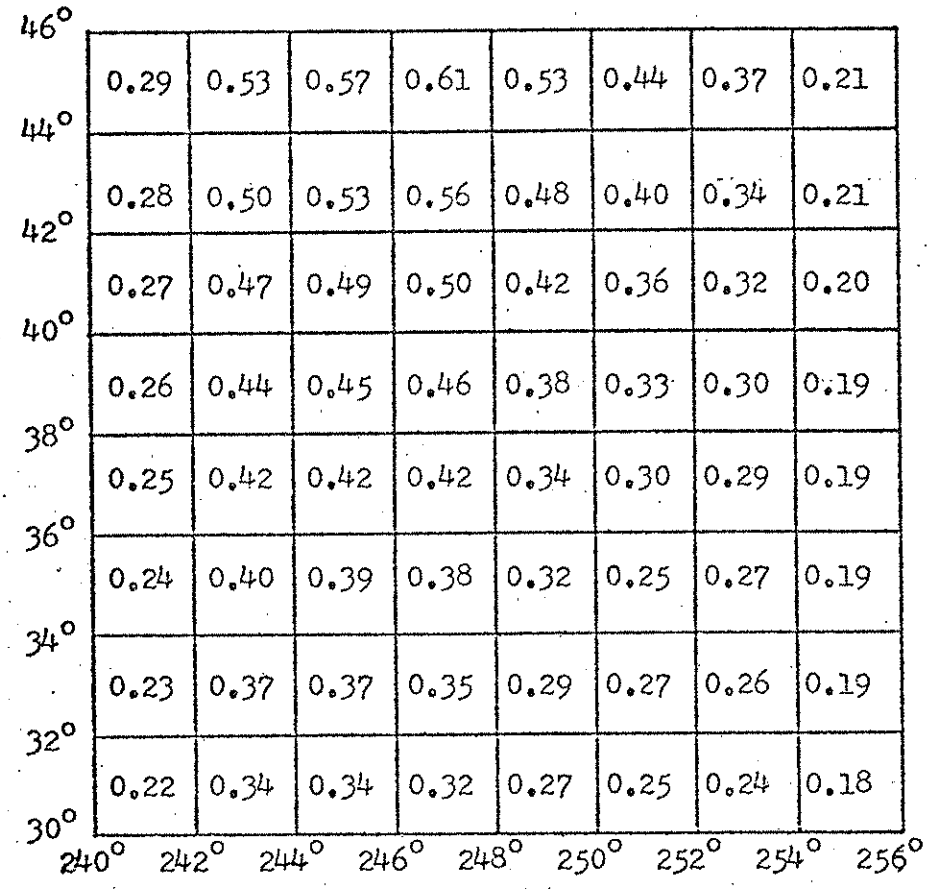

Figure 18 Standard Errors of Recovered Gravity Anomalies (mgal.) (Rotating Gradiometer, Solution 2.2, 250 kilometer Orbit).

inclined to say that the results of this solution are embarassingly good.

7.3.3.3 Experiment Combining Data at 250 and 300 Kilometer Altitude

We know that a satellite orbit at the relatively low altitudes envisioned for gradiometer missions will decay rapidly due to atmospheric drag. Consequently, one can expect to obtain data from more than one altitude. In fact, the simulated perturbed orbits generated for these experiments ranged about ± 20 kilometers about the nominal altitudes. As a result we have from both the simulated orbits the possibility of gradiometer observations over a range of about 230 kilometers to 320 kilometers altitude. Assuming that the orbital life is sufficiently long, say about 40 days, a considerable amount of data may be collected over any region of the earth within this range of altitudes. To test the value of combining observations over a range of altitudes, solution 3.1 combined all of the data generated for solutions 1.3 and 2.2

Resulting anomaly errors and uncertainties for this combined altitude solution are shown in Figures 19 and 20. Significant statistics of this solution are:

16° x 16° adjusted mean anomaly	=	1.00 mgal.
Mean difference in adjusted anomalies	=	-0.00 mgal.
RMS difference in adjusted anomalies	=	0.33 mgal.
Mean error imposed on observations	=	-0.000 E
RMS error imposed on observations	=	0.01 E
Mean observation residual after adjustment	=	0.005 E

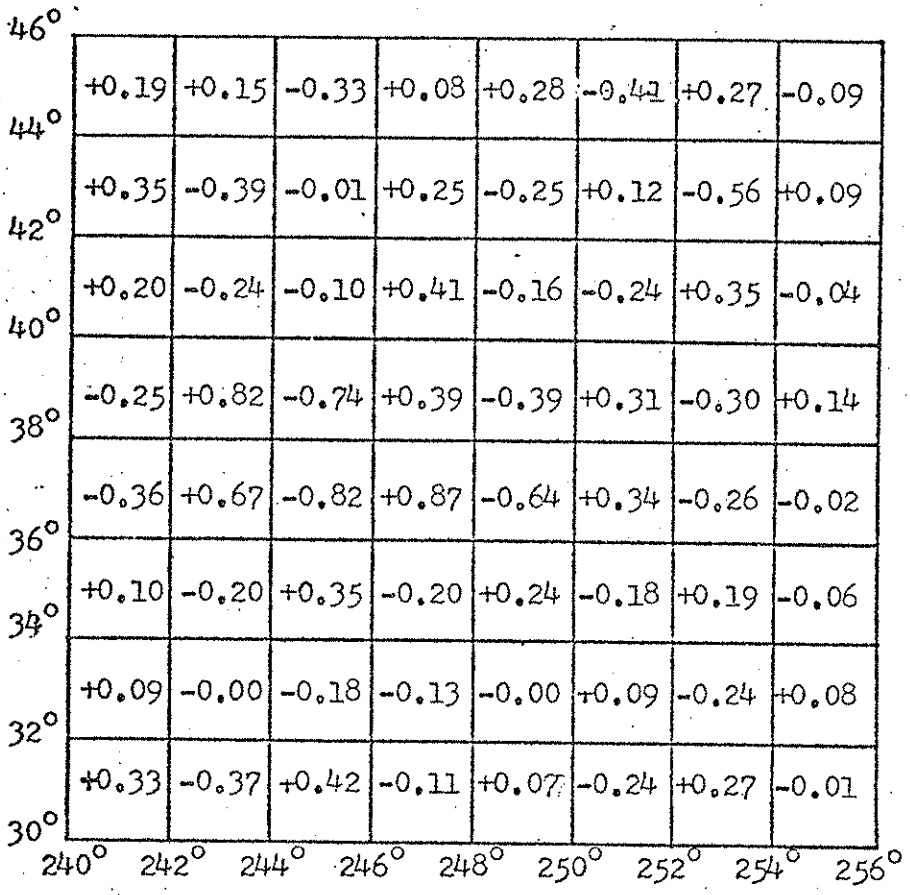

Figure 19 Errors in Recovery of Gravity Anomalies (mgal.) (Rotating Gradiometer, Solution 3.1, Truncation at 0.01 E, Errors Imposed, Zeroth Degree Constraint, Combination of 250 and 300 kilometer Oribts).

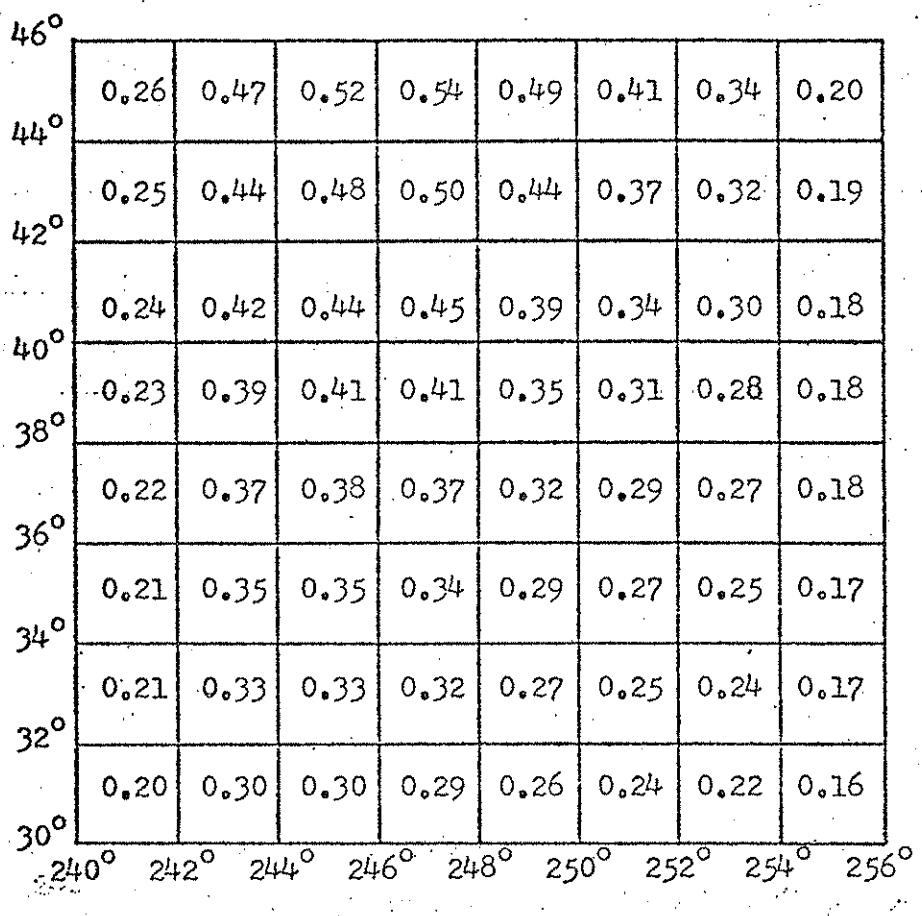

Figure 20 Standard Errors of Recovered Gravity Anomalies (mgal.) (Rotating Gradiometer, Solution 3.1).

RMS observation residual after adjustment	=	0.01E
Standard error of unit weight after adjustment	=	1.23

A somewhat surprising result of this solution may be seen by comparing the correlations here with those for solution 2.2. The pattern of the correlation coefficient given below show a slight degradation of the cross-track block separation for immediately adjacent blocks:

1	-0.80	+0.45	-0.25
-0.25	+0.20	-0.10	+0.05
+0.05	-0.05	+0.02	-0.02
-0.02	0.01	-0.00	0.00

Further comparing the error in anomaly recovery with solution 2.2 indicated 21 errors were increased. The only significant reduction in error occurred in the 6 interior blocks along the northern edge. We also see little or no differences in the uncertainties. Thus we can conclude that combining rotating gradiometer data over the full range of orbital altitudes does not enhance the solution; hence, would be an unjustifiable effort.

A comment should be made here concerning the fairly poor cross-track correlation in the solutions to this point. The sensitive axes of a rotating gradiometer are oriented generally the direction of the vertical and along the plane of the orbit. It seems reasonable then that the lack of cross-track directivity causes the correlations to be higher east and west.

7.3.3.4 Experiment with 300 Kilometer High Orbits Over 5° x 5° Anomaly Blocks

Solution 4.1 for the simulated rotating gradiometer used data generated from 20 days of a simulated orbital arcs over model region B. A total of 840 simulated gradiometer observations were generated over the region. The gravity model used 40 5° x 5° residual gravity anomalies (set A). Although the amount of data used is probably much more than necessary to solve for 5° x 5° anomalies, this solution does show what the gradiometer may be able to do with sufficiently smoothed data. In this solution the anomalous gradients were computed by four point quadrature of the 5° x 5° blocks. The signal amplitude was truncated at 0.01E and normally distributed errors were added to the computed signal amplitude. No conditions were added to the solution.

The anomaly error and uncertainties are shown in Figures 21 and 22. Of interest in this solution is the nearly constant negative errors of the recovered anomalies. A possible explanation might be a slight bias in the reconcilation of the terrestrial gravity data with the satellite derived harmonics which was carried out by Needham (1970).

The typical correlation pattern for this solution still shows the tendency to high cross-track correlations:

1	-0.40	+0.10
-0.04	+0.02	-0.01
+0.01	+0.01	-0.00

Note the unusual pattern of positive and negative correlations as compared to the previous solutions. This solution does give an indication that the rotating gradiometer system potentially can resolve harmonic terms over a broad band.

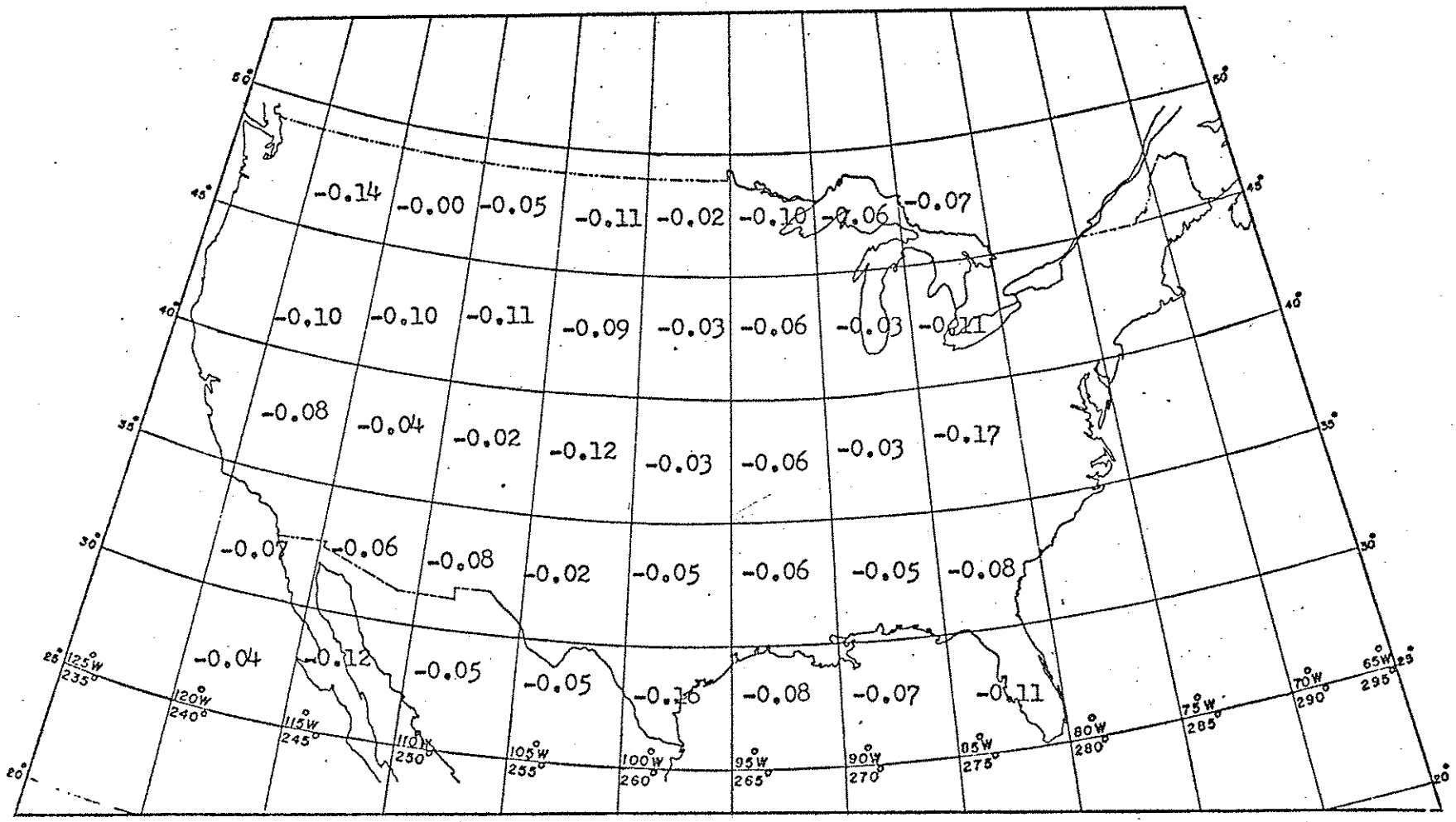

Figure 21 Errors in Recovered Anomalies (mgal.), (Rotating Gradiometer, Solution 4.1, Truncation at 0.01 E, Errors Imposed, 300 kilometer Orbit).

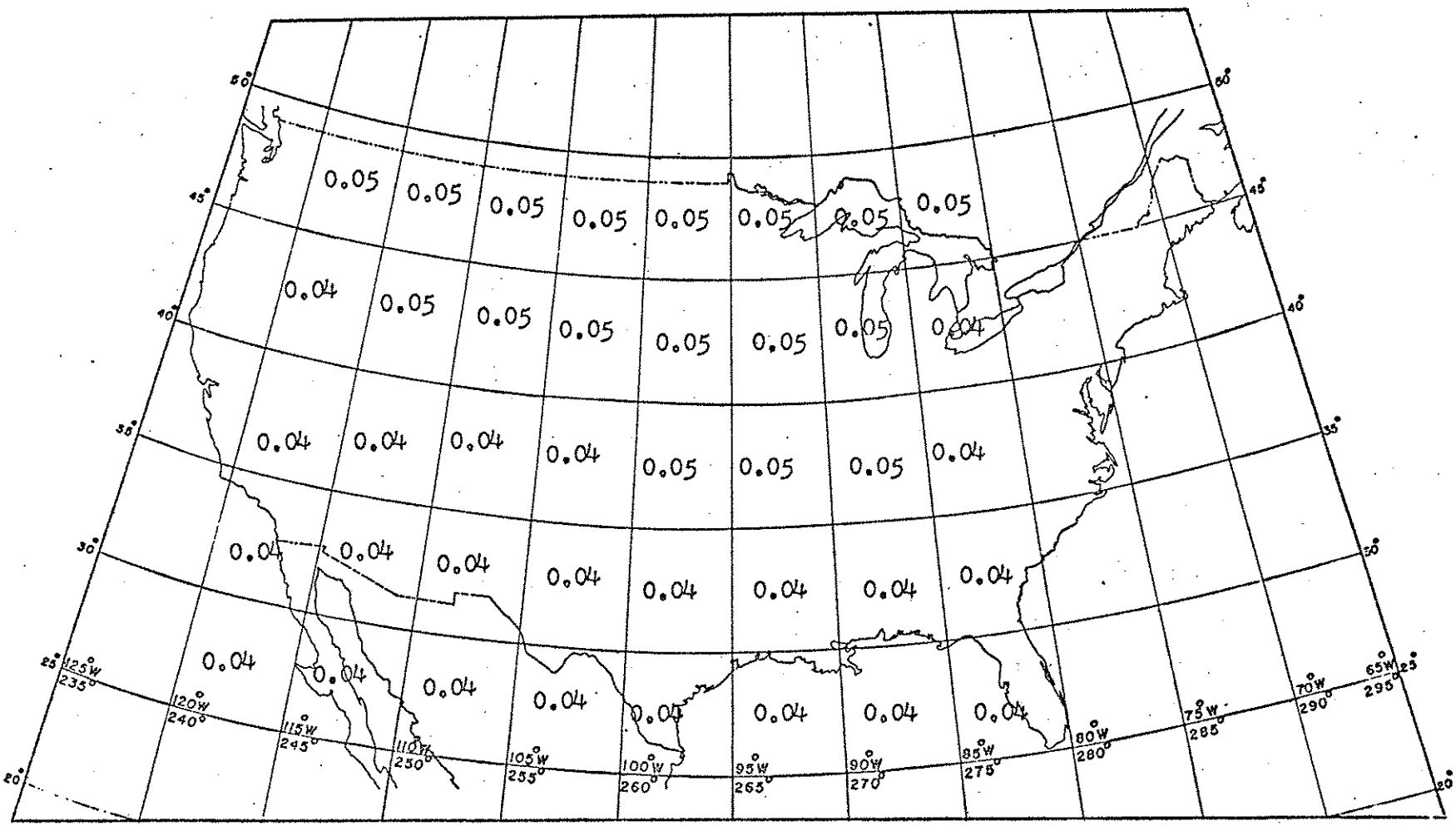

Figure 22 Standard Errors in Recovered Anomalies (mgal.)
(Rotating Gradiometer, Solution 4.1).

7.3.3.4 Subconclusions (Rotating Gradiometer Solutions)

Comparison of the statistics for solutions 1.3 and 2.2 indicate that the gravity anomalies were recovered best from the 250 kilometer orbit with smaller standard errors. This tends to confirm an analysis by Glaser and Sherry (1972) that 250 kilometers is the maximum optimum altitude for resolution to degree 90. In addition, the differences in the two solutions can be attributed in part to improved geometry for the 250 kilometer altitude as greater care was taken in positioning the data points over the anomaly blocks. Solution 2.2 is judged to be the best solution for the rotating gradiometer.

7.3.4 Simulated Hard-Mounted Satellite Gradiometer Solutions

Generally the simulation experiments performed for the hard-mounted gradiometer system were similar in principle to those described in the previous section. It would be possible to hypothesize several hard-mounted gradiometer configurations where the components of the gravity gradient tensor are measured individually or in various combinations. This was not done in this investigation. The tensor components assumed to be measured in all of the experiments described below are as follows:

$$V_{11},\ V_{12},\ V_{13},\ V_{22},\ V_{23}$$

7.3.4.1 Experiments Wtih 300 Kilometer High Orbits

Since orientation parameters are included in the adjustment model for the hard-mounted system as observables, an apriori estimate of the accuracy of these parameters is required. Grosch, et al (1969) and Grosch

(1967) in analytical studies and actual satellite experiments with the Self-Contained Navigation System on ATS-III found that the RMS three axis attitude errors were in the range of 20 seconds to 1.5 minutes of arc. The better accuracy being obtained when the satellite was in the earth's shadow.

In preliminary tests, it was found that weights on the orientation parameters based on standard errors up to about 0.1 degree did not materially influence the results. This tends to confirm the analysis of allowable gradiometer orientation errors made in Gardner, et al (1972), assuming a measuring sensitivity of 0.01E. Subsequent experimental solutions with the hard-mounted system assume a standard error of 30 seconds of arc in the three Euler angles defining the orientation.

Solution 5.1 was designed to test the effect of equal relative weights on the gradient observations. In this solution the 26 orbital arcs over model region C described in section 7.3.3.1, were used. Since the gravity anomalies are linear functions of the gravity gradients in the mathematical model (see Chapter 6), using simulated data without truncation or addition of errors on the observed gradients, the recovered anomaly errors should be nearly zero. However, even with the addition of the zeroth degree constraint the solution did not approach zero errors. Additionally, observation residuals were relatively large in the cross-gradients.

The problem here appears to be related to the findings in Chapter 4, which indicate that the V_{12}, V_{13}, V_{23} gradient tensor components do not contain significant information to harmonic degree 90 when the measuring sensitivity is only 0.01E. Analysis of the estimates of the gradients remaining at degree

90 show the gradiometer sensitivity required by component to be approximately as follows in the 200-300 kilometer altitude range:

V_{11} and V_{22}	10^{-2} E
V_{12}	10^{-6} E
V_{13} and V_{23}	10^{-4} E

An interpretation of these sensitivities would indicate that the cross-gradient components contribute less information than the diagonal components. If we consider the sum of gradient degree variances by squaring the above sensitivity values, we see that the V_{11} and V_{22} components contribute 10^{8} times as much information as the V_{12} component, and 10^{4} times as much as the V_{13} and V_{23} components. Also note that V_{13} and V_{23} contribute 10^{4} times as much as V_{12}. Relative weights based on the reasoning here should be as follows:

V_{11} and V_{22}	$10^{8}/E^{2}$
V_{12}	$1/E^{2}$
V_{13} and V_{23}	$10^{4}/E^{2}$

Note that this use of relative weights is not the normal procedure in classical adjustment computations where weights are based on apriori estimates of the error covariances of the observed quantities. Normally, the solution is insensitive to the relative weights; however, solutions based on the weighting procedure given here do exhibit sensitivity. This weighting procedure has essentially the effect of allowing the solution to be carried by the V_{11} and V_{22} gradient components.

Now assuming the apriori standard error of unit weight to be 0.01, the

relative weights reduce to:

V_{11} and V_{22}	$10^4/E^2$
V_{12}	$10^{-4}/E^2$
V_{13} and V_{23}	$1/E^2$

The above weights were used in Solution 5.2. Again the simulated gradient observations were untruncated and error free. The zeroth degree constraint was included. The mean difference of the recovered anomalies was -0.00016 mgal., while the RMS difference was 0.0005 mgal., which indicates the relative weights based on the sensitivities are approximately correct. This also tends to confirm the reasonableness of the gradient estimates obtained in Chapter 4. The standard errors resulting from this solution are shown in Figure 23. Edge effects are still evident in the pattern of the standard errors. A typical pattern of correlation coefficients from this solution is shown below:

1	-0.75	+0.45	-0.25
-0.60	+0.50	-0.30	+0.15
+0.30	-0.25	+0.15	-0.05
-0.15	+0.10	-0.05	+0.02

The variation of this pattern for specific blocks is about ±0.05. While this solution is considered to be satisfactory, we must remember that the simulated data used is error free. Also the sensitivities assumed are more appropriately applied to gradients at about a 250 kilometer altitude.

7.3.4.2 Experiments at 250 Kilometer Orbital Altitude

Solution 6.1 used the orbital arcs over model region C described in

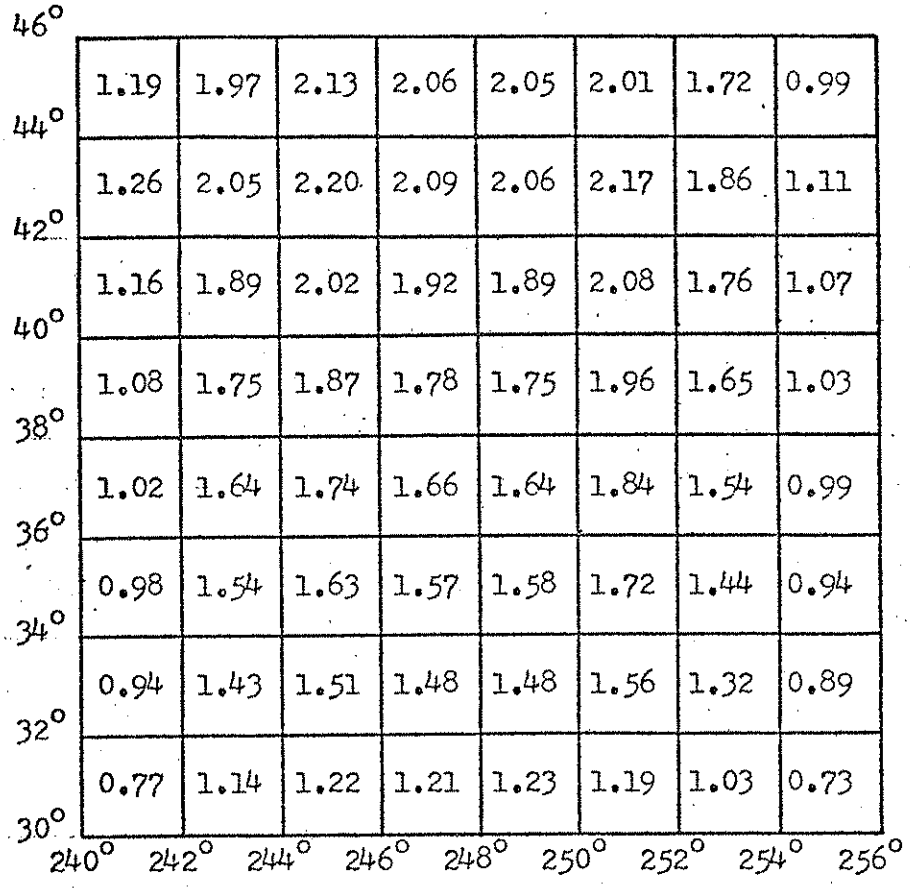

Figure 23 Standard Errors in Recovered Gravity Anomalies (mgal.) (Hard-Mounted Gradiometer, Solution 5.2, Relative Weights Based on Sensitivity, No Truncations, No Errors, Zeroth Degree Constraint, 300 kilometer Orbit).

section 7.3.3.2. Relative weights assigned to the gradient observations were identical to those used in solution 5.2. In this solution the mean anomaly difference was -0.00016 mgal., and the RMS anomaly difference 0.0004 mgal. Resulting standard errors are shown in Figure 24. While there is no marked difference in the recovered gravity anomalies, the standard errors are about half of those obtained at 300 kilometers. Some of this improvement may be attributed to slightly better positioning of the data points although the degrees of freedom for solution 6.1 is slightly greater than in 5.2. In all likelihood, improvement can also be attributed to the fact that the assumed relative weights based on sensitivities are more applicable to the lower altitude gradients. The correlation pattern from this solution is typically as follows:

1	-0.70	0.35	-0.20
-0.50	0.35	-0.20	0.10
0.15	-0.10	0.05	-0.02
-0.03	0.02	-0.02	0.01

Again the variation is about ±0.05. Comparing this pattern with that of the previous solution shows a marked improvement in block separation beyond the immediately adjacent blocks.

Solution 6.2 used the same simulated gradient data at 6.1. However, the gradient values were truncated to the number of digits corresponding to the indicated measuring sensitivity required (see page 143), and normally distributed errors were added to the simulated observations in the manner described on page 124. Figure 25 shows the resulting solution with the zeroth degree

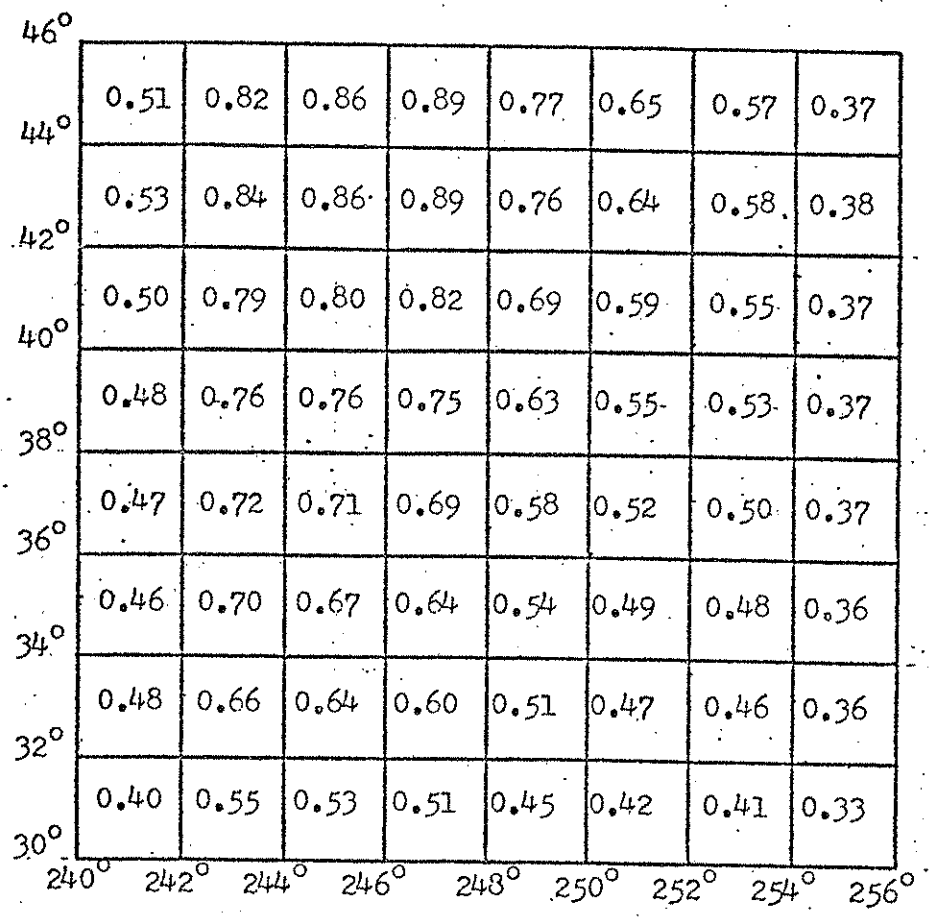

Figure 24 Standard Errors in Recovered Gravity Anomalies (mgal.), (Hard-mounted Gradiometer, Solution 6.1, Relative Weights Based on Sensitivity, No Truncation, No Errors, Zeroth Degree Constraint, 250 kilometer Orbit).

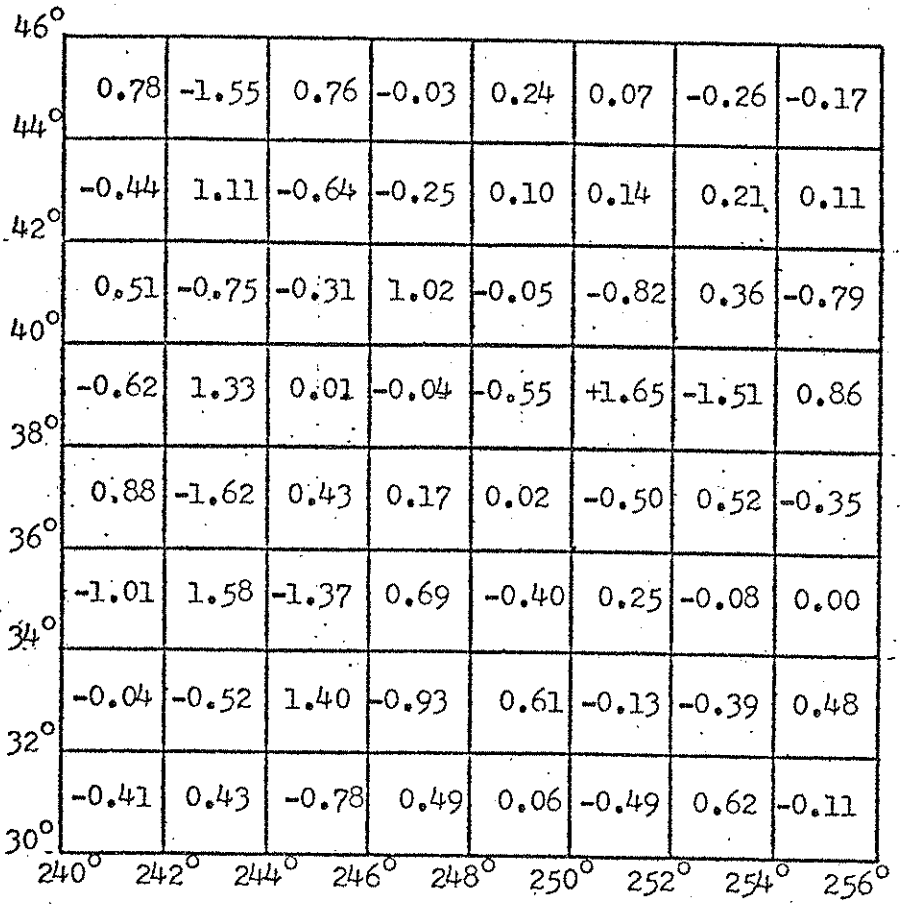

Figure 25 Differences in Recovery of Gravity Anomalies (mgal.) (Hard-mounted Gradiometer, Solution 6.2, Relative Weights and Truncation Based on Sensitivity, Errors Imposed, Zeroth Degree Constraint, 250 kilometer Orbit).

constraint included. The statistics of solution 6.2 are as follows:

16° x 16° mean anomaly after adjustment	=	1.00 mgal.
Mean difference in adjusted anomalies	=	-0.0002 mgal.
RMS difference in adjusted anomalies	=	0.72 mgal.
Mean error imposed on observations	=	-0.0004 E
RMS error imposed on observations	=	0.01 E
Mean observation residual after adjustment	=	-0.02 E
RMS observation residual after adjustment	=	0.04 E
Standard error of unit weight after adjustment	=	1.17

The standard errors and correlation coefficients for this solution are identical to those given for solution 6.1.

While the overall solution may be considered satisfactory, note that the mean and RMS residual reflect a probable systematic bais in the simulated gradient observations. A possible explanation may be attributed to the fact that the sensitivity estimates given on page 143 are order of magnitude estimates only. More accurate estimates of the required gradiometer sensitivities at 250 kilometers altitude based on the development in Chapter 4 are:

V_{11} and V_{22}	1.2×10^{-2} E
V_{12}	1.1×10^{-6} E

V_{13} and V_{23} $\quad 2.3 \times 10^{-4}$ E

However, this may be placing too much credence on the accuracy of the estimated RMS gradients. Additionally, the simulated data may represent a sampling of the external gravity field which does not precisely fit the estimated RMS values. This is especially so since the sample is derived from a model region of limited extent, while the RMS values are essentially global estimates.

From the results of these experiments, it is apparent that a hard-mounted gradiometer system would require cross-gradient sensors of considerably greater sensitivity than that required for the rotating gradiometer system. Development of such a system in view of the apparent technological difficulties associated with achieving a thermally limited threshold sensitivity of 0.01E and a 1σ observational accuracy of 0.01E with the rotating system (Hughes Research Monthly Progress Reports, 1971-72), can be considered highly improbable. Hence the concept of the hard-mounted gradiometer hypothesized in this investigation is not believed to be practical for satellite gradiometry. This conclusion can also be extrapolated to the concept put forth by Moritz (1971) where he proposed using five independent components of the gravity gradient tensor in a collocation solution for determination of spherical harmonics. As was the case in the simulated solutions presented here, the requisite instrumental sensitivities present a serious limitation.

8. SUMMARY AND CONCLUSIONS

This investigation has demonstrated that satellite gradiometry is theoretically capable of providing resolution of the Earth's gravity field to harmonic degree 90 in terms of $2^\circ \times 2^\circ$ mean gravity anomalies. Further, considering the accuracy of the anomalies recovered in the experimental solutions described in the preceding Chapter, one would be inclined to use superlatives.

However, without depreciating the results of this investigation, a word of caution is in order. That is, while we can be optimistic about the potential capabilities of satellite gradiometry, we must recognize that simulation studies based on some hypothetical model are only as valid as the underlying assumptions. For example, will it be technologically possible to achieve a gradiometer sensitivity and accuracy of 0.01E? Will the real data be as smooth as we have assumed in modeling the simulations? Unfortunately, such questions will remain essentially unanswered until an operational gradiometer system is actually placed in orbit about the Earth.

Based upon this investigation, the rotating gradiometer should be chosen over the hard-mounted system by virtue of the extreme sensitivities required in the latter. Comparing the simulation results using the rotating system with analogous results given by Schwarz (1970) for satellite-to-satellite tracking indicates a significant difference in the accuracies of the

recovered gravity field parameters. In the simulation results reported by Schwarz, density layer values in 2° x 2° blocks were recovered to an accuracy of 1 milligals. The rotating gradiometer results obtained here indicate a mean gravity anomaly accuracy of about 0.5 to 1 milligal. Both results are considerably better than the accuracy of 2° x 2° mean gravity anomalies determined by measuring surface gravity along a profile through the block (Moritz, 1963).

The accuracy with which the shape of the geoid can be determined from satellite gradiometry largely depend on the correlations between the anomaly blocks in addition to the accuracy of determining the mean anomaly in a single block. Certainly a combination of satellite gradiometer and altimeter results can be expected to produce heretofore unprecedented global details of the Earth's gravity field.

The excitingly great potential of satellite gradiometry dictates a continuing research and development effort in both the area of instrumentation and data reduction.

APPENDIX A

Point Mass Solutions Using 1° x 1° Mean Anomalies

	West Half Area	East Half Area	Central Area
Latitude limits	25° N - 50° N		
Longitude limits	240° N - 260° E	260°E - 280° E	250° E - 270°E
No. anomalies used in solution	500	500	500
Mass depth (km)	100	100	100
No. of pre-defined masses	-	-	320
No. of unknown masses determined	320[b]	320[b]	320
Mean input anomaly (mgal)	1.20	1.50	1.78[a]
RMS input anomaly (mgal)	17.89	15.99	17.62[a]
Mean residual anomaly after fitting masses (mgal)	1.02	1.41	1.28[a]
RMS residual anomaly after fitting masses (mgal)	7.57	6.23	7.06

[a] Input anomalies have been corrected for predefined masses.

[b] One half of these mass sets were included in the final composite set.

APPENDIX A (CONTINUED)

Summary of Superimposed Point Mass Set Solutions

Depth of Masses (km)	30' x 30'	5' x 5'
Mean Anomaly Block Size Latitude Limits	33°N - 41°N	36°N - 38°N
Longitude Limits	260° E - 265° E	259°.5E - 261°.5E
No. of Anomalies Used in Solution	288	576
No. of Predefined Masses	640	895
No. of Unknown Masses Determined	255	306
Mean Input Anomaly	0.56	-0.11
RMS Input Anomaly	9.40	7.10
Mean Residual Anomaly After Fitting Masses (mgal)	0.64	-0.21
RMS Residual Anomaly After Fitting Masses (mgal)	1.86	1.77

APPENDIX B

RAPPS SPHERICAL HARMONIC

POTENTIAL COEFFICIENTS AND THEIR ACCURACY TO (14, 14)

		C		S	
		ADJUSTED	STANDARD	ADJUSTED	STANDARD
N	M	VALUE	ERROR	VALUE	ERROR
2	0	-484.1750	0.0120		
2	2	2.3706	0.0551	-1.3422	0.0551
3	0	0.9365	0.0314		
3	1	1.8556	0.0497	0.2434	0.0531
3	2	0.7130	0.0491	-0.5486	0.0460
3	3	0.6331	0.0653	1.5234	0.0687
4	0	0.5522	0.0197		
4	1	-0.5513	0.0309	-0.4470	0.0272
4	2	0.2971	0.0437	0.5844	0.0441
4	3	0.8729	0.0305	-0.1975	0.0271
4	4	0.0936	0.0759	0.2741	0.0800
5	0	0.0496	0.0283		
5	1	-0.0816	0.0393	-0.0635	0.0390
5	2	0.5228	0.0419	-0.2134	0.0392
5	3	-0.3560	0.0456	0.0273	0.0461
5	4	-0.0492	0.0479	0.0744	0.0460
5	5	0.0859	0.0593	-0.5689	0.0600
6	0	-0.1366	0.0297		
6	1	-0.0647	0.0261	-0.0194	0.0226
6	2	0.0283	0.0396	-0.2835	0.0396
6	3	-0.0535	0.0411	0.0602	0.0373
6	4	-0.0250	0.0507	-0.4123	0.0518
6	5	-0.2906	0.0339	-0.4509	0.0316
6	6	-0.0087	0.0546	-0.1843	0.0540
7	0	0.0702	0.0327		
7	1	0.1289	0.0489	0.1060	0.0480
7	2	0.3065	0.0372	0.1372	0.0354
7	3	0.1796	0.0430	0.0092	0.0433
7	4	-0.1931	0.0430	-0.0906	0.0415
7	5	0.0704	0.0450	0.0355	0.0461
7	6	-0.1654	0.0441	0.0917	0.0426
7	7	0.0679	0.0464	-0.0298	0.0464
8	0	0.0460	0.0345		
8	1	-0.0433	0.0365	0.0250	0.0343
8	2	0.0401	0.0441	0.0981	0.0439
8	3	-0.0044	0.0388	0.0380	0.0379

		C		S	
N	M	ADJUSTED VALUE	STANDARD ERROR	ADJUSTED VALUE	STANDARD ERROR
8	4	-0.0922	0.0422	0.0188	0.0431
8	5	-0.0630	0.0405	0.0818	0.0403
8	6	-0.1070	0.0423	0.2869	0.0424
8	7	0.0256	0.0348	0.0300	0.0370
8	8	-0.1041	0.0412	-0.0168	0.0402
9	0	0.0248	0.0341		
9	1	0.1325	0.0405	-0.0872	0.0388
9	2	0.0125	0.0328	0.0000	0.0327
9	3	-0.0753	0.0411	-0.0303	0.0412
9	4	0.0400	0.0406	-0.0154	0.0400
9	5	-0.0465	0.0399	0.0258	0.0405
9	6	-0.0102	0.0391	0.0432	0.0393
9	7	0.0421	0.0373	0.0181	0.0380
9	8	0.2074	0.0377	-0.0032	0.0378
9	9	0.0129	0.0382	-0.0345	0.0384
10	0	-0.0127	0.0290		
10	1	0.0788	0.0326	-0.0645	0.0311
10	2	-0.0402	0.0359	-0.0706	0.0362
10	3	-0.0499	0.0371	-0.1314	0.0370
10	4	-0.0310	0.0353	-0.0866	0.0356
10	5	-0.0046	0.0364	0.0037	0.0369
10	6	-0.0622	0.0363	-0.0202	0.0366
10	7	0.0745	0.0352	-0.0160	0.0352
10	8	0.0439	0.0337	-0.1039	0.0343
10	9	0.0934	0.0344	-0.0026	0.0341
10	10	0.0678	0.0347	-0.0690	0.0348
11	0	-0.0880	0.0218		
11	1	0.0244	0.0329	0.0120	0.0319
11	2	0.0304	0.0313	-0.0245	0.0315
11	3	-0.0049	0.0317	-0.0049	0.0318
11	4	-0.0196	0.0320	-0.0597	0.0318
11	5	0.0087	0.0313	-0.0615	0.0317
11	6	0.0339	0.0310	0.0098	0.0311
11	7	0.0088	0.0308	-0.0801	0.0309
11	8	0.0409	0.0297	0.0106	0.0297
11	9	0.0334	0.0289	0.0060	0.0293
11	10	-0.0140	0.0294	-0.0109	0.0295
11	11	0.0752	0.0297	0.0167	0.0298
12	0	-0.0068	0.0236		
12	1	-0.0643	0.0302	-0.0596	0.0283
12	2	-0.0184	0.0299	0.0865	0.0305
12	3	0.0683	0.0286	-0.0065	0.0287
12	4	-0.0176	0.0292	-0.0169	0.0287
12	5	0.0318	0.0286	-0.0677	0.0290
12	6	0.0033	0.0281	0.0346	0.0283
12	7	-0.0423	0.0280	0.0270	0.0279

		C		S	
N	M	ADJUSTED VALUE	STANDARD ERROR	ADJUSTED VALUE	STANDARD ERROR
12	8	0.0101	0.0275	0.0507	0.0275
12	9	-0.0112	0.0263	0.0627	0.0267
12	10	-0.0033	0.0263	0.0027	0.0263
12	11	-0.0179	0.0267	0.0039	0.0269
12	12	0.0255	0.0272	-0.0313	0.0272
13	0	0.0462	0.0258		
13	1	-0.0098	0.0240	-0.0172	0.0228
13	2	-0.0008	0.0233	0.0061	0.0236
13	3	0.0198	0.0235	0.0535	0.0235
13	4	0.0092	0.0238	-0.0293	0.0236
13	5	0.0516	0.0236	-0.0476	0.0239
13	6	-0.0353	0.0233	0.0308	0.0235
13	7	0.0078	0.0230	0.0228	0.0231
13	8	-0.0460	0.0230	-0.0033	0.0229
13	9	0.0014	0.0224	0.0520	0.0227
13	10	0.0162	0.0219	-0.0576	0.0219
13	11	-0.0434	0.0218	-0.0011	0.0220
13	12	-0.0137	0.0222	0.0644	0.0225
13	13	-0.0203	0.0225	0.0465	0.0226
14	0	-0.0103	0.0222		
14	1	-0.0177	0.0243	0.0057	0.0232
14	2	-0.0533	0.0202	0.0006	0.0206
14	3	0.0179	0.0205	0.0149	0.0207
14	4	0.0218	0.0205	-0.0038	0.0203
14	5	0.0745	0.0204	-0.0631	0.0206
14	6	0.0144	0.0202	-0.0374	0.0203
14	7	0.0571	0.0199	0.0310	0.0198
14	8	-0.0159	0.0195	-0.0208	0.0195
14	9	0.0346	0.0193	0.0720	0.0193
14	10	0.0546	0.0191	-0.0461	0.0191
14	11	0.0120	0.0187	-0.0106	0.0187
14	12	0.0254	0.0190	-0.0073	0.0192
14	13	0.0145	0.0197	0.0171	0.0197
14	14	-0.0308	0.0197	-0.0075	0.0197

REFERENCES

American Bosch Arma (1966) "Gravity Gradient Instrument Study", Final Report, NASA DS-66-R371-10.

Anthony, D. (1971) "Gradiometer Applications and Status of Sensor Development", AFCRL Environmental Research Papers, No. 355, Bedford, Mass.

Bell, C.C., R.L. Forward and H.P. Williams (1970) "Simulated Terrain Mapping with the Rotating Gravity Gradiometer", Advances in Dynamic Gravimetry, W.T. Katlner, Editor, Instrument Society of Pittsburg, pp. 115-129.

Chovitz, B.H. J.R. Lucas and F. Morrison (1972) Gravity Gradients at 300 Km Altitude, NOAA, NOS, Rockville.

DeWitte, L. (1965) "On Derivations and Properties of Stokes' Gravity Formula", Aerospace Corporation, Report No. TDR 469 (S 5230-37)-1.

DeWitte, L. (1966) "Truncation Errors in the Stokes and Vening-Meinesz Formulae for Different Order Spherical Harmonic Gravity Terms", Aerospace Corporation, Report No. TR-669 (S 6230-37)-5.

DeWitte, L. (1969) "Altitude Extension of the Three Anomalous Gravity Components", Bulletin Geodesique, No. 93, pp. 287-305, 1 Sept. 1969, Paris.

Flugge, A. (1956) Encyclopedia of Physics, Vol. 47, Part I, pp. 215-219.

Forward, R.L. (1971a) "Geodesy with Orbiting Gravity Gradiometers, Research Report 442, Hughes Research Laboratories, Malibu.

Forward, R.L. (1971b) "Gravitational Field Measurements of Planetary Bodies with Gravity Gradient Instrumentation"; Research Report 448, Hughes Research Laboratories, Malibu, August 1971.

Forward, R.L. (1971c) Development of a Rotating Gravity Gradiometer for Earth Orbit Applications, Preprint and paper presented at the Advanced Applications Flight Experiments (AAFE) Program Review, 5-6 October 1971, NASA Research Center, Hampton, Va.

Gardner, J.A., et al (1972) "Earth Physics Satellite Gravity Gradiometer Study", Document No. 760-70, Jet Propulsion Laboratory, C.I.T. Pasadena.

Glaser, R. and E.J. Sherry (1971) Relationship of Gravity Gradients to Spherical Harmonics, Jet Propulsion Laboratory, C.I.T. Pasadena.

Glaser, R. and E.J. Sherry (1972) Comparison of Satellite Gravitational Techniques, Jet Propulsion Laboratory, C.I.T., Pasadena.

Glaser, R.J. (1972), "Satellite Gradiometry Data Reduction", Thesis, California Institute of Technology, September 1972.

Grafarend, E., (1972a) Inverse Potential Problems of Improperly posed type in Physical Geodesy and Geophysics, Paper presented to the International Sumposium on Earth Gravity Models and Related Problems, August 16-18, 1972, St. Louis, Mo.

Grafarend, E. (1972b) Attempts for a Unified Theory of Geodesy, Paper presented at the 5th Symposium on Mathematical Geodesy (2^{d}Hotine Symposium), October 25-26, 1972, Florence, Italy.

Grafarend, E. (1972c) Private Communication

Grosch, C.B. (1967), "Orientation of a Rigid Torque-Free Body by Use of Star Transits," Journal of Spacecraft and Rockets, Vol. 4, No. 5, pp. 562-566, AIAA, May 1967.

Grosch, C.B. et al (1969). "The SCNS Attitude Determination Experiment on ATS-III, Edina Space and Defense Systems, Control Data Corporation, Paper presented at the Spacecraft Attitude Determination Symposium, El Segundo, Calif. Sept. 30, Oct. 1-2, 1969.

Gulick, L.J. (1970), "A Comparison of Methods for Computing Gravitational Potential Derivatives", ESSA Technical Report C&GS 40, U.S. Dept. of Commerce, Environmental Science Services Administration, Coast and Geodetic Survey, Rockville, Md.

Heffron, W.G. (1971) Gravity and Gravity Gradient From Spherical Harmonics-Case 310, Bellcomm, Washington, D.C., 31 August 1971.

Heiskanen, W.A. and H. Moritz (1967), Physical Geodesy, W.H. Freeman and Co., San Francisco.

Hirvonen, R. and H. Moritz (1963) "Practical Computation of Gravity at High Altitudes", OSU Report No. 27, May 1963 Columbus.

Hobson, E.W. (1965) The Theory of Spherical and Ellipsoidal Harmonics, Chelsea Publishing Co., New York.

Hotine, M. (1957) Metrical Properties of the Earth's Gravitational Field, A.I.G., Toronto.

Hotine, M. (1969) "Mathematical Geodesy", ESSA Monograph 2, U.S. Dept. of Commerce, ESSA, Washington, D.C.

Hughes Research Laboratories (1971-1972), "Development of a Rotating Gravity Gradiometer for Earth Orbit Applications (AAFE)", Monthly Progress Reports for NASA Contract NAS 1-10945.

IAG (1967): "Resolutions Adopted at the General Assembly," International Association of Geodesy, Lucerne, Bulletin Geodesique, No. 86.

IAG, (1970): "Geodetic Reference System 1967," A special publication of the Bulletin Geodesique, Bureau Central de L'Association International de Geodesie, Paris.

IBM (1968): System/360 Scientific Subroutine Package (360A-CM-03x) VersionIII Programmer's Manual, White Plains, New York, International Business Machines Corporation, Form H20-0205-3.

Kaula, W.M. (1963) "Determination of the Earth's Gravitational Field", Rev. Geophysics 1, pp. 507-551, 1963.

Kaula, W.M. (1966a) "Tests and Combination of Satellite Determinations of the Gravity Field with Gravimetry", JGR, Vol. 77, No. 22.

Kaula, W.M. (1966b), Theory of Satellite Geodesy, Blaisdell Publishing Co., Waltham, Mass.

Kaula, W.M. (1967), "Theory of Statistical Analysis of Data Distributed over a Sphere", Reviews of Geophysics, Vol. 5, No. 1, February, 1967.

Kaula, W.M. (editor) (1969a), "Solid Earth and Ocean Physics", Report of a Study at Williamstown, Mass., to the National Aeronautics and Space Administration. Sponsored by NASA Electronics Research Center, MIT Measurement Systems Laboratory, Cambridge.

Kaula, W.M. (1969b) "The Appropriate Representation of the Gravity Field for Satellite Geodesy," Publ. No. 760, Institute of Geophysics and Planetary Physics, University of California, Los Angeles.

Kaula, W. M. (1971a) Implications of New Techniques in Satellite Geodesy, Institute of Geophysics and Planetary Physics, University of California, Los Angeles.

Kaula, W. M. (1971b) Letter to Dr. Martin J. Swetnik, NASA Headquarters, June 16, 1971.

Koch, K.R. (1968) "Alternate Representation of the Earth's Gravitational Field for Satellite Geodesy", Bullettino di geofisica teorica ed applicata, Vol. X, No. 40, December 1968.

Koch, K. (1970) "Gravity Anomalies for Ocean Areas from Satellite Altimetry", Proceedings of the Second Marine Geodesy Symposium, Marine Technology Society, Washington, D.C.

Koch, K. and B. Witte (1971) "The Earths Gravity Field Represented by a Simple Layer Potential from Doppler Tracking of Satellites", NOAA Technical Memorandum No. 59, April 1971.

Kohnlein, W. (1967a) "On the Gravity Gradient of Satellite Altitudes", SAO Special Report 246, July 28, 1967, Cambridge.

Kohnlein, W. (1967b) "Gravity Gradients on the Earth's Surface as Deduced from Satellite Orbits", SAO Special Report 249, August 25, 1967, Cambridge.

Krarup, T. (1969) "A Contribution to the Mathematical Foundation of Physical Geodesy," Report No. 44, Danish Geodetic Institute, Copenhagen.

Kreyszig, E. (1959) Differential Geometry, Mathematical Expositions No. 11, University of Toronto Press, Toronto.

Loomis, et al (1972) "Earth and Ocean Physics Applications Planning Study", Document No. 760-72, Jet Propulsion Laboratory, California Institute of Technology, Pasadena.

Lundquist, C.A., Geo. Giaizglia, K. Hebb and S.G. Main (1969) "Possible Geopotential Improvement from Satellite Altimetry," Special Report 294, Smithsonian Astrophysical Observatory, Cambridge.

MacMillan (1958) The Theory of the Potential, Dover Publication, New York.

Marussi, A. (1949) "Fondements de Geometrie Differentielle Absolne du Champ Potential Terrestre, Bulletin Geodesique, No. 14, pp. 411-439, Dec., 1949.

Marussi, A. (1967) "Gravity Field, Inner Geometry of", Dictionary of Geophysics, pp. 683-685.

Meissl, P., (1971), "A Study of Covariance Functions Related to the Earth's Disturbing Potential," Report No. 151, Department of Geodetic Science, The Ohio State University.

Michal, A.D. (1947) Matrix and Tensor Calculus, John Wiley & Sons, Inc., New York.

Moritz, H. (1963), "Accuracy of Mean Gravity Anomalies Obtained from Point and Profile Measurements", Reports of the Institute of Geodesy, Photogrammetry and Cartography. Report No. 29. The Ohio State University, Columbus.

Moritz, H. (1967) "Kinematical Geodesy", Report No. 92, Department of Geodetic Science, The Ohio State University, Columbus.

Moritz, H. (1970) "Least Squares Estimation in Physical Geodesy", Report No. 130, Department of Geodetic Science, The Ohio State University, Columbus.

Moritz, H. (1971) "Kinemetical Geodesy II", Report No. 165, Department of Geodetic Science, The Ohio State University, Columbus.

Moritz, H. (1972) Private Communication.

Mueller, I.I. (1960) The Gradients of Gravity in Geodesy, Doctoral Dissertation, The Ohio State University, Columbus.

Mueller, I.I. (1961) "The Determination of the Regional Part of the Vertical Gradient Anomaly by a Geodetic Method", Geofisca Pura Applicata, Vol. 48 (1961/I), pp. 1-6, Milano.

Mueller, I.I. (1963) "Geodesy and the Torsion Balance", Journal of the Surveying and Mapping Division, Proceedings of the American Society of Civil Engineers, SU 3, October 1963, pp. 123-155, New York.

Mueller, I.I. (1964a) The Horizontal Gradients of Gravity in Geodesy, Department of Geodetic Science, The Ohio State University, Columbus.

Mueller, I.I. (1964b) "Vertical Gradient of Gravity", Journal of the Surveying and Mapping Division, Proceedings of the American Society of Civil Engineers, SU 2, July 1964, pp. 83-107, New York.

Needham, P. E. (1970) "The Formation and Evaluation of Detailed Geopotential Models Based on Point Masses", Report No. 149, Department of Geodetic Science, The Ohio State University, Columbus.

Obenson, G. F. T. (1970) "Direct Evaluation of the Earth's Gravity Anomaly Field from Orbital Analysis of Artificial Earth Satellites", Report No. 129, Department of Geodetic Science, The Ohio State University, Columbus.

Pollack, H. N. (1972), Spherical Harmonic Representation of the Gravitational Potential Arising from a Point Mass, Spherical Cap, and Spherical Rectangle, With Applications to Field Modeling, Paper presented at the International Symposium on Earth Gravity Models and Related Problems, St. Louis, Mo., August, 1972.

Rapp, R. H. (1966) "A Fortran Program for the Computation of the Disturbance Components of Gravity", Report No. 76, Department of Geodetic Science, The Ohio State University, Columbus.

Rapp, R. H. (1967) The Geopotential To (14,14) From A Combination of Satellite and Gravimetric Data, Presented at the XIV General Assembly IUGG/IAG, Lucerne, Switzerland.

Rapp, R. H. (1972), Improved Models for Potential Coefficients and Anomaly Degree Variances, Department of Geodetic Science, The Ohio State University, Columbus. (In print)

Reed, G. B. (1972) "Trip Report-Orbital Rotating Gravity Gradiometer Contract Review Conference-NASA Langley Research Center, Hampton, Va., 15 February 1972", Department of Geodetic Science, The Ohio State University, Columbus.

Savet, P. H. et al (1967) "Gravity Gradiometry", Report RE-313, Grumman Aircraft Engineering Corporation, Bethpage, N. Y. Final Report prepared for NASA under contract NAS 8-21130, December 1967.

Savet, P. H. (1963) "Gravity Field Exploration by a New Gradient Technique", Journal of Spacecraft and Rockets, Vol. 6, No. 6, 6 June 1969, pp. 710-716.

Savet, P. H. (1970) "New Developments in Gravity Gradiometry", Advances in Dynamic Gravimetry, W. T. Kettner, Editor, Instrument Society of America, Pittsburg, pp. 46-58.

Schwarz, C.R. (1970) "Gravity Field Refinement by Satellite-to-Satellite Doppler Tracking", Report No. 147, Department of Geodetic Science, The Ohio State University, Columbus.

Thompson, L.G., et al (1965) Gravity Gradient Sensors and Their Application for Manned Orbital Spacecraft, Third Goddard Memorial Symposium, American Astronautical Society, Washington D.C.

Trageser, M.B. (1970) "A Gradiometer System for Gravity Anomaly Surveying", Report R-588, C.S. Draper Laboratory, Massachusetts Institute of Technology, Cambridge.

Uotila, U.A. (1967), Introduction to Adjustment Computations with Matrices, Department of Geodetic Science, The Ohio State University, Columbus.

Vinti, S.P. (1971) "Representation of the Earth's Gravitational Potential", Celestial Mechanics, 4 (1971), pp. 348-367, D. Reidel Publishing Co., Dordrecht, Holland.

Witte, B. (1968) "Die Berechnung von Horizontalalabeitungen der Schere-storungen in Aussenraum der Erde aus einer Entwicklung des Potentials nach Kugelfunctionen", Deutsche Geodetische Kommission bei der Bayerischen Akademic der Wissenscheffen, Series C; Dissertation, No. 122, 1968, Munich, West Germany.

Witte, B. (1970a) "Die Berechnung des Vertikalgradienten der Schwere in Aussenraum", Professor Dr. Ing. Helmut Wolf, zum 60, Geburtstag, 1970, pp. 133-142, Institut fur Kartographie und Topographie der Universitat Bonn, West Germany.

Witte, B. (1970b) "Die Bestimnung von Horizontalableitungen der Schwere in Aussenraum aus einer Weiterentwicklung der Stokesschen Funktion", Gerlands Beitrage Zur Geophysik, Vol. 79, No. 2, 1970, pp. 87-94, Akademische Verlagsgesellschaft, Geest and Portig K. -G., Leipzig, East Germany.

Witte, B. (1971) "Computational Procedures for the Determination of a Simple Layer Model of the Geopotential from Doppler Observations", NOAA Technical Report NOS 42, U.S. Dept. of Commerce, National Oceanic and Atmospheric Administration, National Ocean Survey, Rockville, Md.